1-27-2020

Low-cost solid state nanopore biosensing technology towards early disease detection

Julian Bello
Rowan University

LOW-COST SOLID-STATE NANOPORE BIOSENSING TECHNOLOGY TOWARDS EARLY DISEASE DETECTION

by
Julian Bello

A Thesis

Submitted to the
Department of Biomedical Engineering
College of Engineering
In partial fulfillment of the requirement
For the degree of
Master of Science in Biomedical Engineering
at
Rowan University
December 13, 2019

Thesis Adviser: Jiwook Shim, Ph.D.

Acknowledgements

This work would not be possible if it were not for the constant collaboration and support of the students in our undergraduate engineering clinic and the interns we had throughout the years. This includes Maksudul Mowla, Nicholas Troise, Joanna Soyring, Christopher Moran, Julia Borgesi, Olivia Sergeant, and Liza Gunner. I hope you all got as much out of this experience as I got from mentoring you. I would like to especially thank my co-worker, fellow graduate student, and friend, Trang Vu, for being there as a sounding board for ideas, support when things did not work out, and cheers when they did. I also want to give special thanks to Thomas Christiani, who set an example of what a graduate student should be and mentored me along the way. I would also like to thank my graduate committee and the Biomedical Engineering Department Faculty for their support and guidance, and our funding sources for supporting this work.

In addition, I would like to thank my mother, Aida Bello, and my father, Alexis Bello, for pushing me when I was young and always stressing the importance of my education. Ustedes plantaron una semilla cuando yo era pequeño, que crecio a ser un bosque de oportunidades. Gracias. I hope I have made you proud. I would like to thank my younger sister, Gisela. You have motivated me to try and be a good role model for you. I want to thank my dog, Riley. You have made me a more patient person and you have made the stressful times these past two years more tolerable with your unconditional love. And last, but surely not least, I would like to thank my loving fiancée, Claudia Alarcon, who has endured all the ups and downs with me and supported me all along the way. Throughout this experience, I have come to believe that there isn't anything that we can't do if we have each other, and I am extremely excited about our future life together.

Abstract

Julian Bello
LOW-COST SOLID-STATE NANOPORE BIOSENSING TECHNOLOGY TOWARDS EARLY DISEASE DETECTION
2019-2020
Jiwook Shim, PhD.
Master of Science in Biomedical Engineering

Solid-state nanopore based biosensors are cost effective, high-throughput engines for single molecule detection of biomolecules, which is useful for detecting epigenetic modifications on DNA; one of these being the potentially cancerous hypo, or hypermethylation of CpG islands. Despite its immense potential in the realm of disease diagnostics, nanopore detection as it stands faces various limitations that inhibit it from widespread commercial use. These include the complex method of solid-state nanopore fabrication, fast DNA translocations through the pore causing poor resolution, and poor signal to noise ratio. The following work aims to improve the efficacy of the solid-state nanopore biosensing platform as a disease diagnostic tool by improving ease of fabrication with automated MATLAB instrument control and controlled dielectric breakdown fabrication technique and increase signal resolution by using lithium chloride salt concentration gradients. In addition, methylated DNA labeled with certain methyl-binding proteins were tested in an attempt to localize areas of methylation on the DNA strand. These experiments yielded transport events that showed multilevel electrical signals that, in some instances, were able to distinguish between regions of bound protein and unbound DNA on the same strand. Increasing the accuracy of these multilevel event readings will aid in pinpointing localized regions of methylation on DNA and thereby increase the efficacy the solid-state nanopore platform for biosensing.

Table of Contents

Table of Contents (Continued)

List of Figures

Figures **Page**

List of Tables

Tables **Page**

Chapter 1

Introduction

Nanopore biosensing is an emerging and ever-changing field that has seen itself as an integral part of genome sequencing and is trending in the direction of disease diagnostics. In very rudimentary terms, nanopore sensors embody versatility with various types of pores available, including biological, synthetic, and hybrid varieties, each with their own unique capabilities and strengths. Consequently, each variety does also come with its unique set of challenges and limitations that mandates method optimization and modification of experimental conditions in order to overcome them and make this a viable platform. However, the end goal of providing real-time, high throughput disease diagnostics at an affordable cost makes the nanopore biosensing platform worth exploring regardless of the nuances.

With many of the world's diseases now treatable when caught at an early enough stage, including many cancers that see mortality rate drop when caught and treated before stage 1, the challenge is now to find ways to facilitate early diagnostics to a wide population and make it affordable, robust, and accessible enough to catch diseases before they progress into uncurable states. Although still raw in its development, the nanopore platform as a biosensor demonstrates promise in addressing these challenges. The key to this concept is the detection of epigenetic modifications. In recent discovery, diseases have been found exhibit epigenetic changes, or alterations in gene expression and cellular function without changes to the original DNA sequence, prior to presenting the host with any detectable physical symptoms. With the ability to detect epigenetic modifications through nanoscopic changes on DNA molecules, nanopores serve as a very early

screening tool that allows for intervention before disease progression initiates. Early detection coupled with constant advances in medicine, with more targeted therapies, provides hope that one day diseases which were formerly considered death sentences, will become manageable chronic conditions, or even curable ailments.

The following work explores the solid-state nanopore platform for the detection of biomolecules, such as DNA. In particular, the focus was put on the widely used silicon nitride (SiNx) solid-state nanopore as it has been well studied as a biosensor already. The following chapters of this thesis investigate how modification of experimental parameters and optimization of conditions and techniques can improve signal resolution, robustness of results, and overall viability of the solid-state nanopore biosensor for diagnostic purposes and disease detection. Chapter 2 dives deeper into the nanopore platform including a brief history, its role in genomic sequencing and biosensing thus far, and current areas of possible improvement to the sensing platform. These areas of improvement provide the motivation for the research presented in the remainder of the text. Chapter 3 demonstrates the use of automation, a novel method of nanopore fabrication, as well the use of an experimental buffer solution that is not typically used in the field. Chapter 4 builds on the previous research and further explores how creating a concentration gradient of the aforementioned experimental buffer across the experimental chamber can have a two-fold benefit of increasing molecule translocation incidence and increasing signal resolution. Chapter 5 takes all of the knowledge acquired from the previous two chapters and applies it towards the detection of a potentially cancerous biomarker, methylation of certain cytosine bases, with the aid of different protein labels. This section also introduces the use of software and automation in terms of data analysis.

Chapter 6 explores just a few of the possible directions that may be traveled in the further refinement of this platform for diagnostic purposes.

Nanopore biosensing for disease diagnostics is an interesting reimagining of a reliable tool for genome sequencing. Although raw, the hopes are that with sufficient modification and optimization, nanopore biosensors can fit in the space of diagnostic tools to provide real time feedback and improve outcomes. This work aims to contribute to this attempt at optimization that stretches across the nanopore field.

Chapter 2

Nanopores For Sensing: A Review of the Field

2.1 An Introduction to Nanopores

A nanopore is a nanoscale sized aperture in an insulating membrane that separates two sides of a chamber filled with electrolyte solution. Nanopores are generally used in experiments for detection of biomolecules through principles of electrophoresis and ionic current spectroscopy. [1-3] The nanopore is placed in an experimental apparatus and submerged in an electrolyte buffer. A biased voltage is applied across the membrane through Ag/AgCl electrodes and the passing current is observed through a data acquisition board and a computer. When no molecule is passing through the pore, a steady open pore current is observed. As a biomolecule is introduced into the cis side of the chamber, it is drawn towards the trans compartment by the applied electrical field and begins to pass through the pore. As this occurs, part of the pore diameter is blocked, and a characteristic current drop is observed relative to the size of the molecule in relation to the pore size. When the molecule passes through, or translocates to the trans side, the current level returns to baseline level. There are two main types of nanopores: Solid-state and biological. The biological nanopore is a protein channel that gets inserted into a manmade lipid bilayer membrane. Artificially created lipid bilayer membranes can provide a biological environment in which ion channels and other transmembrane proteins can be incorporated *ex vivo* and can be studied for an extended duration in a cost-effective manner. Ever since the first artificial lipid bilayer membrane was created *ex vivo* in the early 1960s, [4, 5] artificially constructed model membranes have been extensively used to elucidate the functions of transmembrane proteins, [6-8] to study

membrane biophysics, [9-13] and to create protein-based sensors, such as biological nanopore based biosensors. [5, 14-18] The solid-state nanopore is a synthetic channel that is created manually in a dielectric membrane. This type of nanopore will be highlighted further later in this chapter and will be the focus of this entire thesis.

2.2 Nanopores for Sequencing

Nanopore technology is especially attractive for the application of DNA sequencing. DNA sequencing has been transformed over the past decade through the commercialization of new and relatively inexpensive short sequence reading technology. [19] However, although technology has improved sequence throughput and has decreased its cost, full genome analysis still requires several days and thousands of dollars to complete. [20, 21] Biological and solid-state nanopores offer a low-cost alternative that is driving the advancement of DNA sequencing even further. Nanopore sequencing devices are capable of the single-molecule detection of a wide variety of analytes of medical interest, ranging from small molecules to post-translationally modified proteins. The most widely used and well-studied biological nanopore protein used is alpha hemolysin (αHL), which is an exotoxin secreted by the bacterium *Staphylococcus aureus*. This nanopore structure remains functionally stable at temperatures close to 100 °C within a wide pH range, [1] and because of its proximity in size to single-stranded DNA molecules, [1] αHL can discriminate among single nucleotides by using ionic current inside the nanopore. In fact, the only available nanopore sensing device to date, the MinIon by Oxford Nanopore, uses a biologically inspired nanopore to analyze single stranded DNA base by base to genetically sequence it.[22] Although a useful research tool because of its well-defined structure, αHL has various drawbacks including

instability when introduced to slight changes in experimental conditions, errors in long DNA sequences, and a fixed inner dimension that sometimes creates obstacles for DNA detection. [23, 24] Lastly, nanopore sequencing methods, both biological and solid-state, are also plagued by ultrafast translocation speeds that do not allow for distinguishable base discrimination. [25]

2.3 Solid-State Nanopores as a Biosensor for Disease Detection

The benefits of the solid-state platform directly juxtapose the drawbacks of the biological platform. Solid-state experiments can be run at different temperatures, pH, salt types and concentrations, and high voltage without any discernable failure in the nanopore structure, or integrity. Another benefit is that you can adjust the size of the solid-state pore in a process called “tuning” to accommodate the size of the specific analyte that is being tested.[26-29] The most common and best characterized type is the silicon nitride (SiNx) nanopore membrane, although graphene, Al_2O_3, HfO_2, and even glass nanopore have been used for various applications. [30-33] Although solid-state pores are undoubtedly more robust than biological pores, typical use of solid-state nanopores for DNA sequencing is not seen because of erratic baseline currents, high signal to noise ratios and lower sensitivity to DNA bases when compared to biological pores. Because of this, it is difficult for a solid-state nanopore sensor to compete with what is already commercially available. An area that solid-state nanopores do fit into is the area of disease diagnostics. There is a clinical need for low cost biosensors and diagnostic tools for drug and disease screening, especially in developing countries and rural areas where these resources are not readily available. Furthermore, routine health screenings do not do enough to check for diseases like cancer that manifest slowly yet

become lethal if left untreated. In the United States, cancer is the second leading cause of death behind cardiac disease. Each year, millions of new cancer cases are diagnosed, with over 600,000 deaths relating to cancer per year. Globally, cancer is the cause of death of every 1 in 7 patients. [34] Oftentimes, a cancer diagnosis is made once a patient has already experienced symptoms or located a tumor. In most cases, this is already too late to intervene with the outlook of any beneficial outcomes. However, cancer detected in stage 0 or 1 can increase positive outcomes up to 90% for some cancer types. [34, 35] Cancer research is often centered around early detection and finding tumors before they metastasize.

DNA methylation, the covalent transfer of a methyl group (CH_3) onto the 5-carbon position of cytosine through DNA methyltransferases, is a natural epigenetic modification in DNA.[36, 37] Methylation regulates cell growth and proliferation by silencing repetitive transcription, or transposition areas, silencing retroviral elements, and regulating tissue-specific gene expression.[38] While DNA methylation is normal in the body, both hypomethylation and hypermethylation can be associated with cancer-specific diseases.[39, 40] Global DNA hypomethylation, the loss of methylation at typically highly methylated repeat sites, causes cancer by activating oncogenes and creating genomic instability. It also affects repetitive sequences, imprinted genes, tissue-specific genes, and genes associated with invasion and metastases. Regionally-specific hypermethylation, over-methylation of specific sections of DNA, commonly occurs at the promoter of *CpG* islands (CGIs) of tumor suppressor genes, causing the tumor suppressing gene to be silenced and the tumor to grow unregulated.[41] DNA methylation at the 5-carbon position of the cytosine nucleotide has been shown to

correspond to pre-cancerous genes including p16INKa, p15INK4b, RASSF1A, MLH1, GSTP1, CDH1, APC, and DAPK1.[42-50] By identifying these aberrant methylation patterns, researchers and medical professionals may be able to detect and diagnose cancer at early stages, decreasing the mortality rate and financial impact of the disease.

However, current methods of analyzing genome wide methylation rely heavily on bisulfide genomic sequencing. [51] This method requires a large sample volume due to DNA degradation during the bisulfite conversion and exhibits low PCR efficiency. [52-54] Previous studies have reported the feasibility of detecting cancer by methylation pattern analysis from genomic extracts of human bodily fluids such as plasma, serum, urine, and stool. [54-56] However, only a very small amount of methylated DNA can be obtained from the bodily fluids. [53] As a result, most conventional methylation assays are not suitable for detecting the extremely low level of methylated DNA in bodily fluids. This presents a need for a less labor intensive and direct method to characterize methylation in a cost effective and timely manner. Nanopore technology has the potential for detecting and characterizing biomolecules including DNA [5, 29, 57], RNA and proteins [58, 59], viruses [60], and polysaccharides [61]. As mentioned previously, when biomolecules pass through the nanopore, they cause ionic current blockages, which can be analyzed to characterize physical and chemical properties of the biomolecule.[1, 29, 62, 63] Previous work has investigated the possibility of nanopore based devices for detection of hypermethylation, coarse quantification of methylation sites, and coarse profiling of single dyad methylation pattern. Thus, there is promise in the nanopore technology toward precancerous and early-stage cancer detection. [43, 64] Nanopore technology is a cost effective, high throughput platform that could assist in these various

medical applications such as drug delivery devices and targeted biorecognition platforms. [65]

Solid-state nanopores' ability to operate in various liquid media and pH conditions as well as their production being scalable and compatible with other detection techniques [66, 67] and common nanofabrication techniques makes the platform an easy choice for use as a diagnostic tool.[68] However, certain obstacles, such as controlling molecule translocation time and discriminating between nucleotide bases and proteins, introduce complications that limit possible commercial use of the solid-state nanopore. The topic of signal resolution will be visited many times in this thesis. As also seen in biological pores, the velocity of DNA transport is in some cases the biggest deterrent from integration of nanopore sensing into mainstream disease diagnostics. Factors affecting transport time range anywhere from the polarity of the molecule being tested, the makeup of the environment the molecule sits in, the strength of the electrical field applied, and the properties of the nanopore being used. As can be seen, there are many variables to this problem and many possible routes to travel along to try to solve these issues. Possible ways to address these shortcomings in signal resolution include upgrading the sensitivity of the data acquisition system, which in many cases may not be possible depending on the technology available, or the financial resources available to the area. Other more malleable methods to address this is by adjusting experimental conditions and techniques, which is the route we decided to go in for this following work that will be presented. Another major challenge facing solid-state nanopores lies within the fabrication process.[69] Nanopores are typically developed using beams of high energy particles either with a transmission electron microscope (TEM), or an ion beam

sculpting tool.[70] This equipment is expensive, requires an experienced operator, and is often impractical as nanopores can be easily destroyed in the process. These drawbacks make nanopore sensors impractical to researchers and discredit its viability in the clinical setting as a diagnostic tool.

Thus, this reveals the motivation for this graduate research. Improving the solid-state nanopore platform signal resolution and fabrication method will not only help advance the field, but it will bring the tool one step closer to making an impact in the lives of the hundreds of thousands of people that are affected by diseases like cancer each year.

Chapter 3

Fabrication of Solid-State Nanopores Using Controlled Dielectric Breakdown in LiCl Buffer[1]

3.1 Background

As mentioned previously, the most common and well-studied method of solid-state nanopore fabrication is TEM drilling. This technique allows researchers in the field to create nanopores in a variety of medium and obtain clear visual evidence of nanopore size and shape. Although very precise, with sub nanometer reproducibility, and widely utilized in the research field, this method lacks practicality in that it requires a transmission electron microscope with a focused electron beam as well as a skilled operator to accurately fabricate a nanopore device. The microscope itself presents a barrier for smaller labs and companies in that it is large and ranges in price anywhere from $95,000 for Jeol or Philips models to over $100,000 for higher end Hitachi instruments. In addition, dry fabrication of the nanopore by TEM drilling requires the membrane to then be mounted into the testing apparatus, introducing various degrees of potential experimenter error that can damage the pore. These reasons create hesitation when considering nanopore sensors for more widespread use. The benefits of nanopore sensors in lower cost, real time sensing capabilities are in a way muted by the cost and time of creation when using the TEM drilling method. An alternative to TEM Drilling, called controlled dielectric breakdown, has been briefly explored as a viable method for solid-state nanopore creation in thin membranes.[71] This heavily biophysical model of nanopore formation was further investigated throughout my research and MATLAB code, coupled with a graphic user interface, was developed to control the fabrication of

[1] Adapted, with permission, from J. Bello, 2018, "Solid-state nanopore fabrication in LiCl by controlled dielectric breakdown," *Biomedical Microdevices* 20(2): p. 38.

the nanopores with ease. Although, controlled dielectric breakdown, has shown promise, as will be shown in the coming sections, it is not free from drawbacks. In the way that TEM drilling demonstrates great precision and control in terms of nanopore size and shape, controlled dielectric breakdown does not see the same accuracy.

Another explanation for lack of prevalence of nanopore biosensors in disease diagnostics is the immensely fast translocation times of single molecules through the pore cavity.[24] Oftentimes, molecule transport is so fast that, depending on the size of the nanopore, it is difficult to even detect a signal. This poses issues when the basis of nanopore detection depends on detecting changes in signal stemming from an occluded pore. Further, certain biomarkers for diseases, such as methylcytosine, are present only on certain nucleotide bases. So, not only is it difficult to track the DNA as it passes through the pore because it is so fast, but the area of interest on said DNA is very small. Consequently, careful control of pore size and experimental conditions are integral to success of detection. However as mentioned previously, where TEM drilling flourishes in control of pore size, controlled dielectric breakdown finds difficulties in achieving sub nanometer precision. Additional limitations for detection included the acquisition propensity of our data acquisition board. Therefore, other avenues were to be explored in hopes of increasing molecule resolution while bypassing limitations in data acquisition and inconsistent nanopore fabrication. With this in mind, a sensible direction to travel in was to alter experimental conditions to slow down DNA translocation velocity to a point that our current data acquisition systems can detect our analytes of interest.

Varying experimental parameters such as temperature, salt concentration, viscosity, and the electrical voltage across the nanopore as well as applying gel media to

physically entrap the transporting DNA strands has been utilized to slow DNA transport through solid-state nanopores.[72-74] Although effective, none of these methods has done much single handedly impact molecule resolution. Perhaps combining two, or more of these methods could have better outcomes, but varying many parameters is a large undertaking. Forced DNA-DNA interactions within pores have also been shown to increase molecule residence time when transporting through the nanopore by tethering one DNA molecule in the pore nanocavity and recording other molecules from the experimental sample that pass through the pore.[75]. However, in this case the behavior of one DNA molecule interacting with another is extremely unpredictable and would not lend itself to work well as a diagnostic tool.

Kowalczyk et al. utilized a buffer solution comprised of varying concentrations of lithium chloride to increase DNA molecule residence time within the nanopore.[76] Different monovalent cations (K^+, Na^+, Li^+) impose different degrees of charge reduction on double stranded DNA[76, 77] with Li^+ possessing the strongest binding affinity to dsDNA out of the three. With the overall net negative charge reduced, thereby making the DNA more net positive, the applied electrical field has less of an impact on drawing the DNA molecule through the nanopore and causes the DNA to slow down. This explains why potassium chloride and sodium chloride buffers have been traditionally used in nanopore experiments, but inexplicably, lithium chloride buffer had not been readily used. As shown in Kowalczyk et al., the increased binding affinity of lithium in their LiCl buffer resulted in dwell time increase of up to 10 fold when compared to experiments run in KCl.[76] Similar results were reported in Kwok et al. when using 3.6 M LiCl buffer instead of 1 M KCl for their DNA experiments. [71] It is important to note

that higher concentrations of salt have even been shown to increase dwell time long enough to detect previously undetectable moieties such as DNA knots translocating through solid-state pores.[78]

In the coming sections, our method of controlled dielectric breakdown of SiNx dielectric membranes in LiCl buffer is shown. The use of controlled dielectric breakdown is aimed to increase experimental efficiency and practicality while the fabricated in LiCl buffer is aimed to increase resolution. In addition, fabrication of the pore directly in LiCl not only minimized transfer of the nanopore device after fabrication, but it also resulted in a more stable pore immediately post fabrication.

3.2 Materials and Methods

For all experiments in this section, 10 nm thick SiNx membranes deposited on a 200 μm SiO_2 substrates with a 0.05 x 0.05 mm window were used to fabricate our nanopore devices using controlled dielectric breakdown. Although these devices can be made in house with the proper instrumentation, they are also commercially available and were purchased from Norcada (Alberta, Canada) to ensure quality and consistency. The membrane chips were pretreated with a solution consisting of 1:1 hydrogen peroxide and 70% isopropyl alcohol to promote hydrophilicity of the SiNx surface and discourage the attachment of air bubbles during fabrication. Air bubbles impede electrical current from freely passing from one side of the experimental chamber to the other. This poses issues in fabrication, as the leakage current through the membrane is suppressed and the experimenter cannot discern when a pore has actually formed, and also causes issues during experimentation as air bubbles within the pore nanocavity block the pore and do

not allow for free molecule translocation. Air bubbles in nanopore experiments should be prevented and avoided at all costs.

The experimental apparatus for the nanopore device consisted of the SiNx purchased from Norcada sandwiched in between two custom-made PMMA chambers. Each separate chamber holds about 200 μL of solution and has a small opening on its side. Upon pore formation, a complete channel is created that connects one chamber to the other. A schematic of our experimental setup is shown in Figure 1.

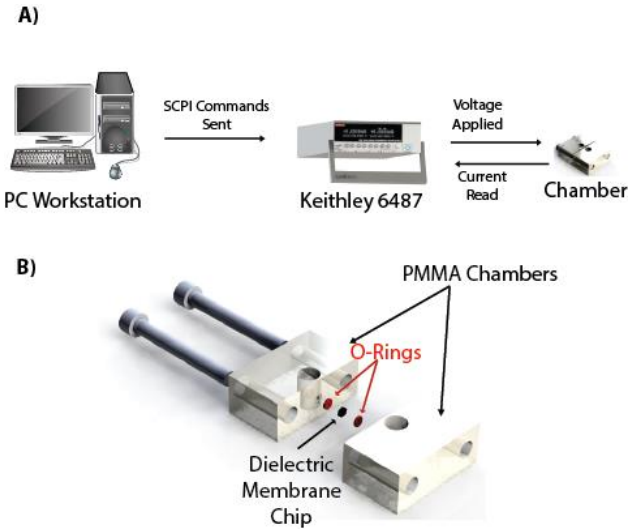

Figure 1. Schematic of Nanopore Experimental Setup. A) A Keithley 6487 Pico Ammeter/Voltage source applies a sustained high voltage electrical field across a dielectric membrane fastened in between our experimental chamber. The voltage source is controlled through a MATLAB script that is run through the PC workstation. As the voltage is being applied, the leakage current is measured simultaneously by the voltage source. B) Horizontal experimental chamber sandwiches a dielectric membrane in between two PMMA compartments tightened by screws. Two rubber O-rings are used to create an airtight seal. The openings in the O-rings create a nanotunnel that focuses the possible area of fabrication into a smaller region of the free-standing membrane.

Fabrication of nanopores in these experiments occurred exclusively through controlled dielectric breakdown. Controlled dielectric breakdown offers benefits to nanopore fabrication that include in situ fabrication and experimentation, a reduction of experimenter error in handling the delicate membrane, and a reduction in the overall instrumentation cost associated with the process. The principle of this method relies on applying sustained high voltage electrical field across an insulating dielectric membrane submerged in an ionic solution. Simultaneously, one must monitor the induced leakage current until a pore is formed. Biophysically, the applied electrical field causes ions in the buffer to move across the membrane. Here free electrons produced by redox reactions between the material surface and the surrounding ions in the solutions cause defects, known as traps, to migrate to a localized region in the conductive path thereby fatiguing it.[71, 79, 80] This allows ions to break across the compromised region of the dielectric material and leads to a distinct breakdown event until a pore spontaneously opens. The mechanism by which this occurs is a phenomenon typically observed in semiconducting capacitors and transistors called trap-assisted tunneling.[71, 79-84] A schematic diagram of the principles of the process is provided in Figure 2.

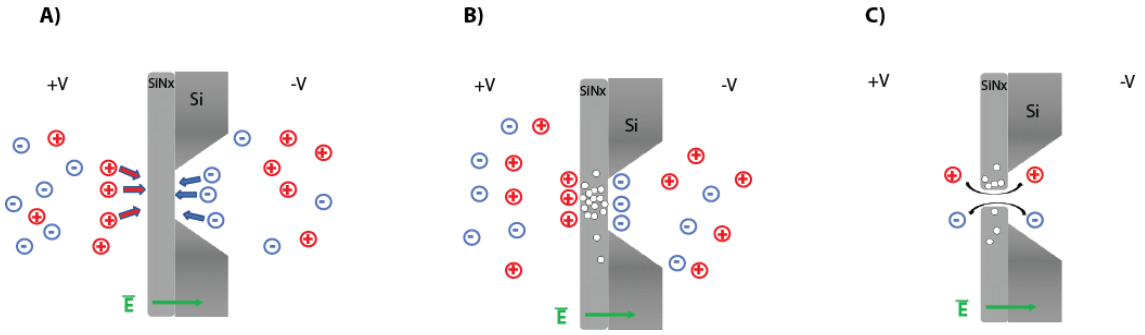

Figure 2. Schematic of SiNx Membrane Undergoing Controlled Dielectric Breakdown. A) The sustained applied voltage field causes a repulsion of the ionic species in the buffer and drives them towards the membrane surface. B) The surface of the membrane reacts with the ions in solution causing redox reactions that produce free electrons. These electrons cause material defects in the silicon known as "traps" to migrate towards the free-standing portion of the membrane device. C) The accumulation of traps creates localized regions of fatigued material that are susceptible to mechanical failure. Driven by the electrical field, the ions in solution can tunnel through the membrane at these localized regions and pass through, thus creating a cylindrical nanopore.

The transport of ions towards the dielectric membrane is shown in Figure 2A. Figure 2B shows the production of free electrons that promote the accumulation of traps on the free-standing membrane region. Figure 2C illustrates the ultimate formation of a cylindrical pore due to localized fatigue caused by the aggregation of traps and the continued flow of ions. A study reported in Kwok et al. found pore formation to be a function of applied voltage, membrane thickness, buffer composition and concentration, and pH.[71, 85, 86] By altering these parameters, the group was able to control pore size with sub-nanometer precision and control time to pore formation without the need of using TEM.[71]

Breakdown was performed in neutral pH ionic buffer solutions (pH 7.2) of either 1 M KCl (the gold standard experimental buffer) and 1 M LiCl. Both experimental solutions were buffered with 10 mM Tris and 1mM EDTA at pH 7.2. The buffer was filtered through a 25 mm PES filter with 0.2 μm pore and degassed to remove air bubbles

from the solution. The membranes were confirmed to have no defects prior to fabrication by observation of insulating behavior when exposed to a biased voltage field of 1 V using an Axopatch 200B current amplifier. Ag/AgCl electrodes were created by soldering silver wire to the ends of typical silicone encased copper wire and curing in a 1:10 dilution of sodium hypochlorite in water. These electrodes were submerged in both reservoirs of the chamber and a sustained voltage ranging from 7 V-9 V was applied across the membrane by a Keithley 6487 Picoammeter/Voltage Source. The Voltage source was controlled remotely through a MATLAB script that simultaneously applies a sustained electrical field across the membrane while measuring current passing through the dielectric membrane. Post fabrication modification included a series of 0-2 V square wave pulses for the refinement of the nanopore inner walls. Refined pores exhibited non-fluctuating baseline current levels when observed through our data acquisition board.

Because nanopore fabrication through dielectric breakdown creates a nanoscopic aperture in a membrane the size of 50 microns^2, it is nearly impossible to find the nanopore post fabrication for determination of size and for imaging. Fortunately, nanopore size was able to be estimated by using conductance measurements and comparing it to effective pore diameter with the assumption of a single cylindrical pore as was described in Kowalczyk et. al. and later used in Kwok et al.[71, 87-90] The exact relation used was $G = \sigma\left[\frac{4t}{\pi d^2} + \frac{1}{d}\right]^{-1}$, where G represents the average conductance of the pore in question, σ is the bulk conductivity of the buffer solution, t represents membrane thickness, and d denotes pore diameter. The relation assumes uniform decay at the initial breakdown point due to the infusion of electrons through the SiNx membrane creating a cylindrical geometry.[91, 92] As shown in previous studies, this relation yields a

reasonable approximation for pore diameter fabricated in solution.[88] Current-voltage (I-V) characteristic curves were recorded both immediately after fabrication and after soaking for a period of time in a 3.6 M LiCl stabilization buffer for all pores in this study.

DNA use for these experiments were 3 kbp NoLimits Individual dsDNA fragments were purchased from ThermoFisher Scientific. DNA was freeze-thawed and introduced into the cis chamber of the experimental apparatus in a final concentration of 10 nM prior to each experimental session after the nanopore was created and characterized. Filtered and degassed 1 M KCl, 1 M LiCl, and 3 M LiCl buffers were used for DNA experiments. Experiments were conducted by applying biased voltage of 200-600 mV in increments of 100 mV and acquiring data at each level for 5 minutes per individual run. During each run, data was acquired and recorded by an Axopatch 200B current amplifier and Digidata 1550B data acquisition board from Molecular Devices. Data acquisition was visually displayed in real time through Clampex data acquisition software. Data were low-pass filtered at 10kHz using the built in 8-pole Bessel filter, and recorded at 100 kHz sampling rates. Translocation events were analyzed using the Clampfit data analysis module and data for dwell time was fit with a single exponential curve. Event occurrence rate was determined by analyzing the time between a current blockage return to baseline and the next drop in current, an instance called a “level 0 event” where level 0 denotes the baseline current level. The reciprocal value these level 0 events were calculated to obtain the frequency of events. Just as with dwell time and frequency, current blockage amplitude was analyzed using Clampfit. The values of current blockages were obtained by fitting current blockage histogram with a Gaussian function.

3.3 Results and Discussion

3.3.1 Automated fabrication using MATLAB. MATLAB's instrument control toolbox was used to remotely control the picoammeter/voltage source. Communication occurred through a series of SCPI code that translated MATLAB commands to messages that could be understood and applied by the voltage source. Although the capability is available to apply voltage application and monitor current through MATLAB SCPI commands, the single channel connection between the instrument and the computer only allows one of these states, voltage application and current reading, to be altered at a time. Although this is an inconvenience, the initial MATLAB script was written in a way that would apply a voltage and then change the channel to monitor current while leaving the voltage channel unaltered. This work around momentarily addressed the issue but did not allow us to change the voltage once the script was initiated. As will be shown below, distinct current levels were determined empirically that when reached, the code would break and result in pores that were formed and of sizes that could be used for DNA experiments.

Prior to initializing the code, an undamaged SiNx was mounted into the experimental apparatus and fastened with screws. The membrane surface was hydrated with experimental buffer and visually inspected to check for air bubbles. When the code was started, an initial voltage of 1 V was applied and held for a short amount of time. If the membrane was intact, no initial distinguishable leakage current would be read by the instrument, indicating a membrane with no physical defects and no nanopore initially present. This is significant in order to have the most control possible surrounding nanopore size and shape. Once a membrane was determined to be intact by the code, a

preset higher voltage was then applied to cause the breakdown. A plot of the leakage current vs. time was plotted as this occurred and allowed the experimenter to track the evolution of the leakage current through the membrane. Throughout the active breakdown of the SiNx, two distinct regions were observed as shown in Figure 3.

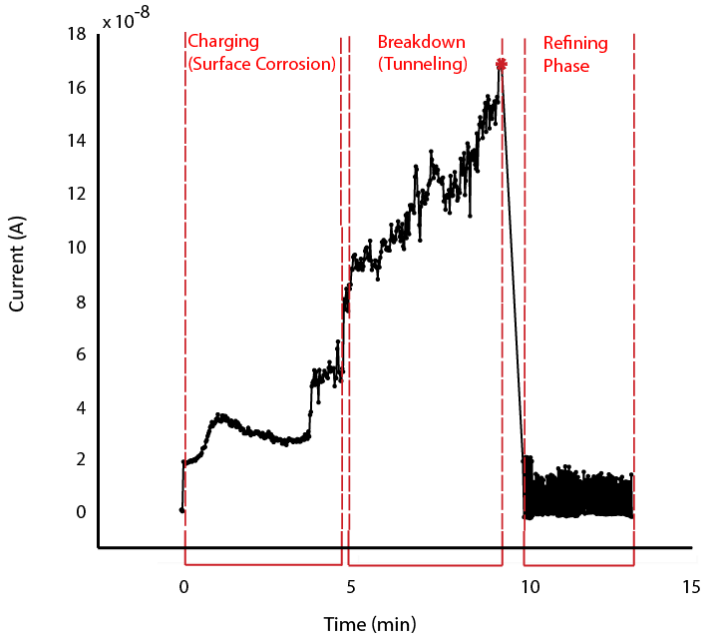

Figure 3. Sample Current Characteristic Trace of Controlled Dielectric Breakdown Session. Ionic current fluctuations are measured at a fixed applied voltage (8 V). Plot generated by the MATLAB script used for controlled dielectric used for controlled dielectric breakdown describes the mechanism by which the breakdown occurs and highlights two distinct regions that are indicative of the molecular interactions occurring at that time point. The current level at which the applied voltage was turned off is denoted by the red asterisk. At this point, preliminary characterization is performed by the code to ensure an irreversible leakage current, accounting for the lapse in time between the cutoff point and the subsequent drop off in current. The drop in current initiates a series of short electrical square wave pulses to refine the pore.

Although there were some differences from membrane to membrane, each current trace had the same general shape, which allowed us to make certain important inferences about what was going on during each region of the fabrication process. More examples of sample current traces generated by our MATLAB code can be found in Appendix A.

During the first of these regions, marked Charging (surface corrosion), breakdown is presumed to be driven by uniform surface charge corrosion slowly degrading the surface of the dielectric material by both the hydrolysis of the cation in solution and the migration of the chlorine.[93, 94] This correlates to the what was discussed in Figure 2A and Figure 2B. In the beginning of this time period, the membrane retains charge, somewhat like an electrical capacitor, which is denoted by the initial upward spike and slow plateau as the membrane becomes fully charged. This charging, caused by the induced electric field originating from the applied voltage, can also contribute to the effect of electroosmotic flow, which is likely to govern the flow of solution through the pore post fabrication and drive the passage of charged molecules, such as DNA, through the nanopore.[95-98] It is important to note that a nanopore is not yet present at this point. If the experimenter would remove the applied voltage, the entirety of the accumulated charge would dissipate and the measured leakage current after time would trend back down to zero. A nanopore is presumed to be formed once a sustained leakage and irreversible leakage current can be observed at lower applied voltage levels.[71]

The second region on the current characteristic plot shows a steady upward trend in leakage current after the plateau of the charging phase. This denotes the accumulation of traps at the localized breakdown region and the initial breakthrough of transporting ions across the membrane and coincides with what was discussed in Figure 2C. Although

a small irreversible leakage current is read at any point of this upward climb when the applied high voltage is removed, the inner pore conductance determined from the I-V relationship estimates that the pore size is too small. Even though technically a nanopore, the small pore would be unable to allow transport and detection of even the smallest single stranded DNA molecules. The inner conductance of the nanopore is related to the polarity and magnitude of the voltage applied.[99] This affects the electrical double layer with and electric field of greater magnitude ultimately being more capable of pulling cations through the pore and promoting flow.[99, 100] A further explanation for how conductance was used to determine pore size is provided in the following section. We found that stopping the applied voltage at various points of this breakdown region resulted in forming pores of varying size. This "cut-off current", denoted by the asterisk on the current characteristics plot, can be preset into the MATLAB script, so that the code automatically stops the applied voltage once the desired nanopore size is obtained.

The code then follows with a series of square wave pulses of 0.2-0.3 V per nanometer of thickness of the membrane as previously reported by Beamish et al. and Kwok et al.[29, 71, 86] The purpose of these pulses was to refine and stabilize the newly formed pore, resulting in a more stable open pore current level when compared to a pore that did not undergo the refining step. Although the pore is assumed to open as a smooth cylinder, the nature of the fabrication process lends itself to irregular pore shapes and even pore enlargement and shrinking if post treatment does not occur. Untreated pores after fabrication are also more prone to insertion of air bubbles. As can be seen in Figure 3 immediately, after the cutoff current and before the refining phase, there is a visible lapse of time on the current characteristic plot. During this time, the code performs a

preliminary I-V evaluation to determine if the observed spike in leakage current is irreversible. Over this ~1-minute period, the applied voltage goes down to zero to allow for any residual charge to dissipate from the SiNx membrane surface and nanopore inner channel. Thereafter, four separate current measurements are taken at 1 V applied and the refining phase commences only if the average of these measurements exceeds a preset accepted level that was determined empirically. More examples of this current trace for other pores are provided in Appendix A and illustrate the same trend in fabrication for nanopores drilled in KCl and LiCl experimental buffers.

To address one of the main concerns of nanopore fabrication, the need for extensive training in correct fabrication techniques, one of the goals for this experiment was to develop a user friendly interface that would lessen the learning curve needed to produce a solid-state nanopore for molecule detection. This was accomplished by using MATLAB's built in graphic user interface design tool called GUIDE. A screen shot of the final version of our GUI is shown in Figure 4.

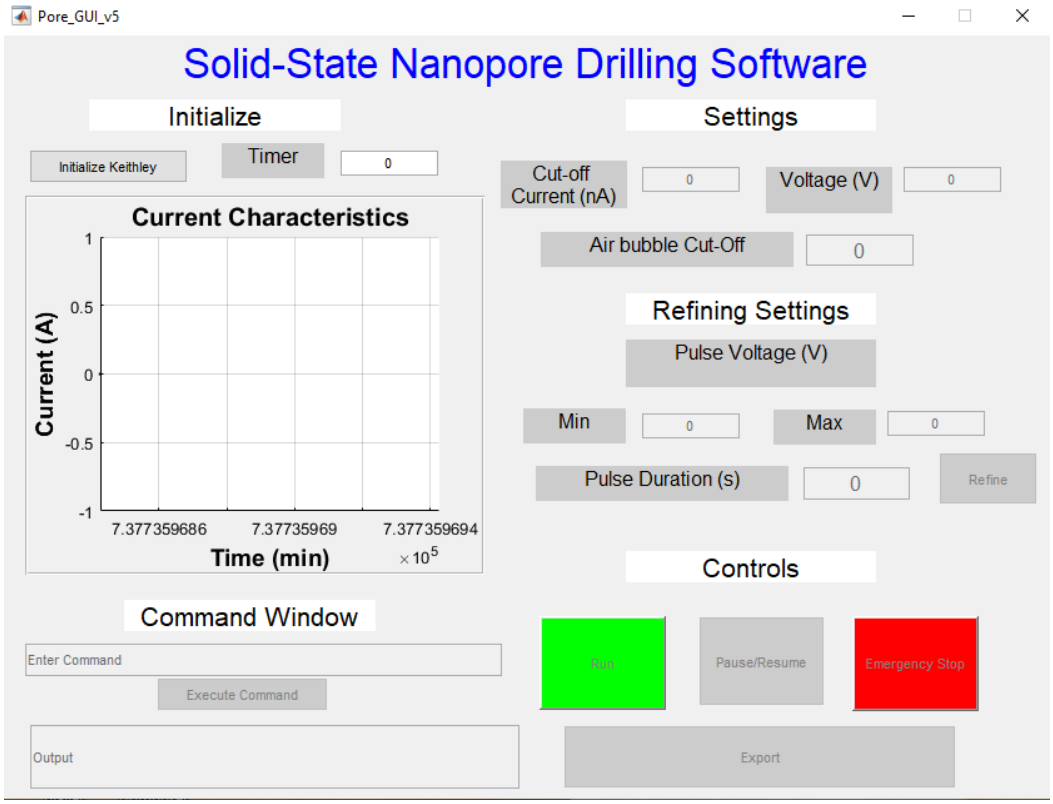

Figure 4. Solid-State Nanopore Fabrication Software User Interface. The entire right side of the application window is grayed out until the "Initialize Keithley" button is pressed and connection between the instrument and computer is determined

Not only does the graphic user interface allow for simple button presses to initiate the fabrication process instead of requiring knowledge in MATLAB coding to change settings and start the code, but it also allows for in process, real time adjustments to experimental parameters. This would prove to be useful in later experiments in different lots of SiNx membranes, who had slightly different material properties, and required some in run modification to achieve the same results. When the pore fabrication GUI application is started, the "initialize" button is pressed to connect the Keithley picoammeter/voltage source to the computer. Settings such as cut-off current levels and applied voltage can be preset, and the current trace can be monitored in the display

window. Voltage and cut-off current can also be adjusted mid run by changing the field and then pressing ENTER on the computer keyboard. This monetarily switches the channel form reading current to changing voltage on the instrument, and then subsequently switches it back so that the current plot may be updated. A minimum threshold can be set to stop the applied voltage when an air bubble is suspected. This allows the operator to check for and remove bubbles before continuing the breakdown experiment. There are fields where one can preset the voltage levels for refining pulses as well as the total duration of the pulses. The refining automatically starts after a pore is determined to be formed as previously described, but the GUI provides the added feature of allowing the refining to commence at any point in the process with just the push of a button. This is useful if the initial refining step did not suffice, or if the operator wanted to resize the pore manually without proceeding through an entire fabrication run. The "pause/resume" button brings the applied voltage to zero and halts the fabrication process, while the "emergency stop" button completely stops the code and closes the application. Upon completion of the fabrication run, the current plot and a summary log of all changes pre run and during the run are saved in a predetermined location on the user's computer. The user interface aimed to give the operator the most control possible, while still maintaining a "press and play" level of functionality and automation that makes the nanopore fabrication easy to perform. The full code used to run the nanopore fabrication software is provided in Appendix B.

3.3.2 Current/voltage relationship and pore size determination. While investigating the relationship between cutoff current and pore size, certain trends were observed as shown in Figure 5A. As the cutoff current increases for any amplitude of applied voltage during fabrication, the pore size subsequently increases as well. This trend is consistent between fabrication in both 1 M KCl and 1 M LiCl. A sustained electric field of 7 V tended to exhibit a less steep breakdown region than a sustained field of 8 V or 9 V, which consequently resulted in a less spontaneous nanopore formation and more precise control of the pore size. It should be noted that applied voltage levels below 7 V for fabrication either resulted in pores that never formed, or pores that took hours to form. This may allude to a minimum threshold voltage required for breakdown to occur. Conversely, applied voltage greater than 9 V resulted in erratic breakdown periods and was not controllable. All pores in this study were fabricated in a time range of 5 to 17 min, which is comparable to the time needed for a trained operator to create a nanopore with TEM drilling.

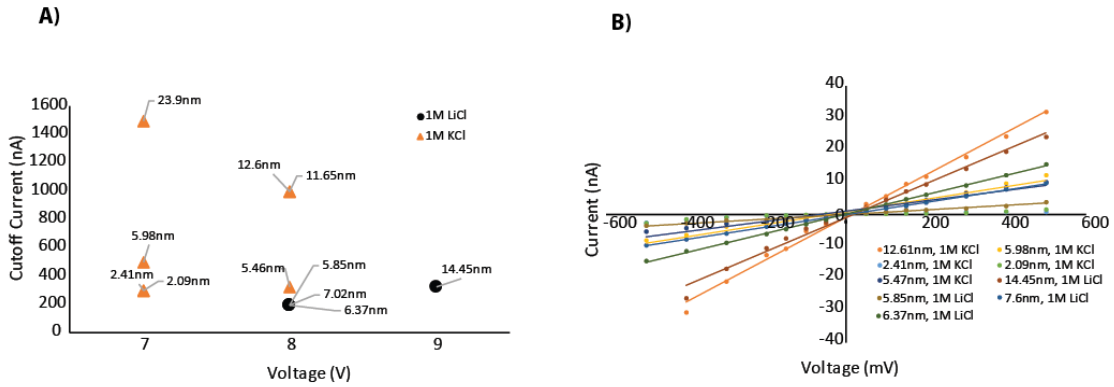

Figure 5. Nanopore Post Fabrication Characterization: Determination of Pore Size. A) Scatterplot of size of nanopores fabricated in LiCl and KCl with respect to the leakage current at which applied voltage was removed. B) A plot of Current vs. Applied Voltage was recorded for each of the nanopores fabricated in both 1 M KCl and 1 M LiCl buffer. The size of the pores was estimated using a relation between observed conductance to nanopore diameter. Symmetry about the origin and linear trendlines correlate to well-wet, cylindrical pores.

Experimental data has allowed us to develop various combinations of cutoff currents, applied voltage, and buffer conditions (salt concentration and salt type) that allow us to have precise control of our pore size. Control of pore size is crucial to have to ability to create pores small enough to detect single stranded DNA as well as pores large and robust enough to detect double stranded DNA. The ability to further tune the pore size up to ~10 nm in diameter allows for the detection of larger molecules such as DNA/antibody or DNA/protein complex as will be shown in later sections of this thesis.

An increase in pore stability and a minimal fluctuation in pore size has been demonstrated after soaking the pore in 3.6 M LiCl overnight and allowing it to equilibrate subsequently after fabrication in KCl buffer.[101] This was consistent with our findings when observing I-V curves immediately after fabrication in 1 M KCl and reexamining the I-V curve after soaking overnight in 3.6 M LiCl buffer. Although this proves it is possible to fabricate in one electrolyte and then replace the solution post fabrication, there

is an increased risk of contamination and damage to the membrane if the nanopore device is left out sitting for any extended amount of time. Furthermore, there lies the possibility of evaporation of the buffer and crystallization of the salt within the buffer, which also damages the pore. The benefits of creating a nanopore in a single buffer and performing experiments *in-situ* are paramount as there is significant reduction in associated risks and allows for experimentation on the same day as the nanopore is created, resulting in greater efficiency.

When fabricated directly in 1 M LiCl buffer instead of being fabricated in KCl and then switched over to LiCl, pores initially exhibited very favorable I-V relationships immediately after fabrication as shown in Appendix C. These pores displayed no significant improvement in linearity after only 1 hour of soaking in the same 1 M LiCl buffer in which it was drilled as shown in Figure 6 (Left).

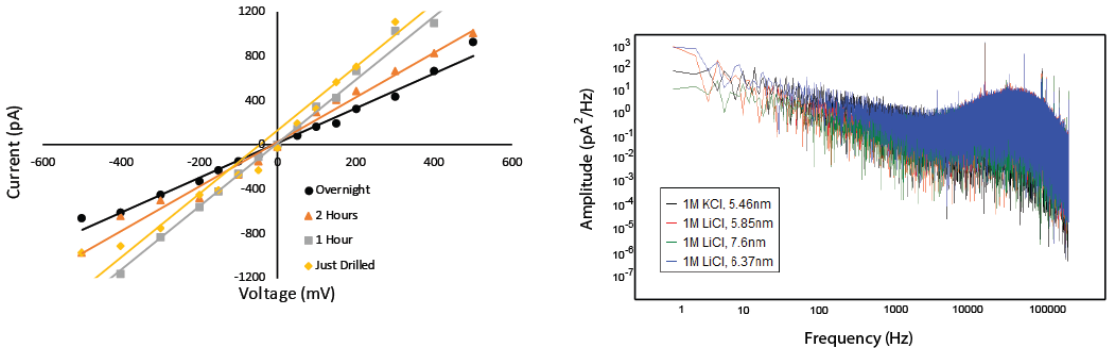

Figure 6. Nanopore Post Fabrication Characterization: Pore Hydration and Noise. (Left) A nanopore was fabricated via controlled dielectric breakdown in 1 M LiCl buffer and an IV curve was taken just after fabrication, after 1 hours of soaking in the 1 M LiCl fabrication solution, after 2 hours of soaking in 1M LiCl fabrication solution, and after soaking in 1 M LiCl fabrication solution overnight. The plots show an improvement in the linearity of the I-V relation after just 1 hour of stabilization in its own fabrication buffer and a significant improvement after 2 hours. A linear, symmetric I-V relationship implies a well-wet inner pore structure that promotes biomolecule transport. (Right) 1/f noise was characterized by recording current fluctuations at constant voltage levels of 0 mV, 100 mV, and 200 mV. The trace was acquired using an Axopatch 200B current amplifier with sampling rate set to 500 kHz and Bessel filtering set to 100 kHz. A representative example of noise characterization recorded at 200 mV for four separate nanopores is provided.

Pores in this study that were fabricated directly in LiCl buffer yielded I-V relationships consistent with fully wet, stable nanopores in a far shorter amount of time than pores fabricated in KCl and transferred to a LiCl stabilization buffer. A similar method of fabrication has yielded success with even higher concentrations of LiCl (3.6 M).[102] Nanopores drilled in 1 M LiCl buffer via controlled dielectric break displayed similar trends in nanopore size in relation to cutoff current as seen in pores drilled in KCl with the same sub-nanometer control of pore size as shown in Figure 5A. This suggests that drilling in LiCl can offer the same experimental control during fabrication with the added benefit of being able to run DNA experiments after only an hour of fabrication. Further characterization of our pores can be seen in Figure 6 (Right) included power

spectral density measurements that revealed good 1/f noise levels that are consistent with well wet pores.

3.3.3 DNA experiments with naked dsDNA. The detection of dsDNA was performed using 4 separate nanopores in 10nm thick SiNx fabricated via controlled dielectric breakdown under different experimental conditions to display a broad range of testing scenarios. 3 kbp dsDNA was introduced to the cis chamber of the experimental apparatus and detected using: a 1) ~5.47 nm pore in 1 M KCl, 2) ~5.85 nm pore in 1 M LiCl, 3) ~7.6 nm pore in 1 M LiCl, and 4) ~6.37 nm pore in 3 M LiCl. A sample of the raw data traces for a representative experimental condition of 300mV applied biased voltage is shown in Figure 7A.

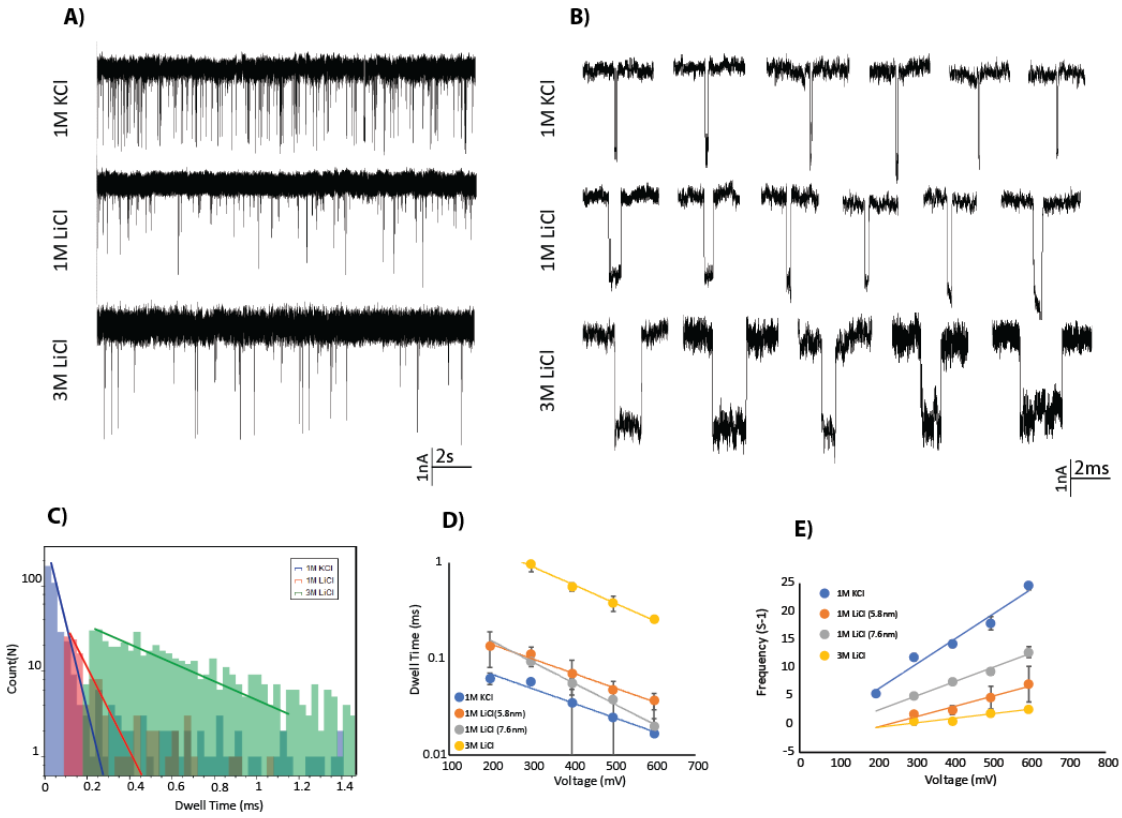

Figure 7. Analysis of DNA Translocation Experiments in Symmetric KCl and LiCl. A) Representative data traces are presented for experiments run in 1 M KCl (top), 1 M LiCl (middle) and 3 M LiCl (bottom) at an applied biased voltage of 300 mV. 10 nM 3 kbps dsDNA was inserted into the cis chamber and DNA translocation events were recorded for multiple runs at a range of 200 mV-600 mV. B) Zoomed in view of individual DNA translocation events in 1 M KCl (top), 1M LiCl (middle), and 3 M LiCl (bottom) at 300mV. C) Histogram of dwell time for 1 M KCl, 1 M LiCl, and 3 M LiCl at 300 mV. The data was presented on a linear-log scale and fit with an exponential decay function. D) graphical representation of average dwell time for each experimental condition. E) Graphical representation of the event frequency for each experimental condition.

The top data trace in this section shows dsDNA translocation events in 1 M KCl, the middle trace for 1 M LiCl, and the bottom trace for 3 M LiCl. From the traces, one can see a decrease in event frequency when using LiCl buffers as opposed to KCl. One can also see the display of events of different amplitudes in the data traces for experiments run in LiCl buffer. This can be attributed to bumping events which can mean

inefficient capture of DNA molecules through the pore. This can also explain the drop in the event frequency. Figure 7B shows zoomed-in individual sample DNA transport events in each salt solution and illustrates the effect of each salt type and concentration on the molecule residence time within the pore. Prolonged events are shown in LiCl when compared to KCl and even longer events are shown at increased LiCl molarity. A histogram for the average dwell time values of the representative condition of 300 mV applied biased voltage is shown in Figure 7C and shows a decreased slope of the fitting line as well as a shift of the fitting line in the positive x direction as you go from 1 M KCl to 1 M LiCl and then to 3 M LiCl. As expected, dwell time was shown to decrease with an increase of the applied voltage as shown in Figure 7D. The general trend agreed with previous findings and showed that DNA experiments run through pores in LiCl chloride produced longer dwell times than pores in KCl. A summary of the mean dwell times for each condition is provided in Table 1.

Table 1

Translocation Event Dwell Time for Pores in KCl and LiCl Buffers

Condition	**Est. Pore Size (nm)**	τ_{200mV} **(ms)**	τ_{300mV} **(ms)**	τ_{400mV} **(ms)**	τ_{500mV} **(ms)**	τ_{600mV} **(ms)**
1M KCl	5.47	0.063 $\pm$ 0.009	0.058 $\pm$ 0.003	0.035 $\pm$ 0.028	0.025 $\pm$ 0.02	0.0169 $\pm$ 0.022
1M LiCl	5.85	0.136 $\pm$ 0.054	0.113 $\pm$ 0.02	0.07 $\pm$ 0.028	0.048 $\pm$ 0.011	0.037 $\pm$ 0.007
1M LiCl	7.6		0.094 $\pm$ 0.01	0.0555 $\pm$ 0.007	0.038 $\pm$ 0.001	0.02 $\pm$ 0.004
3M LiCl	6.37		0.97 $\pm$ 0.16	0.56 $\pm$ 0.05	0.38 $\pm$ 0.07	0.26 $\pm$ 0.02

A similarly sized nanopore tested in 1 M LiCl showed the same trend in decline of dwell time when increasing the biased voltage amplitude. However, the pore under these conditions displayed about a 2-fold increase in dwell time of dsDNA molecules when compared to the pore tested in KCl. The increase in dwell time can be seen in Figure 7B as the length of the drop in current from the baseline current level is longer in 1 M LiCl were compared to 1 M KCl and in 3 M LiCl when compared to 1 M LiCl. When increasing the salt concentration to 3 M LiCl, about an 8-fold increase in dwell time was observed for applied voltage levels of 300 mV, 400 mV, and 500 mv when compared to experiments run in 1 M LiCl as shown in Table 1. At 600mV, a slightly less drastic 7-fold increase in dwell time was observed. This data well agrees with previous findings. [76] The increase in salt concentration creates an environment with more available cations to bind to the DNA molecule, thereby reducing the effective charge of

the DNA and making it move slower without interreacting with the pore walls. Similar results have been reported for single stranded DNA.[76]

As shown in Figure 7E, the experiment conducted in 1 M KCl produced more frequent events in general than experiments conducted in similar sized pores in 1 M LiCl. It is important to note that for experiments in KCl, it is not uncommon to see upwards of tens of thousands of events per applied voltage level and concentration. These events often vary slightly in blockage amplitude as DNA molecules sometimes compact to form knots.[78] For this study, events with deeper current blockages were utilized for consistency. When changing the experimental buffer to 1M LiCl, a reduction in event occurrence frequency is observed. This reduction can also be attributed to DNA-cation interactions. The high affinity of lithium ions to the DNA backbone induces a lower net charge when compared to potassium ions. The binding of Lithium ions causes lower DNA mobility. This phenomenon decreases the perceived “capture radius” of the nanopore, reducing the probability of DNA capture and obstructing DNA from threading efficiently. The capture radius represents the distance at which the DNA is irreversibly captured by the electrical field of the nanopore and transported through the pore. [103-106] For example, measured capture radius for nanopores in standard 1M KCl and 2M LiCl buffer have been shown to have a capture range of 150 nm and 1000 nm respectively.[69] Upon increasing the concentration of LiCl to 3 M, the event occurrence further decreased dramatically. [76, 107, 108]. A summary of the event occurrence frequencies for the various experimental conditions is provided in Table 2.

Table 2

Translocation Event Occurrence Frequency for Pores in KCl and LiCl Buffers

Condition	**Est. Pore Size (nm)**	τ_{200mV} **(s^{-1})**	τ_{300mV} **(s^{-1})**	τ_{400mV} **(s^{-1})**	τ_{500mV} **(s^{-1})**	τ_{600mV} **(s^{-1})**
1M KCl	5.47	5.544 ± 0.28	11.892 ± 0.61	14.345 ± 0.63	17.93 ± 1.16	24.716 ± 0.82
1M LiCl	5.85		1.861 ± 0.42	2.48 ± 0.77	4.756 ± 2.04	7.161 ± 3.17
1M LiCl	7.6		5.066 ± 0.31	7.578 ± 0.37	9.421 ± 0.63	12.802 ± 0.95
3M LiCl	6.37		0.532 ± 0.04	0.592 ± 0.06	2.00 ± 0.16	2.675 ± 0.11

Consequently, DNA transport event occurrence was seen to not only be salt type dependent, but also salt concentration dependent. The increase in concentration of LiCl from 1 M to 3 M further decreases DNA mobility and effective charge and thereby explains the additional drop in event frequency.

A general trend of increased blockage amplitude was observed as the applied biased voltage was increased as shown in Figure 8.

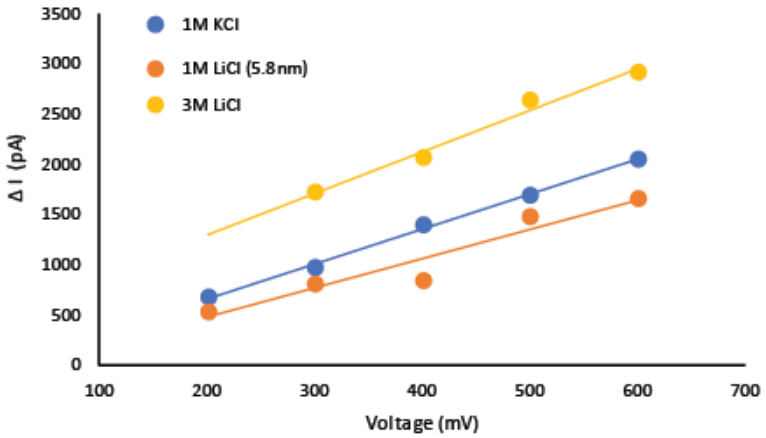

Figure 8. Current Blockage Amplitude of DNA Transport in Symmetric KCl and LiCl. Experiments were carried out in 1 M KCl, 1 M LiCl, and 3 M LiCl at applied biased voltages ranging from 200 mV-600 mV. A general trend of increased blockage amplitude is observed as applied voltage increased. A deeper blockage was also observed in the experiment run in 1 M KCl when compared to a pore of comparable size in 1 M LiCl.

Interestingly, a similar sized pore tested in 1 M LiCl displayed smaller current blockage amplitudes than the one in 1 M KCl at the same applied voltages. This can possibly be explained by the lower conductivity of lithium ions in solution in relation to potassium. [109, 110] Lithium ions' smaller size in comparison to potassium increases its resistivity, inherently decreasing its mobility in solution, which in turn influences conductivity.[111] Conductivity of solution has been shown to positively correlate to blockage amplitude.[112] Additionally, varying the concentration of salt within the same salt species effects blockage amplitude. [112] This was confirmed as the pore tested in 3 M LiCl exhibited about a 2-fold increase in current blockage amplitude when compared to the pore of similar size (<1 nm difference) measured in 1 M LiCl. A summary of the current blockage amplitudes for each condition is given in Table 3.

Table 3

Translocation Event Current Blockage Amplitude for Pores in KCl and LiCl Buffers

Conditions	**Est. Pore Size (nm)**	τ_{200mV} **(pA)**	τ_{300mV} **(pA)**	τ_{400mV} **(pA)**	τ_{500mV} **(pA)**	τ_{600mV} **(pA)**
1M KCl	5.47	677.053 ± 1.54	973.425 ± 1.6	1398.65 ± 6.03	1692.45 ± 5.72	2048.18 ± 3.19
1M LiCl	5.85	541.93 ± 3.17	821.89 ± 8.01	842.838 ± 4.83	1480.97 ± 1.17	1661.6 ± 7.06
1M LiCl	7.6		1059.4 ± 194	1500.05 ± 0.98	1737.19 ± 2.53	2214.78 ± 3.10
3M LiCl	6.37		1733.96 ± 0.9	2067.64 ± 12.51	2640.22 ± 14.13	2922.56 ± 6.11

3.4 Conclusion

This chapter aimed to explore alternatives to traditional solid-state nanopore fabrication methods, including the use of different and less expensive fabrication instruments and alternate experimental conditions to increase experimental efficiency and increase signal resolution for better results. Controlled dielectric breakdown was used to fabricate all nanopores in this study. A functional MATLAB code was written to control all aspects of the fabrication process and allowed us to achieve sub-nanometer precision when using the fabrication settings that were determined through experimentation within the lot of SiNx membranes we used. It was later found, however, that when purchasing a new lot for subsequent experiments, the material properties of the SiNx differed enough that it created different current characteristic trends and different responses to the applied voltage level. The membranes within this new lot did have consistent behavior and after minor adjustments to the fabrication settings, were also able to reliably produce

nanopores of usable size. Nonetheless, our study concluded that controlled dielectric breakdown can be performed in various ionic buffer solutions, with fabrication in lithium chloride resulting in a better wet pore that is stable and ready to undergo DNA experiments within 1 hour. This allows researchers to test their analytes very shortly after fabrication, thereby increasing experimental efficiency.

Although the DNA experiments run in LiCl displayed an overall increase in dwell time, the trend of decreased dwell time in response to increased applied voltage was consistent among all pores. This is significant because the increase in voltage also correlates to an increase in event amplitude and frequency, which are traits that are desired for characterization of analytes. A way to increase dwell time without compromising the event frequency and current blockage amplitude is desired to move forward towards the practical implementation of nanopore biosensors.

The following chapter builds on these experiments and explores the use of a salt gradient to help counteract the negative effects of the LiCl concentration on the frequency of transport events shown. Frequent events are necessary to build statistical significance and reliability for biosensor devices. Asymmetric concentration of buffer between the *cis* and *trans* chambers has been shown to increase capture affinity of solid-state nanopores as well as increase dwell time.[107]

Chapter 4

Optimization of Experimental Conditions to Slow DNA Transport Through Solid-State Nanopores[2]

4.1 Background

The major challenge facing nanopore technology for single molecule detection is the intrinsically fast DNA translocation velocities.[1, 3, 113] In order to enhance the practicality of solid-state nanopores as a biosensor, it is necessary to impede translocation velocity enough so that individual nucleotides can be fully examined and characterized. As shown previously, ionic solution comprised of lithium chloride (LiCl) significantly decreased translocation velocities of DNA transport through solid-state nanopores.[76] In the presence of monovalent cations in solution, such as K^+, Na^+, and Li^+, the cations covalently interact with the negatively charged phosphate backbone. The ions aggregate on the DNA and increase the molecular weight of the complex. In addition, the partial negative charge of the DNA backbone is slightly reduced, thus decreasing the mobility tendency of the complex as it attempts to move in solution.[76, 77, 114] When compared to more commonly used salts, such as KCl, LiCl electrolyte solution has been shown to have a greater binding affinity to dsDNA and thereby reduce velocity of DNA translocation by up to 10-fold.[76, 77] However, previous studies have shown a lack of DNA translocation occurrence when using LiCl electrolyte solutions in exchange for the reduction of DNA velocity.[115]The frequency of observable translocation events was shown to decrease at low applied biased voltages such as 200 mV as well as increased

[2] Adapted, with permission, from J. Bello, 2018, "Increased Dwell Time and Occurrence of dsDNA Translocation Events Through Solid-state Nanopores by LiCl Concentration Gradients," *ELECTROPHORESIS*, 40: 1082-1090.

concentrations of LiCl (3 M). Unfortunately, increasing the experimental voltage in hopes of increasing transport events correlates to increased transport speed, which reduces detectability and signal resolution. The same can be said about lowering the concentration of the salt in the buffer.

Sufficient DNA translocation events are as crucial to nanopores as diagnostic devices as the resolution of the transport events we observe. Amassing tens of thousands of transport events aids in developing significance in the data and reliability in the assay, especially because nanopore data is assessed as trends and distributions instead of singular occurrences. Therefore, a need was present for a method to increase the event occurrence while still maintaining the prolonged dwell times that have been observed in experiments with LiCl.

DNA translocation speeds have been shown to be adjustable through the use of varying salt concentrations on both the cis and trans experimental compartments.[107] The interionic effects of cations in solution, which occur when ions are submerged in an ionic space with a net charge opposite of the ion's charge, have been found to increase at higher concentrations, thereby increasing the resistivity of the ionic solution.[73, 116] The result is a drag force with a magnitude proportional to the concentration of the ionic solution. A weak electrolyte solution generally promotes weak effects whereas a strong electrolyte solution promotes strong effects. In the cis chamber, NDA can freely move, but upon saturation with counterions in the trans chamber, the net charge on the DNA molecule will be decreased and therefore the speed of transport will be altered.

Transport is also influenced by forces near the wall of the channel. At this interface, the ion distribution is strongly influenced by the size of the ions and shear

viscosity.[117] Shear stress can be related to strain with a linear consecutive relationship. Consequently, the shear viscosity near the nanopore wall dramatically increases with the concentration of salt as well as what type of salt, which will leads to slower translocation times.[117] A study reported in Wanunu et al. showed that salt gradients on either end of the nanopore can also increase nanopore sensitivity and mean translocation time of DNA transport.[24, 107] The use of asymmetric salt conditions allowed for positive K^+ ions to be pushed in the trans-to-cis direction more efficiently than negatively charged Cl^- ions moving in the opposite direction.[107] To build on previous success with LiCl, our approach was to take these principles and apply them to our system to see what kind of results would be observed.

A salt concentration gradient of KCl on either side of the nanopore has also been shown by Wanunu to increase the capture rate of DNA.[107, 118] Regarding event occurrence, KCl has been shown to yield more frequent DNA translocation events than LiCl at the same applied voltage. This can be attributed a higher capture range for dsDNA in KCl than in LiCl, a direct result of higher DNA mobility for KCl than in LiCl.[76, 108] This DNA itself "capture" follows a set of chronological steps including the coiling of the polymer, diffusive motion, and capture once the DNA reaches a critical distance.[76, 103, 107] The capture range represents the distance at which the DNA is irreversibly ensnared by the electrical field produced by the applied voltage and near the nanopore opening.[103-106] Nanopores in 2 M LiCl and 1 M KCl have been shown to have a capture range for dsDNA of 150 nm and 1000 nm respectively.[69] The DNA molecules in LiCl buffer experience random drift due to diffusive forces being greater than the DNA molecules in KCl.[103, 104] Because of this, not only is the capture range

a great deal shorter in LiCl than KCl, but the DNA in LiCl buffer takes longer to reach the capture range as well.

One possible explanation to the capture range in LiCl being shorter than KCl is because Li^+ has a higher binding affinity to DNA than K^+.[76] On average, the amount of time that lithium ions remain bound to DNA in a 4 M LiCl system is 50 ps. In a 4 M KCl system, potassium ions bind for an average of only 10 ps.[76] DNA in KCl experience less hydrostatic drag because it has fewer ions bound to the molecule. Because of this, the DNA in KCl have a higher velocity, and a larger capture range. The Li^+ ion, on the other hand, has to overcome higher hydrostatic drag and needs a high electrical field to remove the Li^+ compared to K^+.[104-106] This is beneficial when slowing down translocations, but it also decreases the incidence of biomolecule translocation through the pore and the efficacy of using this salt for biosensing applications.

Creating a salt gradient for experimentation could bypass the shortcomings of the LiCl buffer. A lower concentration of salt in the cis reservoir increases the electric field and capture propensity within the pore without shortening mean translocation times.[107] In the following sections, experiments with varying degrees of salt gradients will be shown in an investigation of the effects of an asymmetric concentration gradient of LiCl on dsDNA transport. This is performed in hopes of increasing event occurrence and slowing down DNA transport through a solid-state nanopore.

4.2 Materials and Methods

Nanopores in this study were fabricated on 10-nm-thick SiN_x membranes deposited on a 200 μm SiO_2 substrate with a 0.05 x 0.05 mm window purchased from Norcada (Alberta, Canada). Fabrication was accomplished through controlled dielectric

breakdown in symmetric 1 M LiCl buffer and by using the MATLAB base fabrication software discussed in the previous chapter. Although the experiments in this section are dealing with asymmetric salt gradients, the fabrication still occurs in symmetric buffer in order to maintain the control of pore size. Pore size was determined using the conductance model used to determine pore size was $G = \sigma\left[\frac{4t}{\pi d^2} + \frac{1}{d}\right]^{-1}$, where G represents the average conductance of the pore, σ is the conductivity of the ionic solution, t represents membrane thickness, and d denotes pore diameter.[88] Following fabrication, refining through the code, and pore size determination, the media on the cis and trans chambers was carefully exchanged in order to create the experimental conditions. The pore was subsequently characterized once more to study the changes in the leakage current when submerged different buffer environments.

For the asymmetric salt experiments, filtered and degassed 0.5 M LiCl, 1 M LiCl, 1.5 M LiCl, and 3 M LiCl solutions were made and buffered with 10 mM Tris, 1 mM EDTA, and titrated to pH 7.2. Concentration gradients of 0.5 M cis/3 M trans, 1 M cis/3 M trans, and 1.5 M cis/3 M trans were used for the asymmetric experiments with DNA. 3 kbps dsDNA were purchased from ThermoFisher Scientific was added to the cis side of the experimental apparatus with a final concentration of 10 nM. Experiments were conducted by applying biased voltage of 200-600 mV in increments of 100 mV and acquiring data at each level for 5 minutes per individual run. One occurrence that was often encountered throughout the asymmetric salt experiments with DNA was a constant "dewetting" of the pore, where the signal appeared to indicate an air bubble had inserted itself into the pore. For these instances, the pore was "electrowet" using cyclic voltage

pulsations ramping from -1 V to 1 V applied by the voltage amplifier. This temporarily increased the hydrophilicity of the membrane. Once the blockage was removed, DNA translocation was restored, and the experiment was continued. Electrowetting and the theory behind dewetting will be discussed in the coming sections.

For all experiments, an Axopatch 200B Amplifier with a built in 8-pole Bessel filter and Digidata 1550B from Molecular Devices were used to record data for their high quality, good signal-to-noise ratio single channel measurements. Data was recorded using the Clampex software at a 100 kHz sampling rate and a lowpass Bessel filter of 10 kHz and data was analyzed in the same manner as the previous chapter.

4.3 Results and Discussion

4.3.1 Increased event occurrence frequency by application of a LiCl gradient.

The previous chapter showed the efficacy of LiCl buffer in increasing dwell time of the dsDNA molecule within the nanopore.[115] This is especially apparent in high concentrations of LiCl, such as 3 M. However, the frequency of event occurrence for these experiments was very low and required multiple data acquisition sessions to obtain sufficient data points. At lower voltages, such as 100 mV to 200 mV and with the same concentration of DNA as shown in other successful experiments (10 nM), DNA translocation events are not detectable as shown in Figure 9. To improve on this and increase the overall practicality of this biosensing device, experiments were conducted with asymmetric salt concentration on either side of the nanopore.

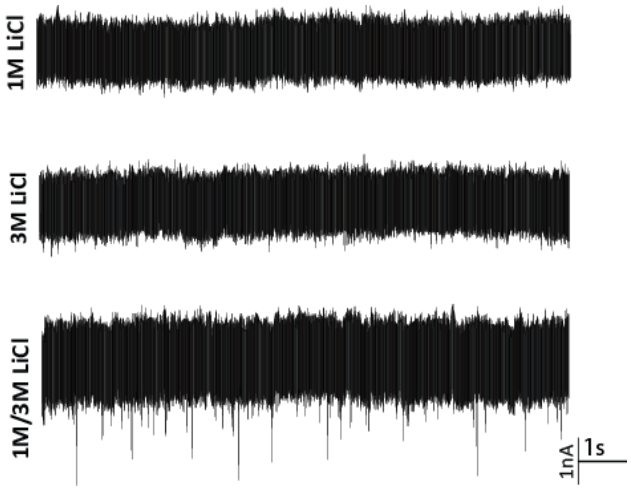

Figure 9. Sample Data Traces of dsDNA Translocation Performed at Low Biased Voltages. 3 kbps dsDNA was inserted into the cis experimental chamber at a concentration of 10 nM (the same concentration used for all other experimental conditions), a voltage was applied, and the sessions were recorded to capture any possible DNA translocation events. In 1 M LiCl, at 150 mV, no DNA translocation events were observed. No events were observed either in 3 M LiCl at a biased voltage level of 150 mV. Interestingly, when recording in asymmetric 1 M/3 M LiCl and maintaining the DNA concentration constant, some DNA transport was observed.

For this study, long dsDNA was inserted into the cis chamber of the experimental apparatus in which a LiCl concentration gradient was applied with the lower concentration of salt being used in cis and the larger concentration used in trans as shown in Figure 10A.

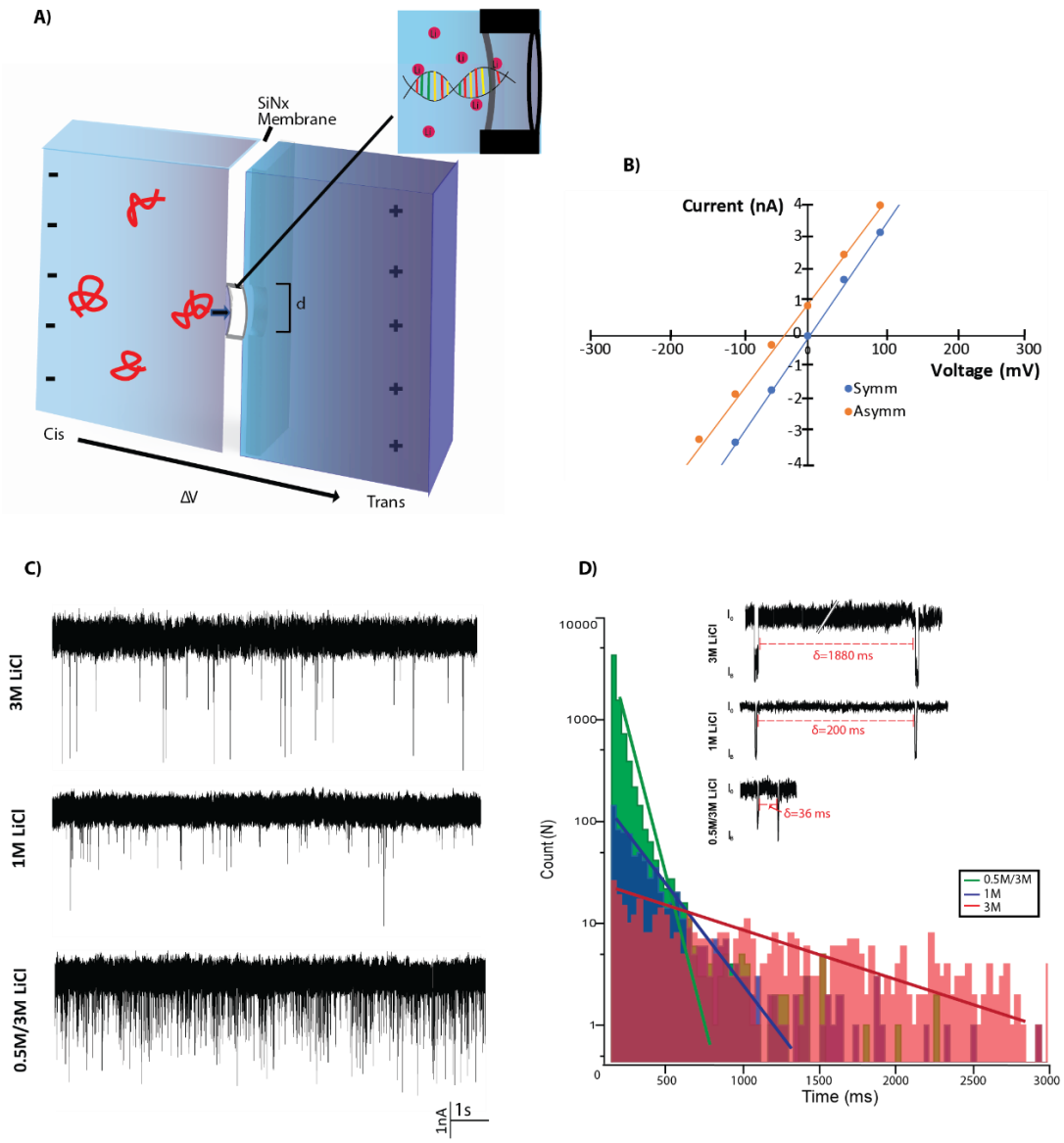

Figure 10. Overview of the dsDNA translocation Experiments in LiCl Salt Gradients. A) Schematic representation of the experimental conditions. Lower concentration of LiCl is denoted by the lighter blue in the cis chamber. The higher concentration is denoted by the darker blue in the trans chamber. dsDNA is shown in the cis chamber and transporting through the nanopore with Li^+ ions attached to the backbone (inset). B) I-V relationship of a 5.0 nm nanopore in both symmetric 1 M LiCl and asymmetric 1 M/3 M LiCl is plotted. Characteristic offset in I-V relationship of a pore in asymmetric salt conditions due to ion flow down the salt gradient is shown. The curve maintains linearity and is parallel to the I-V relationship in symmetric conditions. C) Representative data trace samples of dsDNA translocation event occurrences recorded at 300 mV in 5.8 nm and 6.4 nm pores in symmetric 1 M LiCl and 3 M LiCl respectively as well as a 10.9 nm pore in asymmetric 0.5 M/3 M LiCl. An increase in event frequency is observed. D) Histogram created by fitting the data for I_0 duration for the 0.5 M/3 M LiCl, 1 M LiCl, and 3 M LiCl conditions with an exponential decay function.

Interestingly, when obtaining an I-V relationship from nanopores in asymmetric buffer, the curve was often found to be parallel to the I-V curve from the same pore in symmetric conditions (1M/1M LiCl), but with a marginal offset. This occurrence is shown in Figure 10B for a 5.0 nm pore in a 1 M/3 M (cis/trans) salt gradient. This can be explained by an imbalance in the equilibrium of ions in the two chambers. Upon introducing an asymmetric salt gradient, there is automatically ion flow because of the tendency of ions to move down their concentration gradient. This explains why there is current reading even with 0 V applied. Other examples of this offset are found in Appendix D with only one exception in which a linear behavior was retained, but the slope of the I-V curve was steeper for the asymmetric condition. Although inexplicable, a possible explanation for this could be a pore that was not fully wet at the time of characterization.

For the study, a 5.0 nm pore was used with a concentration gradient of 1 M/3 M LiCl (cis/trans), a 6.0 nm pore was used with a gradient of 1.5 M/3 M LiCl, and a 10.9 nm pore was used with a gradient of 0.5 M/3 M. Nanopores of 5.8 nm and 6.4 nm in symmetric 1 M LiCl and 3 M LiCl respectively were used as controls to compare the change in event occurrence frequency. Qualitatively, the application of salt gradients increased mean translocation event occurrence when compared to the 1 M LiCl and 3 M LiCl controls that were tested in symmetric experimental conditions as seen in Figure 10C. Events were found to occur about 5-times more frequently in 0.5 M/3 M LiCl than in 1 M LiCl and over 50-times more frequently than in 3 M LiCl as shown in Figure 10D. The increase in event occurrence frequency was quantified by analyzing the duration of I_0 (open pore current baseline) between transport events and fitting this data with an

exponential decay function. The frequency was obtained by applying the reciprocal of the mean I_0 durations, the time in between the conclusion of one event and the start of the next, for each experiment. The difference in time between observed events in provided for symmetric 1 M LiCl, 3 M LiCl and for 0.5 M/3 M LiCl in the inset of Figure 10D. The time between events is reduced by about 5-fold in the asymmetric conditions. The comparison of event frequencies among each condition is plotted in Figure 11.

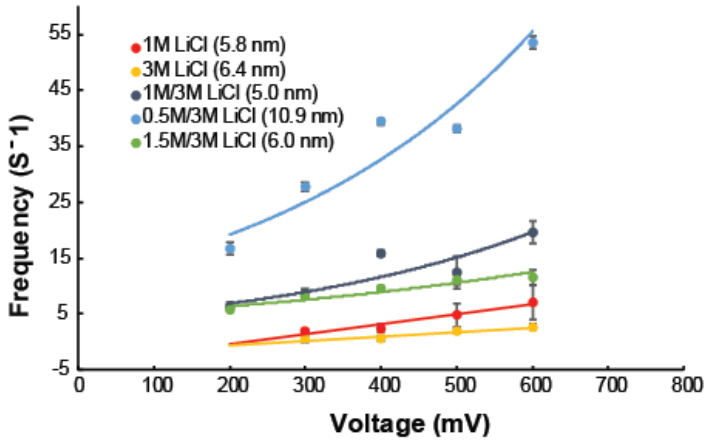

Figure 11. Event Occurrence Frequencies of dsDNA Translocations in LiCl Gradients. Experiments run in symmetric 1 M LiCl and 3 M LiCl and asymmetric 1.5 M/3 M LiCl, 1 M/3 M LiCl, and 0.5 M/3 M LiCl are provided for comparison. Data was recorded at biased voltage levels of 200 mV, 300 mV, 400 mV, 500 mV, 600 mV. An overall increase in event occurrence is observed for experiments run in asymmetric LiCl conditions as opposed to symmetric LiCl.

As shown, all nanopores exhibited the same trend of increasing transport events with increasing applied voltage. Each experiment performed in asymmetric conditions yielded more frequent events than the controls. 0.5 M/3 M LiCl had the highest occurrence rate of dsDNA translocations at $27.78 \pm 0.69\ s^{-1}$ at 300 mV. A summary of

all the event frequencies for every condition at applied biased voltages of 200 mV, 300 mV, 400 mV, 500 mV, and 600 mV are provided in Table 4.

Table 4

Translocation Event Occurrence Frequency in LiCl Gradients

Condition	**Est. Pore Size (nm)**	f_{200mV} (s^{-1})	f_{300mV} (s^{-1})	f_{400mV} (s^{-1})	f_{500mV} (s^{-1})	f_{600mV} (s^{-1})
1 M LiCl	5.8		1.86 $\pm$ 0.42	2.48 $\pm$ 0.77	4.75 $\pm$ 2.00	7.16 $\pm$ 3.20
3 M LiCl	6.4		0.53 $\pm$ 0.04	0.59 $\pm$ 0.05	2.0 $\pm$ 0.16	2.67 $\pm$ 0.11
1 M/3 M LiCl	5.0	6.34 $\pm$ 0.67	8.68 $\pm$ 0.96	15.92 $\pm$ 0.47	12.48 $\pm$ 2.86	19.65 $\pm$ 2.00
0.5 M/3 M LiCl	10.9	16.66 $\pm$ 1.09	27.78 $\pm$ 0.69	39.17 $\pm$ 0.55	38.16 $\pm$ 0.75	53.65 $\pm$ 1.15
1.5 M/3 M LiCl	6.0	5.78 $\pm$ 0.13	8.19 $\pm$ 0.47	9.46 $\pm$ 0.43	11.07 $\pm$ 0.85	11.59 $\pm$ 1.30

As the trend suggests, we can expect to see further increases in event frequency as we apply an even larger gradient of salt. This is significant because it would allow for more data points at lower biased voltages. Application of low voltages may be crucial for relatively sensitive biomolecules, or for particles with high charge density as they are more susceptible to changes in their properties if exposed to higher voltages.[119, 120] Lower voltages also results in a cleaner baseline with less noise. This allows for definitive discrimination between DNA transport events and background noise. When

considering possible applications for automated data analysis or even machine learning applications, the first component of trained machine learning is clean data with little to no ambiguity.

4.3.2 Slowed translocation of dsDNA by use of LiCl gradients. The utilization of salt gradients was also studied in terms of further slowing transport of dsDNA through the nanopore. This was shown to be the case when looking at nanopores in KCl buffer, but it was yet to be seen if the same would be seen in pores in LiCl. Nanopores of 5.8 nm and 6.4 nm in symmetric 1 M LiCl and 3 M LiCl respectively were used as controls to compare the change in dwell time. Transport events were again recorded at biased applied voltage levels ranging from 200 mV to 600 mV in increments of 100 mV. Figure 12A shows samples of raw data traces for the specified conditions at an applied voltage of 300 mV.

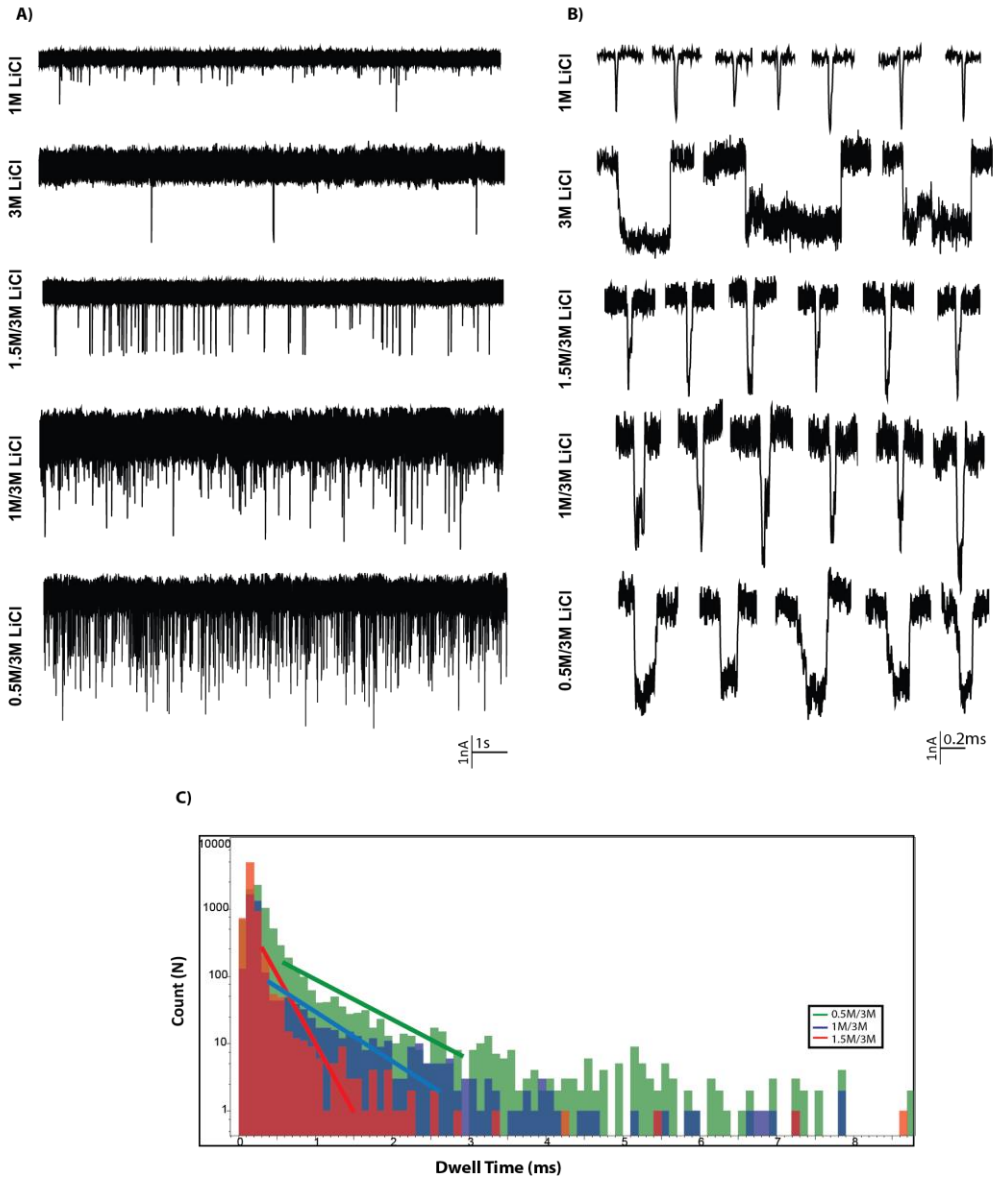

Figure 12. Analysis of DNA Translocation Experiments in LiCl Gradients. A) Representative data traces for experiments run in 0.5 M/3 M LiCl (cis/trans), 1 M/3 M LiCl, and 1.5 M/3 M LiCl. Data traces for similar experiments in symmetric 1 M LiCl (1 M/1 M) and 3 M (3 M/3 M) is provided above as a control. Each data trace was recorded at a biased applied voltage of 300 mV. B) A detailed view of representative individual transport events for the conditions of 1M LiCl,3 M LiCl, 1.5 M/3 M LiCl, 1 M/3 M LiCl, and 0.5 M/3 M LiCl. An increase in dwell time of dsDNA molecules is observed for each experiment run under asymmetric conditions when compared to symmetric 1 M LiCl with 0.5 M/3 M LiCl exhibiting the largest increase out of the samples with a LiCl gradient. C) Histogram created by fitting the data for translocation events for the 0.5 M/3 M LiCl, 1 M/3 M LiCl, and 1.5 M/3 M LiCl conditions with an exponential decay function. A translation to the right as well as a decrease in slope is observed as one increases the LiCl gradient.

Here, the discrepancy in event frequency can be seen between the conditions. Figure 12B shows examples of individual events from the data traces for each condition to illustrate the increase in dwell time. Qualitatively, there is a significant increase in dwell time observed between 1 M LiCl and 0.5 M/3 M LiCl for an applied biased voltage of 300 mV. To quantify the magnitude of the increase, the dwell times were fitted with an exponential decay function as shown in the histogram in Figure 12C. Figure 13 shows a trend between all pores that features a decrease in dwell time as the applied voltage increases.

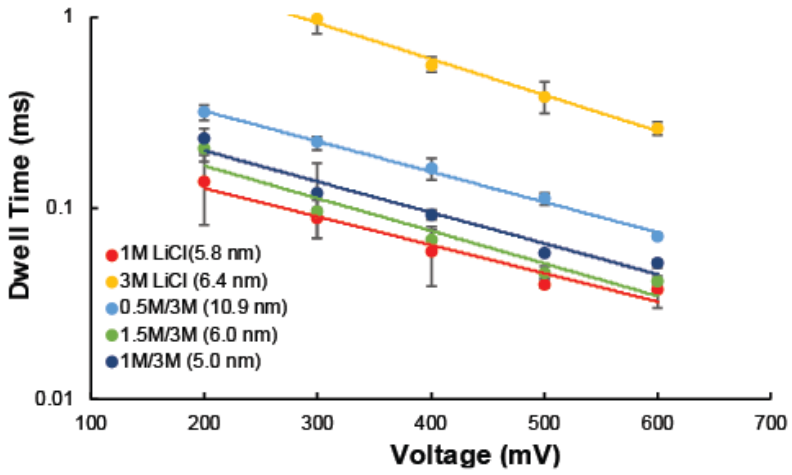

Figure 13. Mean Dwell Times for dsDNA Translocation Events in LiCl Gradients. Experiments run in symmetric 1 M LiCl and 3 M LiCl and asymmetric 1.5 M/3 M LiCl, 1 M/3 M LiCl, and 0.5 M/3 M LiCl are provided for comparison. Data was recorded at biased voltage levels ranging from 200 mV to 600 mV in 100 mV increments.

There is about a 3-fold increase in mean translocation time when comparing 0.5 M/3 M LiCl to 1 M LiCl. The other asymmetric conditions (1 M/3 M and 1.5 M/3 M) exhibit marginal increases as well when compared to 1 M LiCl. However, when

compared to the pore in symmetric 3 M LiCl, there was no observable increase in dwell time in any of the asymmetric cases. A possible explanation for this might be that the effect of the cation binding affinity to the dsDNA backbone, which makes the molecule bulkier. The opposite seems to be true at lower concentration of lithium chloride, such as 1 M. A summary of all the recorded dwell times for every condition at applied biased voltages of 200 mV, 300 mV, 400 mV, 500 mV, and 600 mV is provided in Table 5.

Table 5

Transport Duration in LiCl Gradients

Conditions	**Est. Pore Size (nm)**	$\tau_{200\ mV}$ **(ms)**	$\tau_{300\ mV}$ **(ms)**	$\tau_{400\ mV}$ **(ms)**	$\tau_{500\ mV}$ **(ms)**	$\tau_{600\ mV}$ **(ms)**
1 M LiCl	5.8	0.136 $\pm$ 0.054	0.089 $\pm$ 0.020	0.059 $\pm$ 0.021	0.040 $\pm$ 0.002	0.037 $\pm$ 0.007
3 M LiCl	6.4		0.970 $\pm$ 0.160	0.560 $\pm$ 0.050	0.380 $\pm$ 0.070	0.260 $\pm$ 0.020
1 M/3 M LiCl	5.0	0.228 $\pm$ 0.030	0.120 $\pm$ 0.050	0.092 $\pm$ 0.006	0.058 $\pm$ 0.002	0.051 $\pm$ 0.003
0.5 M/3 M LiCl	10.9	0.314 $\pm$ 0.030	0.219 $\pm$ 0.017	0.160 $\pm$ 0.020	0.111 $\pm$ 0.008	0.071 $\pm$ 0.002
1.5 M/3 M LiCl	6.0	0.203 $\pm$ 0.030	0.0947 $\pm$ 0.005	0.068 $\pm$ 0.009	0.046 $\pm$ 0.003	0.410 $\pm$ 0.001

Figure 14 shows the differences in current blockage amplitude between each pore. Observing the other trends and how well they agree with previous experiments, one would expect the 1 M and 3 M symmetric conditions to be the upper and lower limits,

with the asymmetric conditions falling somewhere in between. However, as can be seen in Figure 14, there is no clear trend as the salt gradient increases or decreases other than a general trend of increased amplitude for each condition as voltage increases. This may be a result of dewetting within the pore nanocavity or could be a result of the previously observed salt gradient offset. Although corrected for the individual offsets observed post fabrication, the characteristic of current blockage amplitude remains an unreliable indicator of nanopore performance because the initial offset tends to fluctuate. However, it should be noted that the purpose of this experiment was to observe improvement in dwell time and capture, which has been demonstrated in previous sections. So overall, there is merit in using salt gradients when the goal is to increase capture efficiency and molecule residence time within the pore nanocavity.

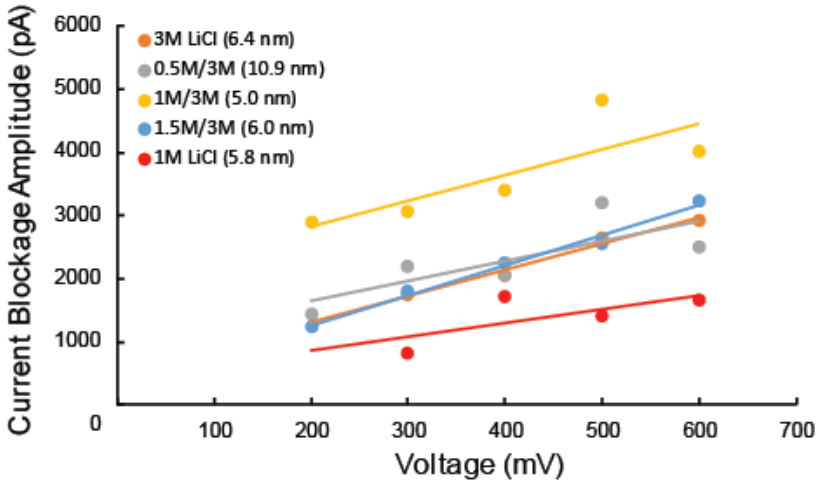

Figure 14. Current Blockage Amplitude of DNA Transport in LiCl Gradients. Experiments were carried out in symmetric 1 M LiCl and 3 M LiCl, and in asymmetric 0.5 M/3 M LiCl, 1 M/3 M LiCl, and 1.5 M/3 M LiCl at applied biased voltages ranging from 200 mV-600 mV. A general trend of increased blockage amplitude is observed as applied voltage increased.

4.4 Conclusion

In the sections above, 2-fold, 3-fold, and 6-fold LiCl concentration gradients were applied on the experimental buffer condition of dsDNA nanopore translocation experiments. When compared to experiments carried out in symmetric 1 M LiCl, the experiments conducted in asymmetric conditions resulted in more prolonged dwell times, with the most significant increase, about 2-fold, observed in 0.5 M/3 M LiCl. This was about 4 times longer than dwell times observed in 1 M KCl in previous studies. Conversely, when compared to 3 M LiCl experiments, the observed dwell times in asymmetric experiments were shorter. However, the unbalanced experimental conditions yielded an overall increase in event occurrence. For instance, 0.5 M/3 M LiCl showed a 5 time and 54 time increase in event occurrence when compared to symmetric 1 M LiCl and 3 M LiCl respectively. This increase in event frequency increases the data generated per run and consequently gives way to more reliable statistical analysis in far less time.

One of the promises of the nanopore platform for diagnostic purposes is the notion of receiving real time results that are accurate. Although the prolonged molecule residence time of symmetric high salt conditions, such as 3M LiCl, would result in better resolution and more accuracy, the lack of data points would then create insignificance in the data. This would result in either an unreliable assay, or a wildly inefficient one if one chooses to opt for accumulating sufficient points under those conditions. The benefit of increased event occurrence retains the inclusion of asymmetric salt conditions in the realm of experimental parameters, even though the observed dwell time in the 6-fold concentration gradient (0.5 M/3 M LiCl) is still faster than in the symmetric 3 M LiCl. Gradients of 10-times or greater could possibly approach the dwell times observed in

symmetric 3 M LiCl, although none of our data supports that a larger gradient would surpass the temporal resolution of the symmetric 3 M LiCl. More could be done to enhance the signal while still being able to use salt gradients for enhanced dwell time and DNA capture.

The use of asymmetric experimental salt solution did not come without its own difficulties that needed to be overcome. The application of the salt gradients had a deleterious effect on signal to noise ratio of the nanopore sensing as well as the overall health of the pore. Although the desired slower translocation times and increased event occurrences were achieved, these findings were coupled with fluctuating baselines and obstruction of the pore that often-impeded further DNA translocation. This obstruction appeared on the signal monitoring as if it were an inserted air bubble, but upon visual inspection, no air bubble was observed. Oftentimes, this required invasive intervention, or in extreme case when nothing else worked, a repeat in the experiment. A possible explanation for this can be the contribution of hydrodynamic slip that occurs as a result of the asymmetric LiCl solution concentration and the inherent hydrophobic properties of the silicon nitride dielectric membranes that was used for the experiments.[121, 122] The LiCl buffer seemingly augmented this occurrence further and created more hydrophobic air pockets within the pore. Transport occurs because fluid in both experimental chambers connects within the pore's cavity. Air pockets in the nanopore can "dewet" the pore and prevent passage of buffer and molecules.[122] Such a phenomenon is reversible through various techniques including electrowetting,[29, 123] which employs a cyclic voltage pulse to enhance the hydrophilicity of the pore albeit while also marginally increasing your pore diameter in the process.[29] Electrowetting allows for continued

data acquisition, although introduces the need for constant monitoring of the data acquisition session to interfere when a hydrophobic blockage occurs. This hinders some of the autonomy that is desired in nanopore biosensors. In addition, as mentioned previously, the pore was in some cases was not able to be rewet, no matter how long the electrowetting took place. This seemed to be more prevalent in steeper salt gradients, raising the question whether there is a limit to how large of a gradient is possible with this particular salt.

To this point, all DNA tested has been naked, which means it has been devoid of any additional epigenetic modification, such as methylation. In the next chapter, knowledge gained from these asymmetric buffer experiments will be used to detect methylated DNA with various protein labels in what is our platform's first preliminary test in detecting disease biomarkers.

Chapter 5

Detection of Local Methylation Sites on DNA Fragments Using Nanopores and Methyl-Binding Proteins

5.1 Background

Proteins that bind to areas of DNA methylation with high affinity are known as methyl-binding proteins (MBPs). These proteins can be used to identify and label methylated *CpG* sites. In this study, we utilize three MBPs; kaiso zinc finger, methyl-binding domain 1, and methyl-binding domain 2.[124] Kaiso zinc finger (KZF) is a Cys2-His2 zinc finger protein with a corresponding DNA binding site. The C-terminal of KZF contains an arginine/lysine-rich area that allows structured loops to form during DNA binding, increasing the risk of nonspecific target binding. KZF wraps 5-6 bps around the DNA when bound, and it requires two consecutive *CpG* pairs to bind to methylated DNA.[125] The protein has a molecular weight of 13.02 kDa.[43] KZF can act in carcinogenesis by silencing certain genes, and it has shown a role in both colorectal and lung cancer.[126, 127]

Methyl-binding domain 1 (MBD1) is the largest member of the methyl-binding domain (MBD) protein family and its corresponding DNA binding site. While there are 13 different isoforms of MBD1, where variants incorporating a third CXXC-type zinc finger domain can bind to DNA independent of its methylation status, isoforms requiring DNA methylation for binding to occur are of greater interest.[126] Nuclear magnetic resonance (NMR) spectroscopy and band-shift studies have demonstrated that CXXC of histone H3K4 methylase MLL binds to one pair of *CpG*s via amino acids located in an extended loop. The loop forms a crescent-shaped structure and is stabilized by eight cysteine residues coordinating with two zinc atoms.[128] Similarly to KZF, MBD1 can

act in carcinogenesis. MBD1 has been associated with lung cancer risk, as well as promyelocytic, leukemia, pancreatic, prostate, and colorectal cancer. Also, MBD1 plays a role in the IFNγ/STAT1 cancer-associated pathway. The effect of MBD1 isoforms on cancer depends on its redundancy and target specificity.[126] The MBD1 DNA binding region is 5-6 bps long, and the protein has a molecular weight of 16.3 kDa.[43] For this study, we used an engineered form of MBD1 classified as MBD1x, which is comprised of only the methyl binding region of the MBD1 protein. Methyl-binding domain 2 (MBD2) is another protein in the MBD family and its corresponding binding site. Unlike MBD1, to the best of our knowledge, MBD2 is not as well studied for binding with methylated DNA. MBD2 is smaller than MBD1 and located 4 Mb away from MBD1 on the "q" arm of chromosome 18.[126] MBD2 can recognize and bind to a single symmetrically methylated *CpG* pair, but it binds with greater affinity in more densely methylated areas of the DNA molecule.[129] As with other MBPs, MBD2 can also act in carcinogenesis, and it has been shown to silence genes in cancers such as colorectal, lung, prostate, and renal.[126, 130] It has been shown to bind preferentially at the *GSTP1* island promoter gene, a *CpG* rich promoter that plays a role in the spread of methylation to neighboring sites.[131]

Methyl-binding proteins can be used to identify areas of DNA methylation through the usage of a nanopore-based methylation assay. Nanopore-based assays study single molecules through ionic current spectroscopy and electrophoresis.[64, 132, 133] The basis behind nanopore sensing with Methyl-binding protein labels is very similar to nanopore biosensing with unlabeled DNA. A nanopore is submerged in ionic solution while a complex of DNA and MBPs is placed into the solution on the cis side of the

experimental chamber. An external voltage is applied across the pore, causing the DNA - MBP complex to pass through the pore.[43, 64, 134, 135] When the molecules pass through the pore, an ionic current blockage occurs, causing a drop in current amplitude. The amplitude of the ionic current blockage is proportional to the size of the molecule relative to the size of the nanopore opening.[136-138] Distinct amplitudes for unbound DNA and DNA bound to MBPs indicate whether the DNA is methylated as the MBP will not bind to non-methylated DNA, resulting in a shallow ionic current blockage when traveling through a nanopore. The difference in nanopore biosensing with protein labels stems from the analysis. For DNA with methylation sites, multilevel events, or events in which the observed signal has more than one peak, may be seen when methyl-binding proteins attach. Observing these events and being able to characterize them could lead to viable localization of methylation on DNA molecules. Being able to detect hypermethylation on DNA and find the general location of the aberrant methylated cytosine can prove to be crucial to future research in the field of cancer epigenetics and diagnostics.

This chapter builds from previous work where we aimed to improve temporal resolution by utilizing different experimental conditions. Herein, detection and characterization of methylation on 100 base pairs double-stranded DNA (dsDNA) is presented by using SiN_x solid-state nanopores as a platform with KZF, MBD1x, and MBD2 protein labels. The DNA used for this study was synthesized to contain consecutive methylated *CpG* sites on opposite ends of the DNA molecule as shown in Figure 15A. This allows experiments to be run with both KZF and MBD proteins with

the same DNA and allows up to two bound proteins to one DNA molecule at any given time as shown in Figure 15B.

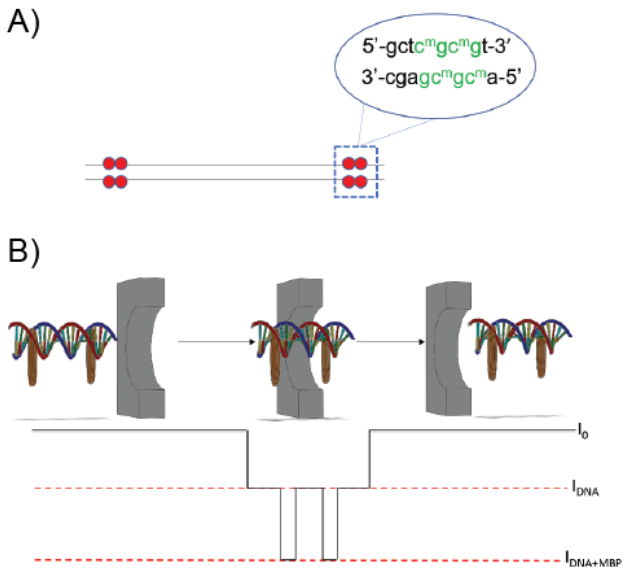

Figure 15. Schematic of dsDNA with Two Methylation Sites. A) Simplified illustration of 100 base pair dsDNA molecule used in the DNA - Protein complexes formed. Two methyl-binding regions, each featuring consecutive methylated CpG islands (inset) are equidistant from each end of the DNA molecule respectively. B) Illustration of expected current blockage signature to be observed when DNA molecule complexed with two methyl-binding proteins translocate through the nanopore. Multilevel current blockages can be expected as regions on the DNA molecule with attached proteins will have a greater diameter and create a greater momentary blockage.

As a DNA molecule with two bound proteins transports through the nanopore, a distinct multilevel current blockage signature is expected. The ability to detect more than one bound protein on the same DNA molecule makes it possible to compare the bound sites to each other. Because hydrophobic interactions within the nanopore wall cause variations in molecule residence time, it is difficult to determine the exact location of methylation based on the location of one protein bound blockage event ($I_{DNA+MBP}$).

However, having more than one protein allows us to compare one $I_{DNA+MBP}$ with another resulting in more meaningful findings. This study aims to compare each protein label to determine which one is most viable at performing this task.

5.2 Materials and Methods

Nanopores in this study were fabricated on 15nm thick custom made SiNx membranes purchased commercially from Norcada. Fabrication took place in 1 M LiCl through dielectric breakdown as has been previously reported[71, 115], and the diameter of each nanopore was estimated using the conductance model previously reported in Kowalczyk et. al.[88] Experiments in this study aimed to investigate the effect of different protein labels on the current signature of 100 base pairs dsDNA transport events. KZF, MBD1x, and MBD2 methyl *CpG* binding proteins were selected as protein labels and were tested electrophoretically in 7.7 nm, 8.3 nm, and 8.4 nm nanopores respectively by applying biased voltage ranging from 200 mV-600 mV. The DNA concentration in all experiments was 10 nM.

The DNA use for these experiments was purchased from Integrated DNA Technologies. The lyophilized DNA was reconstituted and stored in a storage buffer consisting of 10 mM Tris, 1 mM EDTA, pH of 8.0, at 1 μM concentration. The full DNA sequence used is provided in Appendix E. DNA methylation was quantified using methyl-binding proteins that bind to *CpG* methylation sequences. The DNA was complexed with KZF, MBD1x, and MBD2 using standard procedures and were subsequently stored in 4 °C refrigeration. The MBD2 protein was acquired from LumiMac Inc. in Seoul Korea. The MBD1 and MBD2 experiments were performed with symmetric 1 M/ 1 M and asymmetric 1 M/ 3 M LiCl buffer concentrations at 200, 300,

400, 500, and 600 mV voltages. KZF experiments were performed with symmetric buffer concentrations of 0.2 M NaCl, 7.2 pH at 200, 300, 400, 500, and 600 mV voltages.

Instrumentation for data acquisition and MATLAB fabrication code is the same as has been previously reported in the last two chapters. For single level DNA transport events, the same method of data analysis using Clampfit was used as reported in previous chapters as well. For experiments that featured multilevel events, this method could not be used. Multilevel events were analyzed using open source Transalyzer MATLAB GUI based package for nanopore signal analysis that was adapted by our undergraduate clinic for our specific purposes.[33] Screen shots from the software are provided below in Figure 16 and Figure 17.

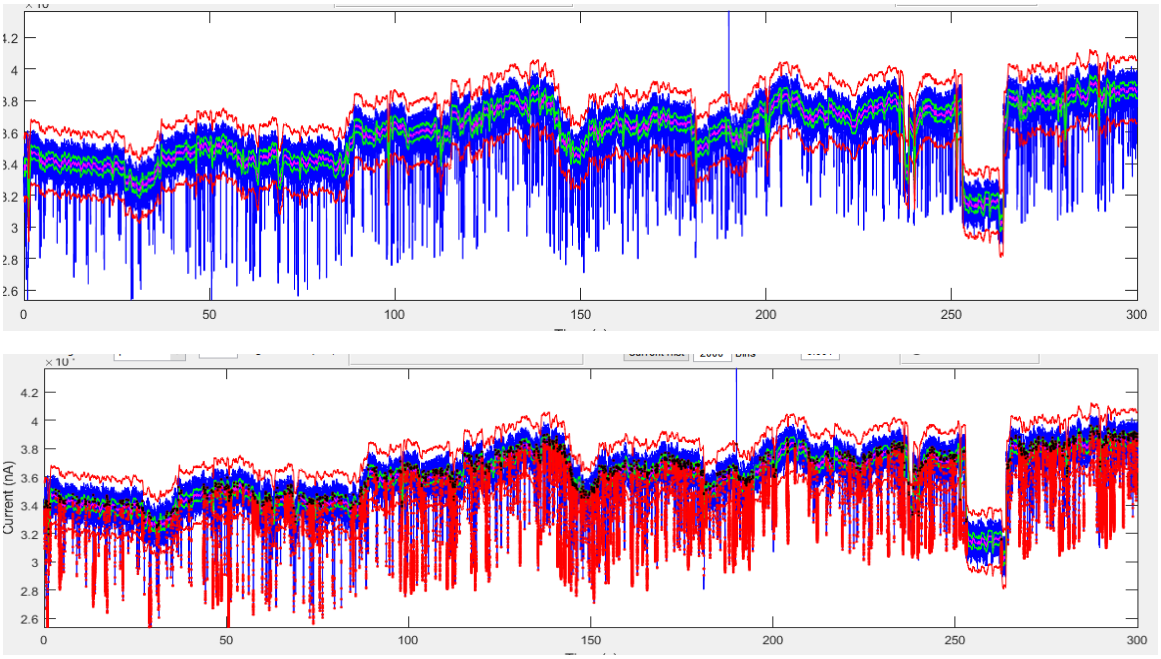

Figure 16. Example of Current Traces in Transalyzer Software. The code uses settings preset by the user to automatically detect the baseline, which is shown by the purple/green line down the center of the solid blue region in the trace (top). The thin red lines that run parallel to the baseline detection illustrate the event detection threshold. Once events are detected, they are highlighted in red (bottom).

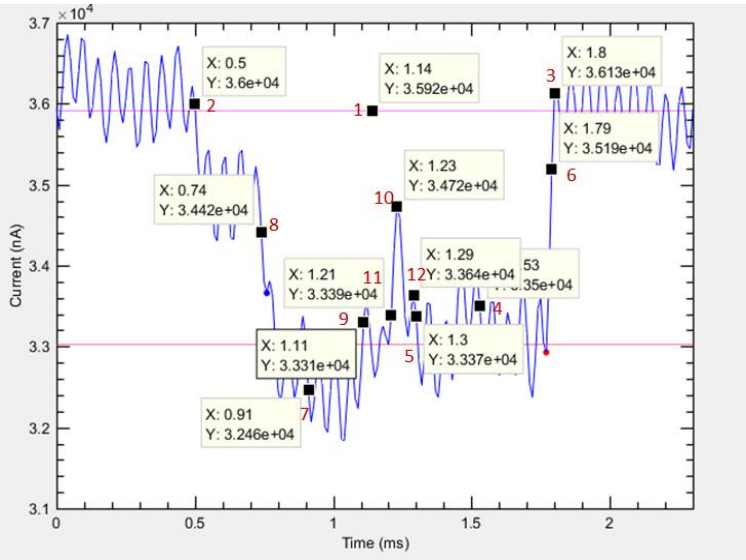

Figure 17. Example of Multilevel DNA Transport Event in Transalyzer Software. The different regions of the multilevel event are manually annotated.

The software automatically detects the baseline of the current trace and uses a preset threshold to determine if a fluctuation in current is a DNA transport event. The automatic detection performs well in following the constantly shifting baseline of the solid-state nanopore current trace. The DNA events that are selected are highlighted in red in the bottom image of Figure 16. As can be seen near the end of this trace, the software does a good job at discerning between a DNA transport event and a momentary complete pore blockage. These blockages do not represent a single molecule of DNA translocating through the pore and can be best attributed to multiple molecules, air bubbles, or pore dewetting. The events can be individually viewed and visually inspected, as shown in Figure 17, to ensure the detection was accurate. This window also allows one to manually annotate the event with the different levels of the multilevel event and export this data into an Excel spreadsheet. Data generated from this software was used to

generate the multilevel event maps that will be shown later in this chapter. Adaption of this software for our purposes was assisted by Brandon Salamone, a consultant from the ECE Department at Rowan University.

A one-way ANOVA test was performed using add-in software in Microsoft Excel 2016 to determine if the mean differences in current amplitudes were significantly different between the complexed and naked DNA at a 0.05 significance level. The one-way ANOVA was selected due to its ability to compare the means of numerous different levels of data for a given factor. The "levels" of the ANOVA test were the complexed protein (KZF, MBD1, or MBD2) or the naked DNA, while the single factor was amplitude. Following the ANOVA test, a Fisher's LSD Post-Hoc test was conducted to confirm where the differences occurred between groups.

5.3 Results and Discussion

5.3.1 Methylation detection with KZF protein labels. Methylated DNA was complexed with KZF in a ratio of 10 nM DNA to 50 nM KZF (1:5) in 0.2 M NaCl buffer to optimize binding. Initially, a 1:1 DNA to KZF ratio was used, but no observable transport events were recorded. 10 nM DNA to 50 nM KZF was used to ensure binding and observable transport events. Experiments were run in symmetric 0.2 M / 0.2 M (*cis* / *trans*) NaCl buffer as well as asymmetric 0.2 M / 2.0 M (*cis* / *trans*) NaCl buffer. A sample of non-complexed DNA (unbound) of the same sequence as the experimental group was also tested in symmetric 0.2 M NaCl buffer and provided as a control. All experimental buffers were titrated to pH 7.2 using 1M HCl. Figure 18A shows average current blockage amplitudes recorded for each condition.

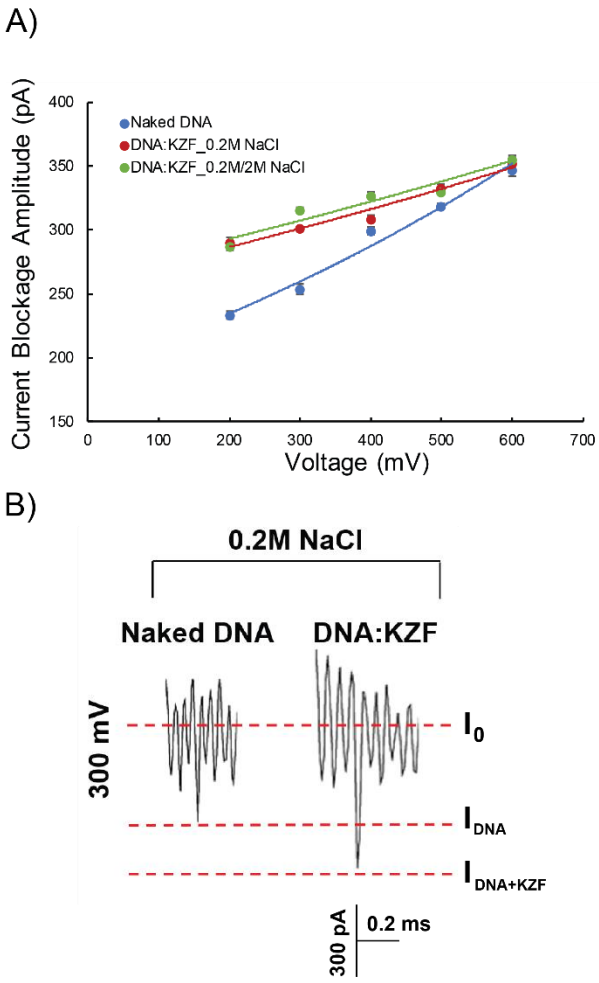

Figure 18. Current Blockage Amplitude of DNA-KZF Transport. A) Graph of Naked DNA in symmetric 0.2 M NaCl, DNA - KZF complex in symmetric 0.2 M NaCl, and DNA - KZF complex in asymmetric 0.2 M/2 M NaCl are shown. A general trend of increasing blockage amplitude was observed with increasing applied voltage. At lower applied voltages (200 mV-300 mV), there was a measurable increase in blockage amplitude of the sample with the complex in comparison to the sample with Naked DNA. B) Examples of events observed in each condition at 300 mV. A 7.69 nm nanopore was used for experiments in these conditions.

A general trend of increased current blockage amplitude is observed as voltage increases. Table 6 shows a tabulated summary of all the average current blockage amplitudes for DNA - KZF complexes in the tested conditions.

Table 6

Current Blockage Amplitude for DNA - KZF Samples

Conditions	**Sample**	$I_{200\ mV}$ **(pA)**	$I_{300\ mV}$ **(pA)**	$I_{400\ mV}$ **(pA)**	$I_{500\ mV}$ **(pA)**	$I_{600\ mV}$ **(pA)**
0.2M / 0.2M NaCl	Naked DNA	233.77 ± 3.17	253.83 ± 4.14	299.36 ± 2.93	318.55 ± 2.00	346.49 ± 4.60
	DNA - KZF	289.96 ± 4.19	300.99 ± 1.72	308.77 ± 2.68	333.24 ± 2.67	352.16 ± 2.46
0.2 M / 2.0 M NaCl	DNA - KZF	286.82 ±2.22	315.53 ± 2.23	327.14 ± 2.34	330.06 ± 2.06	355.24 ± 2.70

A distinct increase in amplitude is observed when looking at the DNA - KZF complex when compared to naked DNA at low voltages (200 mV- 300 mV). Evidently, binding can be presumed as identical experimental conditions while introducing the complex resulted in increased blockage. Interestingly, when making the same comparison at higher voltages (400 mV-600 mV), all three plots converge to the same current amplitude. This can be attributed to increased transport velocity of DNA complex molecules as applied voltage increases. Coupled with fast DNA transport in NaCl ionic solution, the speed of the translocating molecule at high voltages is likely to decrease the mean current blockage amplitude of the complex and not present as a detectable difference between DNA - KZF complex samples and naked DNA.

There is a slight increase in blockage amplitude when comparing the DNA - KZF complex in asymmetric 0.2 M / 2.0 M NaCl (*cis* / *trans*) to symmetric 0.2 M NaCl, however the increase is not significantly different. There is also no evident increase in molecule residence time provided by the asymmetric conditions. The dwell times for

DNA - KZF samples as well as all other samples in this study are given in Appendix G. Although we expected to see multilevel events due to protein bound DNA, as shown in the schematic in Figure 15B, multilevel current blockage events were not present. Previous work has shown multilevel current blockage events with a tighter pore dimension compared to the DNA-KZF complex. [43] Here, a slightly larger nanopore was used and may explain the lack of complex detection. As an alternative, to see the desired multilevel events, the translocation speed would need to be reduced to allow for better molecule resolution with our data acquisition board. Using a salt buffer of LiCl would effectively slow down the translocation speed and improve resolution.[76, 115, 139] However, stability of the KZF protein has not been reported in LiCl and utilizing a different salt might denature the sample. Consequently, in order to expand the repertoire of experimental conditions used and to better observe multilevel events, different protein labels were investigated.

5.3.2 Methylation detection with MBD protein labels. Methyl-binding domain proteins offer a high binding affinity to methylated *CpG* sites, with reported dissociation constants, k_d, of about 30 μM for a single MBD1x binding domain and about 2.1 μM for MBD2. [140-142] MBD proteins have also been shown to be stable in relatively high salt concentrations (up to 1 M).[43] For this study, MBD1x and MBD2 protein monomers were complexed with target dsDNA at a ratio of 10 nM DNA to 10 nM MBD1x (1:1), and 10 nM DNA to 10 nM MBD2 respectively. Experiments were run in symmetric 1.0 M / 1.0 M (*cis* / *trans*) LiCl as well as asymmetric 1.0 M / 3.0 M (*cis* / *trans*) LiCl. A sample of non-complexed DNA (unbound) of the same sequence as the experimental

group was also tested in symmetric 1.0 M LiCl and provided as a control. Experiments in this group were tested at applied biased voltages ranging from 300 mV to 600 mV.

As shown in Figures 19A and 19B, the trend of increased ionic current blockage amplitude with increased voltage is maintained with MBD2x complexes yielding a greater current blockage than MBD1x complexes.

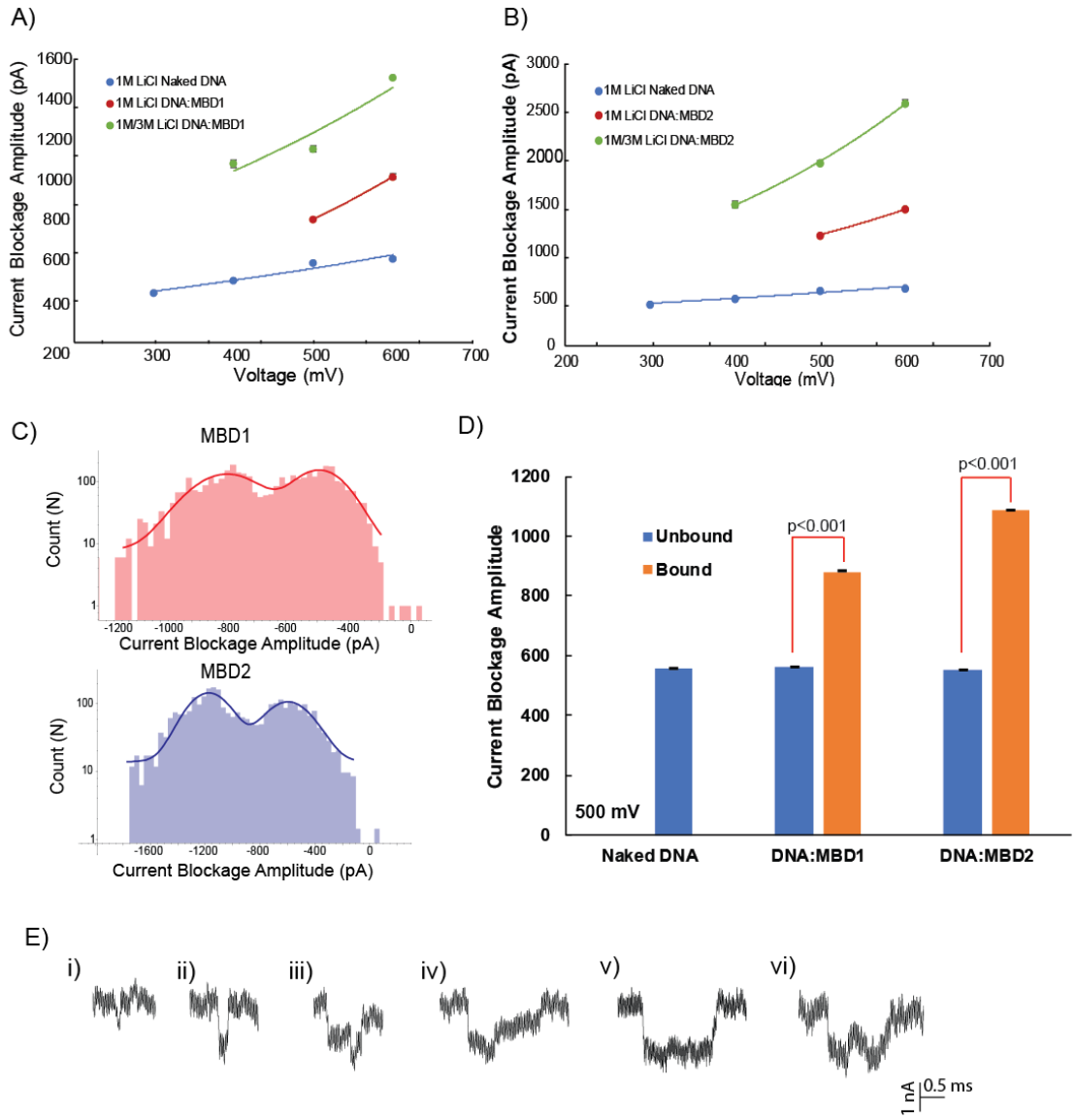

Figure 19. Experimental Results for DNA-MBD Transport. A-B) Graphs illustrating average current blockage amplitude for samples containing DNA - MBD1 and DNA - MBD2 complexes respectively. The complexes were tested in symmetric 1 M LiCl as well as asymmetric 1 M/3 M LiCl with a sample of Naked DNA in symmetric 1 M LiCl provided as a control. The experiments were run over an applied voltage range of 300 mV-600 mV. 8.33 nm and 8.35 nm nanopores were used for these experiments respectively. C) Histograms for current blockage amplitudes of DNA - MBD1 (top) and DNA - MBD2 (bottom) complex samples. Data presented are from experiments run in 1 M LiCl at 500 mV. D) Bar graph representing information from previous histograms with the addition of naked DNA blockage amplitude as a control. A single factor ANOVA with a Fisher LSD post hoc test was used to determine significance between large and small amplitude peaks for both samples. E) Sample DNA transport events from DNA - MBD2 sample in 1 M/3 M LiCl experiments at 500 mV applied voltage. Various and distinct current signatures were observed (i-vi).

At higher voltages (500 mV, 600 mV, and 400 mV for DNA - MBD samples in 1.0 M / 3.0 M LiCl), there were two distinct ranges of current blockage amplitudes observed for DNA - MBD complexes. This difference is most evident in Figure 19C, which shows current blockage amplitude histograms for DNA - MBD1x and DNA - MBD2x samples at 500 mV. There are two distinguishable peaks that denote two different event types. Furthermore, when looking at the data from each peak individually and comparing the higher amplitude peak with the lower amplitude peak, it is observed that the average low amplitude event for DNA - MBD sample has a similar amplitude to the unbound DNA sample. Figure 19D shows the level of ionic current blockage graphically in the form of a bar graph. Statistical analysis was performed on these samples with a single factor Analysis of Variance (ANOVA) and Fisher's Least Significant Difference (LSD) post hoc test. It was determined that there is statistical significance between the groups of high blockage amplitude and low blockage amplitude for DNA – MBD1x and DNA – MBD2x samples. Conversely, there was no significance between the low amplitude groups and the naked DNA tested in symmetric 1.0 M LiCl. Thus, it can be concluded that the two distinct peaks in Figure 19C correspond to bound and unbound DNA molecules. The ANOVA table used to complete this analysis is provided in Appendix H. Consequently, the only transport of DNA - MBD complex to be considered was the deeper amplitude events as the shallow amplitude events describe unbound DNA and would skew results. Since our DNA had two regions of methylation, using a 1:1 DNA to protein ratio resulted in a distribution of DNA that was bound to two proteins, DNA that was bound to one protein, and a distribution of unbound DNA.

Although transport events were observed for both solutions containing DNA and MBD1x and DNA and MBD2x at lower voltages (300 mV and 400 mV in symmetric 1.0 M LiCl, and 300 mV in asymmetric 1.0 M / 3.0 M LiCl), there was only one observable peak. The average current blockage amplitudes for these conditions were very similar to the values for naked DNA. It can be assumed that at these low voltages, there is either no transport of DNA - MBD complex, or the transport of the complex is too infrequent to present with two peaks in the current blockage histogram. A possible reason for a lack of DNA - MBD complex transport can be insufficient electrostatic force at low applied voltages.[139] The reliance of molecule transport on overcoming electrostatic gradient is lessened in asymmetric conditions, which may explain how complex translocation is observed at 400 mV in 1.0 M / 3.0 M LiCl experiments. A summary of current blockage amplitudes for MBD1x complexes, MBD2x complexes, and naked DNA is provided in Table 7.

Table 7

Current Blockage Amplitude for DNA - MBD Samples

Conditions	**Sample**	$I_{300\ mV}$**(pA)**	$I_{400\ mV}$**(pA)**	$I_{500\ mV}$**(pA)**	$I_{600\ mV}$**(pA)**
1.0 M / 1.0 M LiCl	Naked DNA	444.75 $\pm$ 3.76	507.99 $\pm$ 5.27	591.63 $\pm$ 4.47	613.01 $\pm$ 3.88
	DNA-MBD1			809.69 $\pm$ 17.95	1020.73 $\pm$ 16.63
	DNA-MBD2			1180.52 $\pm$ 7.96	1450.96 $\pm$ 15.26
1.0 M / 3.0 M LiCl	DNA-MBD1		1084.42 $\pm$ 37.42	1156.74 $\pm$ 7.89	1512.83 $\pm$ 17.63
	DNA-MBD2		1503.62 $\pm$ 34.10	1945.39 $\pm$ 18.14	2585.56 $\pm$ 26.51

Probably the most fascinating development in the analysis of DNA - MBD complexes was the variations in observed current signatures that included single level blockages (i-ii) and multilevel blockages (iii-vi) as shown in Figure 19E. These sample events were extracted from DNA- MBD2x experiments in 1 M/3 M LiCl at 500 mV applied voltage. The single level blockages observed (i-ii), consist of unbound DNA transport (i), which featured a shallow downward spike, and bound single level DNA transport (ii), which was a much larger downward spike, but only had one distinguishable peak and thereby could not be considered multileveled. The transport observed in (ii) was an anomaly because it was a single deep current blockage that shared blockage amplitudes on par with the deeper blockages of multilevel events but lacked the distinct multiple levels. The amplitude of these events was too large to be naked DNA, but the dwell time was too short to be consistent with the complex. One possible explanation for this can be that the region on the DNA attached to the protein dominates the molecule/pore interaction and the region not bound to protein is not detected. This can stem from the high velocity of molecule transport and the slightly larger size of the nanopore compared to the complex. However, although the amplitude of this event is on par with protein bound DNA transport, there is no definitive way to determine whether one protein, or two proteins are bound.

Aside from this, there was an abundance of DNA bound to MBD that produced current signature event shapes including (iii), which had a long initial blockage (when scanning from right to left) and a subsequent shorter blockage, (iv), which had a short initial blockage and a longer blockage afterwards, and (v), which appeared to be a singular long blockage with a prolonged dwell time. Upon further analysis of these types

of prolonged events, there were some events that included a brief upward spike after the initial long blockage and then a subsequent long blockage at the end as seen in (vi). Events with this current blockage signature are promising in that it shows the rudimentary ability of the nanopore-based biosensor to detect two different protein labels on the same DNA molecule so that the nanopore sensor would profile the methylation pattern on a single dsDNA strand. In addition, observation of events such as (iii) and (iv) provide a benchmark for the discrimination of events such as (v) and (vi), where knowing the amplitude of each protein bound region as well as the overall duration of the molecule transport allows us to analyze less clear events, such as (v), more objectively. Although events such as (v) show only one level, the duration of these transport events are on par with (iii) and (iv) and can be assumed to have more than one protein bound although it cannot definitively be considered multilevel from visual inspection.

When comparing DNA - MBD1x complexes with DNA - MBD2x complexes, DNA - MBD2 complexes had a greater diversity in event current signature types and had a greater occurrence of two bound protein events (v-vi) than MBD1 complexes. Conversely, DNA - MBD1x complexes had a greater number of protein-bound single level events (ii). As they do not offer much in terms of blockage level distinction, these events are not helpful in localization of methylation. Therefore, it is best to continue the analysis with the DNA - MBD2x complex as it has a greater binding affinity and creates a larger overall current blockage, which offers a sharper contrast when looking at different blockage levels.

5.3.3 Localization of methylation using MBD2. To take a closer look into the possible localization of methylated *CpG* islands, two bound protein multilevel events were considered more heavily than single bound protein events. A representative example of a two bound protein multilevel event is provided in Figure 20A.

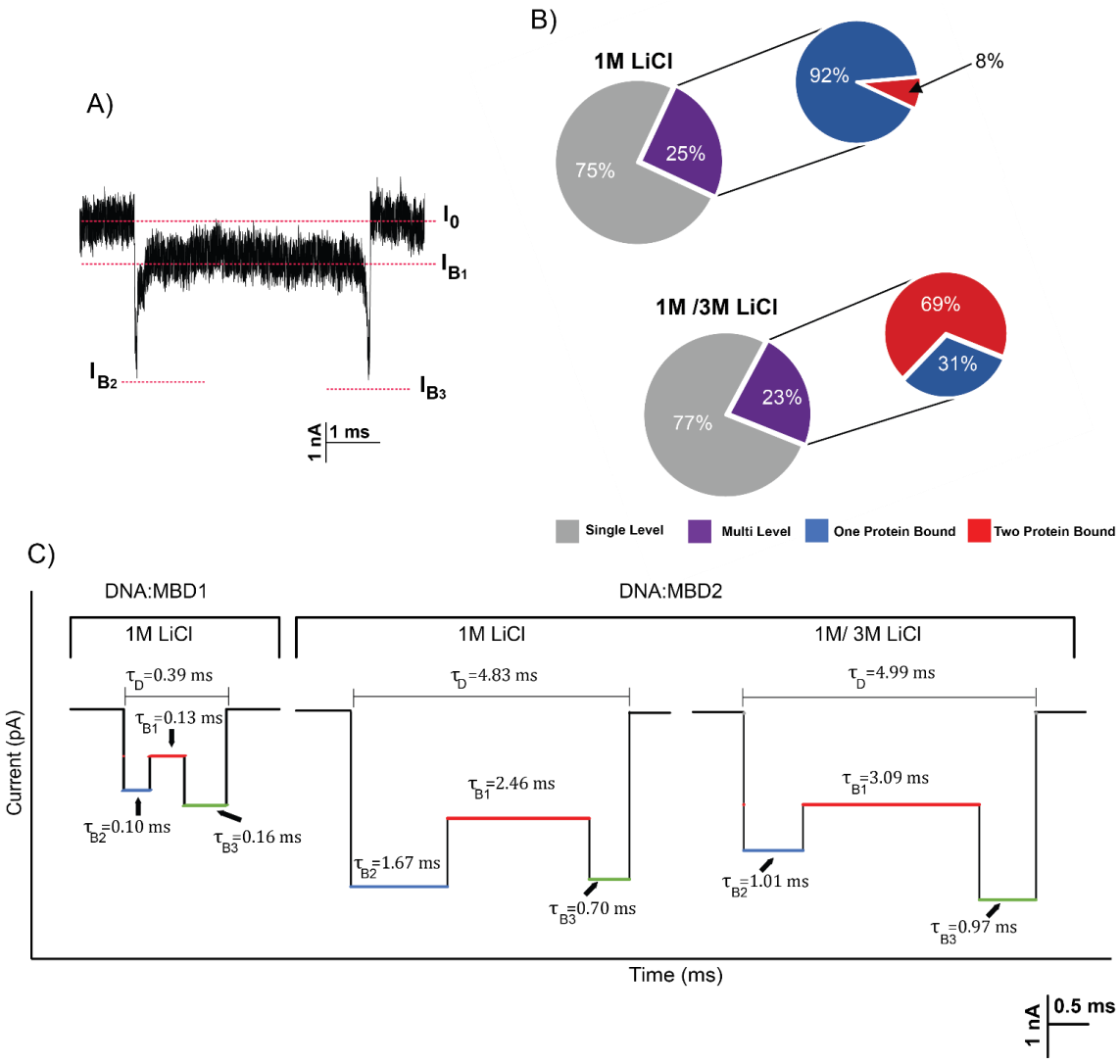

Figure 20. Analysis of Multilevel Current Blockage Events for DNA – MBD Samples. A) Representative multilevel event showing DNA transport with two MBD2 proteins bound. The different current levels, I0, IB1, IB2, and IB3, represent open pore baseline current, DNA blockage current, DNA/protein 1 blockage current, and DNA/protein 2 blockage current respectively. This event was observed in a 1:5 ratio DNA - MBD2 sample in 1 M/ 3 M LiCl at 500 mV. B) Pie chart depicting the distribution of different types of bound protein events observed in 1:5 ratio DNA - MBD2 sample in 1 M/ 3 M LiCl at 500 mV. C) DNA - MBD multilevel event map representing the average temporal duration of each level of current blockage observed in 1:1 ratio DNA -MBD1 samples in 1M LiCl, and 1:5 ratio DNA - MBD2 samples in 1 M LiCl and 1 M/3 M LiCl. This current signature corresponds to sample events in Figure 3v-vi and can be assumed to represent two bound proteins.

Here, our nomenclature for labeling multilevel events is provided as I_0 represents open pore baseline current, I_{B1} is the DNA blockage current (where no methyl-binding protein is present), I_{B2} is the DNA/protein 1 blockage current, and I_{B3} is the DNA/protein 2 blockage current level. Both I_{B2} and I_{B3} were represented separately as we found there were often differences in the amplitude of the signal detected from each of these current blockages. Although if one considers the trajectory of the DNA - protein complex as it enters the nanopore, the first protein that would create a blockage would be B3, the two possible bound proteins were labeled chronologically from left to right to avoid confusion when observing and analyzing the sample events. Since a 1:1 ratio of DNA - protein in the complexed sample yielded a significant amount of unbound DNA, 1:5 ratio DNA - MBD2x was also tested to maximize the amount of two bound protein multilevel events that were observed. Histograms for this experiment are provided in Appendix I and show about 80 % bound DNA, which is a significant improvement to about 50 % bound when testing the 1:1 ratio sample. This is DNA bound to either one, or two MBD2x proteins and includes events like in Figure 19E (ii).

Figure 20B shows the distribution of each type of bound protein event observed in the 1:5 DNA - MBD2x sample at 500 mV applied voltage. As shown, experiments run in symmetric 1.0 M LiCl and asymmetric 1.0 M / 3.0 M LiCl both displayed around 25 % multilevel current blockages out of the 80 % bound DNA events. Multilevel events here denote any event that has a level I_{B1} blockage as well as an I_{B2} and/or I_{B3} blockage. As shown in Figure 19E, DNA complexes with one bound proteins (I_{B2} or I_{B3} blockage) and two bound proteins (I_{B2} and I_{B3} blockage) were both observed. When one looks at the breakdown of multilevel current blockage events, events in symmetric 1.0 M LiCl were

single protein bound multilevel more than 90 % of the time. As discussed previously, the truly valuable type of event to observe is the two bound protein multilevel event, which only makes up about 8 % of the occurrences among multilevel events in symmetric 1 M LiCl. When one looks at events in asymmetric 1.0 M / 3.0 M LiCl, there is a significant increase in two bound protein multilevel events, making up almost 70 %. The distribution of each type of bound protein event observed in DNA - MBD1x samples at 500 mV and 600 mV as well as the distribution of events observed in DNA - MBD2 at 600 mV is provided in Appendix J.

Figure 20C is an event map generated from the average duration and blockage amplitudes of each level in a two bound protein multilevel event. The data was aggregated to show a simplified version of what a two bound protein multilevel event looks like to scale and includes the temporal duration of overall molecule residence, the DNA blockage current (where no methyl-binding protein is present), the DNA/protein 1 blockage current, and the DNA/protein 2 blockage current level, denoted by $\tau_D, \tau_{B1}, \tau_{B2},$ and τ_{B3} respectively. τ_{B1} also corresponds to the temporal duration between the end of the first protein occurrence and the second on the same DNA molecule. As shown in Figure 20C, there is a clear difference between DNA - MBD1 samples and DNA - MBD2 samples when looking at amplitude and event duration. When comparing the symmetric 1 M LiCl map to the 1.0 M / 3.0 M LiCl map for the MBD2 sample, a similar overall dwell time, τ_D, is observed. However, there is an increase in τ_{B1}, which allows one to locate the MBD2 proteins relative to each other. When considering the length of our DNA sequence of 100 base pairs, which translates to about 34 nm in length, each methyl-binding region included on the DNA sequence (consecutive methylated

CpG) encompasses 4 bases, or 4 % of the total length of the strand. The distance between the two methyl-binding regions is 68 bases, or about 23 nm. Relating temporal duration to physical distance can help researchers gain a better sense of where methylation manifests itself spatially on the DNA molecule. Utilizing this information along with improving resolution is crucial for the advancement of nanopore biosensors towards methylation detection. Similar multilevel event maps for other current signatures are provided in Appendix K.

5.4 Conclusion

Nanopore biosensors are promising tools in the diagnostic field that can provide a reliable, low-cost, high throughput alternative to current methods. Although the ability for implementation of nanopore sensors is present, obstacles in the form of fast biomolecule transport and the inability to detect label-free, hinder the platform's progression onto the mainstage of detection of methylated DNA. Protein labels in the form of methyl- binding proteins and asymmetric salt gradients are good ways to bypass some of the sensitivity issues by amplifying and prolonging the signal output in a way that can be distinguished by the naked eye.

In this study, three methyl-binding proteins, KZF, MBD1x, and MBD2, were utilized with the identical methylated DNA sequence to determine which protein label provided the clearest and most distinct signal. To the best of our knowledge, this is the first reported instance of methylation detection with an MBD2 methyl-*CpG*-binding label. DNA - MBD2 complexes in asymmetric 1.0 M / 3.0 M LiCl outperformed the other candidates in terms of current blockage amplitudes, overall dwell time, τ_D, and in distance between protein blockage occurrences on the same DNA molecule. When

looking at τ_D for the DNA - MBD2 complex under asymmetric LiCl conditions, the multilevel event map in Figure 20C showed the τ_D was about 62 % of the duration of the whole transport event on average. Considering the spatial distance between the two methyl-binding sites on the DNA molecule is 68 % of the whole DNA strand, the DNA - MBD2 complex accurately measured the separation of the two proteins.

Although the results in this study are promising, certain aspects must be addressed moving forward. For instance, the methylation map generated and reported in Figure 20C illustrates the compiled average of each current blockage region. As were shown in the sample multilevel events, the start and end points of blockage levels are not always clearly defined and there is a certain amount of subjectivity that comes with the analysis. Automating and standardizing the analysis process is crucial to building reliability in the system and to finding meaningful results. Furthermore, DNA with multiple methyl-binding regions must be tested to see if one is able to distinguish distances between multiple proteins on one DNA molecule with an MBD2 label instead of the distance between just two.

Chapter 6

Conclusions and Future Directions

Solid-state nanopores can be used as inexpensive and high performance biosensors that are capable of the single molecule detection of a wide variety of analytes of medical interest, ranging from small molecules to post translationally modified proteins. [143] Historically, the nanopore biosensing platform has been attractive in the realm of DNA sequencing, but recently, there has been a shift towards detection of different biomarkers that can result in early disease diagnosis. Theoretically sound and endlessly versatile, one can see why the solid-state nanopore platform in particular would be a tantalizing modality for researchers to experiment with experimental conditions, instrumentation, and techniques. However, as mentioned previously and highlighted throughout this work, the sloid-state nanopore platform exhibits several drawbacks, including unstable baseline currents, fast DNA transport, and typically complex and costly fabrication.

Throughout this thesis, some of the capabilities of the solid-state nanopore were demonstrated. The technique of controlled dielectric breakdown was explored, which not only serves practical purposes in that it allows for *in-situ* fabrication and experimentation and cuts down on overall fabrication time, but it also makes nanopore biosensing technology accessible to institutions that normally would not be able to afford to adopt it due to expensive instrumentation. This coincides with our nanopore sensor's ultimate goal of bringing reliable, low-cost diagnostic opportunities to underserved communities and developing nations. The modification of experimental conditions was also investigated, as the traditional and well-studied potassium chloride experimental buffer was substituted for lithium chloride buffer with relative success in terms of increasing

nanopore stability post fabrication and in slowing DNA transport. Salt gradients were introduced to further slow DNA transport and increase the incidence of certain transport events that were previous very infrequent. Also, the engineered binding region novel methyl binding protein, MBD2, was used as a protein label to enhance signal in areas of methylation on DNA and was compared to previously used protein labels. In essence, this is the first step towards the nanopore device to be used for biosensing purposes of biomarker detection. Although this work never reached the advent of testing clinical samples, progress was made in discovering new combinations of techniques and conditions to improve the process.

There is also still much that can possibly be done. One thing that was additionally explored in this research was the possibility of using different MBD2 chain lengths to further enhance our signal. These n-mers (dimers, trimers, and tetramers) of MBD2 were combined with the DNA spoken about in the previous chapter in the same manner as the MBD2 monomer was. Multilevel transport events were only observed at 500 mV and 600 mV, with the majority being observed at 600 mV. All the while, we still saw a lot of large, single spike events that do not have multilevel, but are larger blockages than naked DNA as discussed in the previous chapter. These occurred consistently around 50 % of the time for the trimer and tetramer (1 M symmetric and 1M/3M), and more often for the monomer (almost 70% of the time for 1M/3M LiCl). The exact reason for this occurrence is still unknown. In addition, the change in dwell time from one n-mer to the other is not linear. There is a minor, 2-fold increase in average total dwell time between monomer and trimer, and there was no significant increase in dwell time between the trimer and tetramer even though we expected slower transport in the tetramer with it being a larger

molecule and with us using a smaller pore for that experiment (16.2 nm as opposed to 18.9 nm). Although interesting to pursue, the different n-mers introduced their own set of obstacles. Since they were different sizes, different size pores were required to analyze the complexes. We were able to accommodate this, but it made data between the different n-mers difficult to compare. Also, the proteins themselves are not rigid bodies, so the longer protein chains, once bound to the DNA, could theoretically reorient themselves and fold as they transport through the pore. This could dramatically alter the characteristic signature of the observed signal; a problem that was not encountered when working with the monomer. More sophisticated ways of characterizing these complexes, or analyzing the data has to be implemented to gain any meaningful information from these molecules. Ultimately, the benefits of working with n-mers as opposed to the monomers still await to be seen, but they are still an interesting area to explore for the future.

Another possible direction for this work to head into could look at different materials for the nanopore. This work focused on one material, the silicon nitride membrane for the nanopore device, but solid-state pores can be made of anything from graphene to glass. Graphene pores introduce an interesting group of ultra-thin nanopore membranes that can address some of the issues that were presented in SiNx pores. These "2 Dimensional" materials can resolve nanoscale-spaced molecular structures with a resolution of less than 0.6 nm along the length of the molecule and could lead to an error-free read-out. [144] Atomically thin graphene nanopores, closely resembling the diameter of dsDNA, have a high sensitivity to infinitesimal changes in the outer diameter of the translocating DNA and could exemplify this principal of 2-D materials. [144] However,

graphene nanopores have a strong hydrophobic interaction with DNA, which causes the DNA to attach to the graphene membrane and impedes translocation and requires surface pretreatment to promote transport. [144-146] Alternative materials have been explored to eliminate the need for additional surface treatment protocol. [68] Molybdenum disulfide (MoS2) is a novel atomically thin nanopore membrane material that has an inherent affinity for DNA translocation and single nucleotide base resolution, but requires no special surface treatment to avoid hydrophobic interaction between DNA and the MoS2 surface. [144] It would be interesting to see if MoS2 membranes could be drilled through controlled dielectric breakdown, and whether the 2-D material would do enough to help the resolution issues we experienced during my graduate studies.

Another route that can be explored is the ever-growing realm of artificial intelligence. Although deserving of its own full thesis and deeper dive, a classical machine learning model is, in short, very reminiscent of how people learn by past experiences. The pipeline involves manually labeled data, which is then used to train a modifier, which then allows the computer to make decisions on unlabeled data based on features from the modifier. This would fit in the scheme for nanopore detection because in its current state, analysts are manually labeling data for hours already. Key features from this data could be used to train the computer to discern transport events form baseline noise, multilevel events from normal transport, and typically information one would manually obtain, such as dwell time, and current amplitude. Utilizing a machine learning model to event detection and data analysis could further automate the process and remove analyst subjectivity. However, this method is not foolproof, and although automation and artificial intelligence has made great strides, it is not always the best

solution. Mislabeling is a key concern. Oftentimes, manually labeled data varies from one dataset to the next. Training a computer with contradicting features, or features that are too vague could lead to inaccuracy. As an analogy, labeling a picture of an orange with color and shape as distinguishing features could get accurate results if the computer is shown pictures of different fruit. However, if the computer is presented with a picture of a basketball, it may mislabel the image as an orange. Similarly, if DNA transport data is too vague in criteria for what an event is, machine learning will not be useful. The robustness of artificial intelligence depends on the amount of data it is trained on, and the quality of that data. Although machine learning is an interesting area to explore for this application, the quality and resolution of the data may create more problems than it addresses.

Being able to detect aberrant methylation in a routine lab screening could help locate a tumor site before it begins to form. This could prove to be crucial in terms of early intervention and therapy and ultimately lead to an exponential increase the rate of survival for most cancer patients. Nanopore biosensors can make this a possibility with some fundamental improvements. This work has been one step towards that goal and has shown promise in the platform, but work still remains to be accomplished in the control of translocation speeds, resolution of signature current blockades and in pinpointing the location of attached methyl binding protein labels.

References

[1] Y. Feng, Y. Zhang, C. Ying, D. Wang, and C. Du, "Nanopore-based Fourth-generation DNA Sequencing Technology," *Genomics, Proteomics & Bioinformatics,* vol. 13, no. 1, pp. 4-16, 2// 2015.

[2] L.-Q. Gu and J. W. Shim, "Single molecule sensing by nanopores and nanopore devices," *Analyst,* 10.1039/B907735A vol. 135, no. 3, pp. 441-451, 2010.

[3] B. M. Venkatesan and R. Bashir, "Nanopore sensors for nucleic acid analysis," (in eng), *Nat Nanotechnol,* vol. 6, no. 10, pp. 615-24, Sep 18 2011.

[4] P. Mueller, D. O. Rudin, H. Ti Tien, and W. C. Wescott, "Reconstitution of Cell Membrane Structure in vitro and its Transformation into an Excitable System," *Nature,* 10.1038/194979a0 vol. 194, no. 4832, pp. 979-980, 06/09/print 1962.

[5] J. Bello, Y.-R. Kim, S. M. Kim, T.-J. Jeon, and J. Shim, "Lipid bilayer membrane technologies: A review on single-molecule studies of DNA sequencing by using membrane nanopores," *Microchimica Acta,* vol. 184, no. 7, pp. 1883-1897, 2017// 2017.

[6] R. Coronado, "Recent Advances in Planar Phospholipid Bilayer Techniques for Monitoring ION Channels," *Annu. Rev. Biophys. Biophys. Chem.,* vol. 15, no. 1, pp. 259-277, 1986/06/01 1986.

[7] F. J. Morera, G. Vargas, C. Gonzalez, E. Rosenmann, and R. Latorre, "Ion-channel reconstitution," (in Eng), *Methods Mol Biol,* vol. 400, pp. 571-85, 2007.

[8] C. F. Stevens, "Electrophysiological methods: ion channel reconstitution," (in Eng), *Science,* vol. 234, no. 4779, p. 1016, Nov 21 1986.

[9] L. Bakas, A. Chanturiya, V. Herlax, and J. Zimmerberg, "Paradoxical lipid dependence of pores formed by the Escherichia coli alpha-hemolysin in planar phospholipid bilayer membranes," (in Eng), *Biophys J,* vol. 91, no. 10, pp. 3748-55, Nov 15 2006.

[10] F. S. Cohen and W. D. Niles, "Reconstituting channels into planar membranes: a conceptual framework and methods for fusing vesicles to planar bilayer phospholipid membranes," *Methods Enzymol,* vol. 220, pp. 50-68, 1993.

[11] H. W. Huang, "Deformation free energy of bilayer membrane and its effect on gramicidin channel lifetime," *Biophys J,* vol. 50, no. 6, pp. 1061-1070, 1986.

[12] S. Ladha *et al.*, "Lateral diffusion in planar lipid bilayers: a fluorescence recovery after photobleaching investigation of its modulation by lipid composition, cholesterol, or alamethicin content and divalent cations," *Biophys J,* vol. 71, no. 3, pp. 1364-1373, 1996.

[13] H. Schindler, "Planar lipid-protein membranes: strategies of formation and of detecting dependencies of ion transport functions on membrane conditions," *Methods Enzymol,* vol. 171, pp. 225-53, 1989.

[14] H. Bayley, "Sequencing single molecules of DNA," *Curr. Opin. Chem. Biol.,* vol. 10, no. 6, pp. 628-637, 12// 2006.

[15] H. Bayley and P. S. Cremer, "Stochastic sensors inspired by biology," *Nature,* 10.1038/35093038 vol. 413, no. 6852, pp. 226-230, 09/13/print 2001.

[16] S. Blake, T. Mayer, M. Mayer, and J. Yang, "Monitoring chemical reactions by using ion-channel-forming peptides," (in eng), *Chembiochem,* vol. 7, no. 3, pp. 433-5, Mar 2006.

[17] J. Schmidt, "Stochastic sensors," *J. Mater. Chem,* 10.1039/B414551H vol. 15, no. 8, pp. 831-840, 2005.

[18] T. A. Mirzabekov, A. Y. Silberstein, and B. L. Kagan, "Use of planar lipid bilayer membranes for rapid screening of membrane active compounds," *Methods Enzymol,* vol. 294, pp. 661-74, 1999.

[19] H. Bayley, "Nanopore Sequencing: From Imagination to Reality," *Clin. Chem.,* 10.1373/clinchem.2014.223016 vol. 61, no. 1, p. 25, 2014.

[20] M. C. Schatz, A. L. Delcher, and S. L. Salzberg, "Assembly of large genomes using second-generation sequencing," *Genome Res.,* vol. 20, no. 9, pp. 1165-1173, 2010.

[21] W. W. Soon, M. Hariharan, and M. P. Snyder, "High-throughput sequencing for biology and medicine," *Mol. Sys. Biol.,* vol. 9, pp. 640-640, 01/22

[22] T. Laver *et al.,* "Assessing the performance of the Oxford Nanopore Technologies MinION," *Biomolecular Detection and Quantification,* vol. 3, pp. 1-8, 2015/03/01/ 2015.

[23] L. Song, M. R. Hobaugh, C. Shustak, S. Cheley, H. Bayley, and J. E. Gouaux, "Structure of staphylococcal alpha-hemolysin, a heptameric transmembrane pore," (in eng), *Science,* vol. 274, no. 5294, pp. 1859-66, Dec 13 1996.

[24] D. Branton *et al.,* "The potential and challenges of nanopore sequencing," *Nat Biotech,* 10.1038/nbt.1495 vol. 26, no. 10, pp. 1146-1153, 10//print 2008.

[25] J. Shi, J. Hou, and Y. Fang, "Recent advances in nanopore-based nucleic acid analysis and sequencing," *Microchim. Acta,* vol. 183, no. 3, pp. 925-939, 2016// 2016.

[26] B. N. Miles, A. P. Ivanov, K. A. Wilson, F. Dogan, D. Japrung, and J. B. Edel, "Single molecule sensing with solid-state nanopores: novel materials, methods, and applications," *Chemical Society Reviews,* 10.1039/C2CS35286A vol. 42, no. 1, pp. 15-28, 2013.

[27] J. Li, D. Yu, and Q. Zhao, "Solid-state nanopore-based DNA single molecule detection and sequencing," *Microchimica Acta,* vol. 183, no. 3, pp. 941-953, 2016// 2016.

[28] M. Valentina, F. Paola, F. Giuseppe, R. Luca, and V. Ugo, "Size and functional tuning of solid state nanopores by chemical functionalization," *Nanotechnology,* vol. 23, no. 43, p. 435301, 2012.

[29] E. Beamish, H. Kwok, V. Tabard-Cossa, and M. Godin, "Fine-tuning the Size and Minimizing the Noise of Solid-state Nanopores," *Journal of Visualized Experiments : JoVE,* no. 80, p. 51081, 10/31 2013.

[30] V. Thangaraj *et al.*, "Detection of short ssDNA and dsDNA by current-voltage measurements using conical nanopores coated with Al2O3 by atomic layer deposition," *Microchim. Acta,* journal article vol. 183, no. 3, pp. 1011-1017, 2016.

[31] J. Larkin, R. Henley, D. C. Bell, T. Cohen-Karni, J. K. Rosenstein, and M. Wanunu, "Slow DNA Transport through Nanopores in Hafnium Oxide Membranes," *ACS Nano,* vol. 7, no. 11, pp. 10121-10128, 2013/11/26 2013.

[32] L. J. Steinbock, R. D. Bulushev, S. Krishnan, C. Raillon, and A. Radenovic, "DNA Translocation through Low-Noise Glass Nanopores," *ACS Nano,* vol. 7, no. 12, pp. 11255-11262, 2013/12/23 2013.

[33] C. J. Russo and J. A. Golovchenko, "Atom-by-atom nucleation and growth of graphene nanopores," *Proceedings of the National Academy of Sciences of the United States of America,* vol. 109, no. 16, pp. 5953-5957, 04/06 2012.

[34] R. L. Siegel, K. D. Miller, and A. Jemal, "Cancer statistics, 2019," vol. 69, no. 1, pp. 7-34, 2019.

[35] R. L. Siegel, K. D. Miller, and A. Jemal, "Cancer statistics, 2018," *CA: A Cancer Journal for Clinicians,* vol. 68, no. 1, pp. 7-30, 2018.

[36] G. Strathdee and R. Brown, "Aberrant DNA methylation in cancer: potential clinical interventions," *Expert Reviews in Molecular Medicine,* vol. 4, no. 4, pp. 1-17, 2004.

[37] K. F. Santos, T. N. Mazzola, and H. F. Carvalho, "The prima donna of epigenetics: the regulation of gene expression by DNA methylation," *Brazilian Journal of Medical and Biological Research,* vol. 38, pp. 1531-1541, 2005.

[38] L. D. Moore, T. Le, and G. Fan, "DNA methylation and its basic function," *Neuropsychopharmacology,* vol. 38, no. 1, pp. 23-38, 07/11

[39] M. Ehrlich, "DNA hypomethylation in cancer cells," *Epigenomics,* vol. 1, no. 2, pp. 239-259, 2009.

[40] M. Kulis and M. Esteller, "DNA methylation and cancer," (in eng), *Adv Genet,* vol. 70, pp. 27-56, 2010.

[41] B. Jin, Y. Li, and K. D. Robertson, "DNA methylation: Superior or subordinate in the epigenetic hierarchy?," *Genes & Cancer,* vol. 2, no. 6, pp. 607-617, 2011.

[42] J. Shim *et al.*, "Detection of methylation on dsDNA using nanopores in a MoS2 membrane," *Nanoscale,* 10.1039/C7NR03092D vol. 9, no. 39, pp. 14836-14845, 2017.

[43] J. Shim *et al.*, "Nanopore-based assay for detection of methylation in double-stranded DNA fragments," (in English), *Acs Nano,* Article vol. 9, no. 1, pp. 290-300, Jan 2015.

[44] J. Shim *et al.*, "Detection and Quantification of Methylation in DNA using Solid-State Nanopores," *Sci. Rep.,* Article vol. 3, p. 1389, 03/11/online 2013.

[45] E. R. Fearon and B. Vogelstein, "A genetic model for colorectal tumorigenesis," *Cell,* vol. 61, no. 5, pp. 759-767, 1990/06/01/ 1990.

[46] S. B. Baylln, J. G. Herman, J. R. Graff, P. M. Vertino, and J.-P. Issa, "Alterations in DNA Methylation: A Fundamental Aspect of Neoplasia," in *Advances in Cancer Research,* vol. 72, G. F. Vande Woude and G. Klein, Eds.: Academic Press, 1997, pp. 141-196.

[47] E. Li, T. H. Bestor, and R. Jaenisch, "Targeted mutation of the DNA methyltransferase gene results in embryonic lethality," *Cell,* vol. 69, no. 6, pp. 915-926, 1992/06/12/ 1992.

[48] P. W. Laird, "Cancer epigenetics," (in eng), *Hum Mol Genet,* vol. 14 Spec No 1, pp. R65-76, Apr 15 2005.

[49] P. W. Laird, "The power and the promise of DNA methylation markers," (in eng), *Nat Rev Cancer,* vol. 3, no. 4, pp. 253-66, Apr 2003.

[50] P. W. Laird and R. Jaenisch, "The role of DNA methylation in cancer genetic and epigenetics," (in eng), *Annu Rev Genet,* vol. 30, pp. 441-64, 1996.

[51] A. Murrell, V. K. Rakyan, and S. Beck, "From genome to epigenome," *Human Molecular Genetics,* vol. 14, no. suppl 1, pp. R3-R10, April 15, 2005 2005.

[52] A. Murrell, V. K. Rakyan, and S. Beck, "From genome to epigenome," (in eng), *Hum Mol Genet,* Research Support, Non-U.S. Gov't

[53] C. Grunau, E. Renault, A. Rosenthal, and G. Roizes, "MethDB--a public database for DNA methylation data," (in eng), *Nucleic Acids Res,* Research Support, Non-U.S. Gov't vol. 29, no. 1, pp. 270-4, Jan 01 2001.

[54] P. W. Laird, "The power and the promise of DNA methylation markers," *Nat Rev Cancer,* 10.1038/nrc1045 vol. 3, no. 4, pp. 253-266, 04//print 2003.

[55] J. B. Kisiel *et al.*, "Stool DNA testing for the detection of pancreatic cancer Assessment of Methylation Marker Candidates," (in English), *Cancer,* vol. 118, no. 10, pp. 2623-2631, May 15 2012.

[56] R. Kandimalla, A. A. van Tilborg, and E. C. Zwarthoff, "DNA methylation-based biomarkers in bladder cancer," (in English), *Nature Reviews Urology,* vol. 10, no. 6, pp. 327-335, Jun 2013.

[57] J. Kasianowicz, E. Brandin, D. Branton, and D. W. Deamer, "Characterization of individual polynucleotide molecules using a membrane channel," *Proc. Natl. Acad. Sci. U.S.A.,* vol. 93, pp. 13770-13773, 1996.

[58] C. Dekker, "Solid-state nanopores," *Nature Nanotechnology,* Review Article vol. 2, p. 209, 03/04/online 2007.

[59] H. Bayley and C. R. Martin, "Resistive-Pulse SensingFrom Microbes to Molecules," *Chemical Reviews,* vol. 100, no. 7, pp. 2575-2594, 2000/07/01 2000.

[60] A. McMullen, H. W. de Haan, J. X. Tang, and D. Stein, "Stiff filamentous virus translocations through solid-state nanopores," *Nature Communications,* Article vol. 5, p. 4171, 06/16/online 2014.

[61] B. I. Karawdeniya, Y. M. N. D. Y. Bandara, J. W. Nichols, R. B. Chevalier, and J. R. Dwyer, "Surveying silicon nitride nanopores for glycomics and heparin quality assurance," *Nature Communications,* vol. 9, no. 1, p. 3278, 2018/08/16 2018.

[62] T. Vu, S.-L. Davidson, J. Borgesi, M. Maksudul, T.-J. Jeon, and J. Shim, "Piecing together the puzzle: nanopore technology in detection and quantification of cancer biomarkers," *RSC Advances,* 10.1039/C7RA08063H vol. 7, no. 68, pp. 42653-42666, 2017.

[63] B. M. Venkatesan, B. Dorvel, S. Yemenicioglu, N. Watkins, I. Petrov, and R. Bashir, "Highly Sensitive, Mechanically Stable Nanopore Sensors for DNA Analysis," *Advanced Materials,* vol. 21, no. 27, pp. 2771-2776, 2009.

[64] J. Shim *et al.*, "Detection and Quantification of Methylation in DNA using Solid-State Nanopores," *Scientific Reports,* Article vol. 3, p. 1389, 03/11/online 2013.

[65] T. A. Desai *et al.*, "Nanopore Technology for Biomedical Applications," *Biomedical Microdevices,* vol. 2, no. 1, pp. 11-40, 1999// 1999.

[66] V. Kurz, E. M. Nelson, J. Shim, and G. Timp, "Direct visualization of single-molecule translocations through synthetic nanopores comparable in size to a molecule," *ACS Nano,* vol. 7, no. 5, pp. 4057-69, May 28 2013.

[67] E. M. Nelson, V. Kurz, J. Shim, W. Timp, and G. Timp, "Using a nanopore for single molecule detection and single cell transfection," *Analyst,* vol. 137, no. 13, pp. 3020-7, Jul 07 2012.

[68] J. Feng *et al.*, "Identification of single nucleotides in MoS2 nanopores," *Nat Nano,* Article vol. 10, no. 12, pp. 1070-1076, 12//print 2015.

[69] F. Nicoli, D. Verschueren, M. Klein, C. Dekker, and M. P. Jonsson, "DNA Translocations through Solid-State Plasmonic Nanopores," *Nano Letters,* vol. 14, no. 12, pp. 6917-6925, 2014/12/10 2014.

[70] A. J. Storm, J. H. Chen, X. S. Ling, H. W. Zandbergen, and C. Dekker, "Fabrication of solid-state nanopores with single-nanometre precision," *Nature Materials,* vol. 2, p. 537, 07/13/online 2003.

[71] H. Kwok, K. Briggs, and V. Tabard-Cossa, "Nanopore Fabrication by Controlled Dielectric Breakdown," *PLOS ONE,* vol. 9, no. 3, p. e92880, 2014.

[72] M. Waugh *et al.*, "Interfacing solid-state nanopores with gel media to slow DNA translocations," *ELECTROPHORESIS,* vol. 36, no. 15, pp. 1759-1767, 2015.

[73] D. Fologea, J. Uplinger, B. Thomas, D. S. McNabb, and J. Li, "Slowing DNA translocation in a solid-state nanopore," *Nano letters,* vol. 5, no. 9, pp. 1734-1737, 2005.

[74] P. Krishnakumar *et al.*, "Slowing DNA Translocation through a Nanopore Using a Functionalized Electrode," *ACS Nano,* vol. 7, no. 11, pp. 10319-10326, 2013/11/26 2013.

[75] Z. Liang, Z. Tang, J. Li, R. Hu, D. Yu, and Q. Zhao, "Interaction prolonged DNA translocation through solid-state nanopores," *Nanoscale,* 10.1039/C5NR01954K vol. 7, no. 24, pp. 10752-10759, 2015.

[76] S. W. Kowalczyk, D. B. Wells, A. Aksimentiev, and C. Dekker, "Slowing down DNA Translocation through a Nanopore in Lithium Chloride," *Nano Letters,* vol. 12, no. 2, pp. 1038-1044, 2012/02/08 2012.

[77] R. W. Wilson, D. C. Rau, and V. A. Bloomfield, "Comparison of polyelectrolyte theories of the binding of cations to DNA," *Biophysical Journal,* vol. 30, no. 2, pp. 317-325, 1980/05/01/ 1980.

[78] C. Plesa *et al.*, "Direct observation of DNA knots using a solid-state nanopore," *Nat Nano,* Article vol. 11, no. 12, pp. 1093-1097, 12//print 2016.

[79] D. S. Jeong and C. S. Hwang, "Tunneling-assisted Poole-Frenkel conduction mechanism in HfO2 thin films," *Journal of Applied Physics,* vol. 98, no. 11, p. 113701, 2005.

[80] S. Habermehl, R. T. Apodaca, and R. J. Kaplar, "On dielectric breakdown in silicon-rich silicon nitride thin films," *Applied Physics Letters,* vol. 94, no. 1, p. 012905, 2009.

[81] I. Yanagi, R. Akahori, T. Hatano, and K.-i. Takeda, "Fabricating nanopores with diameters of sub-1 nm to 3 nm using multilevel pulse-voltage injection," *Scientific Reports,* Article vol. 4, p. 5000, 05/21/online 2014.

[82] J. Zhi, Z. Yi-Qi, L. Cong, W. Ping, and L. Yu-Qi, "Influence of trap-assisted tunneling on trap-assisted tunneling current in double gate tunnel field-effect transistor," *Chinese Physics B,* vol. 25, no. 2, p. 027701, 2016.

[83] S. Pud, D. Verschueren, N. Vukovic, C. Plesa, M. P. Jonsson, and C. Dekker, "Self-Aligned Plasmonic Nanopores by Optically Controlled Dielectric Breakdown," *Nano Letters,* vol. 15, no. 10, pp. 7112-7117, 2015/10/14 2015.

[84] J. Wu, L. F. Register, and E. Rosenbaum, "Trap-assisted tunneling current through ultra-thin oxide," in *1999 IEEE International Reliability Physics Symposium Proceedings. 37th Annual (Cat. No.99CH36296)*, 1999, pp. 389-395.

[85] B. Kyle *et al.*, "Kinetics of nanopore fabrication during controlled breakdown of dielectric membranes in solution," *Nanotechnology,* vol. 26, no. 8, p. 084004, 2015.

[86] B. Eric, K. Harold, T.-C. Vincent, and G. Michel, "Precise control of the size and noise of solid-state nanopores using high electric fields," *Nanotechnology,* vol. 23, no. 40, p. 405301, 2012.

[87] I. Vodyanoy and S. M. Bezrukov, "Sizing of an ion pore by access resistance measurements," *Biophysical Journal,* vol. 62, no. 1, pp. 10-11, 1992.

[88] S. W. Kowalczyk, Y. G. Alexander, R. Yitzhak, and D. Cees, "Modeling the conductance and DNA blockade of solid-state nanopores," *Nanotechnology,* vol. 22, no. 31, p. 315101, 2011.

[89] O. V. Krasilnikov, R. Z. Sabirov, V. I. Ternovsky, P. G. Merzliak, and J. N. Muratkhodjaev, "A simple method for the determination of the pore radius of ion channels in planar lipid bilayer membranes," *FEMS Microbiology Letters,* vol. 105, no. 1-3, pp. 93-100, 1992.

[90] O. V. Krasilnikov, R. Z. Sabirov, V. I. Ternovsky, P. G. Merzliak, and B. A. Tashmukhamedov, "The structure of Staphylococcus aureus alpha-toxin-induced ionic channel," (in eng), *Gen Physiol Biophys,* vol. 7, no. 5, pp. 467-73, Oct 1988.

[91] S. Lombardo, J. H. Stathis, B. P. Linder, K. L. Pey, F. Palumbo, and C. H. Tung, "Dielectric breakdown mechanisms in gate oxides," *Journal of Applied Physics,* vol. 98, no. 12, p. 121301, 2005.

[92] Y. Wang, C. Ying, W. Zhou, L. de Vreede, Z. Liu, and J. Tian, "Fabrication of multiple nanopores in a SiNx membrane via controlled breakdown," *Scientific Reports,* vol. 8, no. 1, p. 1234, 2018/01/19 2018.

[93] G. S. Frankel and N. Sridhar, "Understanding localized corrosion," *Materials Today,* vol. 11, no. 10, pp. 38-44, 2008/10/01/ 2008.

[94] M. Bestetti, "Contribution to the study of uniform corrosion by means of the maximum entropy production rate principle," *Protection of Metals and Physical Chemistry of Surfaces,* journal article vol. 52, no. 1, pp. 176-181, January 01 2016.

[95] D. V. Melnikov, Z. K. Hulings, and M. E. Gracheva, "Electro-osmotic flow through nanopores in thin and ultrathin membranes," *Physical Review E,* vol. 95, no. 6, p. 063105, 06/12/ 2017.

[96] M. Mao, J. D. Sherwood, and S. Ghosal, "Electro-osmotic flow through a nanopore," *Journal of Fluid Mechanics,* vol. 749, pp. 167-183, 2014.

[97] K. P. Singh and M. Kumar, "Effect of surface charge density and electro-osmotic flow on ionic current in a bipolar nanopore fluidic diode," *Journal of Applied Physics,* vol. 110, no. 8, p. 084322, 2011.

[98] D.-H. Lin, C.-Y. Lin, S. Tseng, and J.-P. Hsu, "Influence of electroosmotic flow on the ionic current rectification in a pH-regulated, conical nanopore," *Nanoscale,* 10.1039/C5NR03433G vol. 7, no. 33, pp. 14023-14031, 2015.

[99] Z. S. Siwy, "Ion-Current Rectification in Nanopores and Nanotubes with Broken Symmetry," *Advanced Functional Materials,* vol. 16, no. 6, pp. 735-746, 2006.

[100] B. Schiedt, K. Healy, A. P. Morrison, R. Neumann, and Z. Siwy, "Transport of ions and biomolecules through single asymmetric nanopores in polymer films," *Nuclear Instruments and Methods in Physics Research Section B: Beam Interactions with Materials and Atoms,* vol. 236, no. 1, pp. 109-116, 2005/07/01/ 2005.

[101] K. Briggs, H. Kwok, and V. Tabard-Cossa, "Automated Fabrication of 2-nm Solid-State Nanopores for Nucleic Acid Analysis," *Small,* vol. 10, no. 10, pp. 2077-2086, 2014.

[102] T. C. Autumn, B. Kyle, R. H. Adam, and T.-C. Vincent, "Solid-state nanopore localization by controlled breakdown of selectively thinned membranes," *Nanotechnology,* vol. 28, no. 8, p. 085304, 2017.

[103] Y. He, M. Tsutsui, R. H. Scheicher, C. Fan, M. Taniguchi, and T. Kawai, "Mechanism of how salt-gradient-induced charges affect the translocation of DNA molecules through a nanopore," *Biophys J,* vol. 105, no. 3, pp. 776-82, Aug 06 2013.

[104] A. Y. Grosberg and Y. Rabin, "DNA capture into a nanopore: interplay of diffusion and electrohydrodynamics," *J Chem Phys,* vol. 133, no. 16, p. 165102, Oct 28 2010.

[105] F. Nicoli, D. Verschueren, M. Klein, C. Dekker, and M. P. Jonsson, "DNA translocations through solid-state plasmonic nanopores," *Nano Lett,* vol. 14, no. 12, pp. 6917-25, Dec 10 2014.

[106] A. J. Storm, C. Storm, J. Chen, H. Zandbergen, J.-F. Joanny, and C. Dekker, "Fast DNA Translocation through a Solid-State Nanopore," *Nano Letters,* vol. 5, no. 7, pp. 1193-1197, 2005/07/01 2005.

[107] M. Wanunu, W. Morrison, Y. Rabin, A. Y. Grosberg, and A. Meller, "Electrostatic focusing of unlabelled DNA into nanoscale pores using a salt gradient," *Nat Nano,* 10.1038/nnano.2009.379 vol. 5, no. 2, pp. 160-165, 02//print 2010.

[108] E. Stellwagen, Q. Dong, and N. C. Stellwagen, "Monovalent cations affect the free solution mobility of DNA by perturbing the hydrogen-bonded structure of water," *Biopolymers,* vol. 78, no. 2, pp. 62-68, 2005.

[109] A. V. Wolf, *Aqueous solutions and body fluids: their concentrative properties and conversion tables*. Hoeber Medical Division, Harper & Row, 1966.

[110] R. C. Weast, *CRC Handbook of Chemistry and Physics, 70th Edition*. Taylor & Francis, 1989.

[111] T. V. S. L. Satyavani, B. Ramya Kiran, V. Rajesh Kumar, A. Srinivas Kumar, and S. V. Naidu, "Effect of particle size on dc conductivity, activation energy and diffusion coefficient of lithium iron phosphate in Li-ion cells," *Engineering Science and Technology, an International Journal,* vol. 19, no. 1, pp. 40-44, 2016/03/01/ 2016.

[112] R. M. M. Smeets, U. F. Keyser, D. Krapf, M.-Y. Wu, N. H. Dekker, and C. Dekker, "Salt Dependence of Ion Transport and DNA Translocation through Solid-State Nanopores," *Nano Letters,* vol. 6, no. 1, pp. 89-95, 2006/01/01 2006.

[113] I. C. Nova *et al.*, "Investigating asymmetric salt profiles for nanopore DNA sequencing with biological porin MspA," *PLOS ONE,* vol. 12, no. 7, p. e0181599, 2017.

[114] G. S. Manning, "The molecular theory of polyelectrolyte solutions with applications to the electrostatic properties of polynucleotides," *Quarterly Reviews of Biophysics,* vol. 11, no. 2, pp. 179-246, 2009.

[115] J. Bello and J. Shim, "Solid-state nanopore fabrication in LiCl by controlled dielectric breakdown," *Biomedical Microdevices,* vol. 20, no. 2, p. 38, 2018.

[116] H. Falkenhagen, "The principal ideas in the interionic attraction theory of strong electrolytes," *Reviews of Modern Physics,* vol. 3, no. 3, p. 412, 1931.

[117] R. Qiao and N. Aluru, "Ion concentrations and velocity profiles in nanochannel electroosmotic flows," *The Journal of chemical physics,* vol. 118, no. 10, pp. 4692-4701, 2003.

[118] M. M. Hatlo, D. Panja, and R. van Roij, "Translocation of DNA Molecules through Nanopores with Salt Gradients: The Role of Osmotic Flow," *Physical Review Letters,* vol. 107, no. 6, p. 068101, 08/01/ 2011.

[119] Y. Omura, K.-H. Kyung, S. Shiratori, and S.-H. Kim, "Effects of Applied Voltage and Solution pH in Fabricating Multilayers of Weakly Charged Polyelectrolytes and Nanoparticles," *Industrial & Engineering Chemistry Research,* vol. 53, no. 29, pp. 11727-11733, 2014/07/23 2014.

[120] D. Bakewell, *Micro- and Nano-Transport of Biomolecules*. bookboon.com, 2009.

[121] M. Rauscher and S. Dietrich, "Wetting Phenomena in Nanofluidics," *Annual Review of Materials Research,* vol. 38, no. 1, pp. 143-172, 2008.

[122] J. L. Trick, C. Song, E. J. Wallace, and M. S. P. Sansom, "Voltage Gating of a Biomimetic Nanopore: Electrowetting of a Hydrophobic Barrier," *ACS Nano,* vol. 11, no. 2, pp. 1840-1847, 2017/02/28 2017.

[123] S. N. Smirnov, I. V. Vlassiouk, and N. V. Lavrik, "Voltage-Gated Hydrophobic Nanopores," *ACS Nano,* vol. 5, no. 9, pp. 7453-7461, 2011/09/27 2011.

[124] A. Fournier, N. Sasai, M. Nakao, and P.-A. Defossez, "The role of methyl-binding proteins in chromatin organization and epigenome maintenance," *Briefings in Functional Genomics,* vol. 11, no. 3, pp. 251-264, 2012.

[125] B. A. Buck-Koehntop, M. A. Martinez-Yamout, H. J. Dyson, and P. E. Wright, "Kaiso uses all three zinc fingers and adjacent sequence motifs for high affinity binding to sequence-specific and methyl-CpG DNA targets," *FEBS letters,* vol. 586, no. 6, pp. 734-739, 2012.

[126] L. Parry and A. R. Clarke, "The roles of the methyl-cpg binding proteins in cancer," *Genes & Cancer,* vol. 2, no. 6, pp. 618-630, 2011.

[127] G. J. P. Filion, S. Zhenilo, S. Salozhin, D. Yamada, E. Prokhortchouk, and P.-A. Defossez, "A Family of Human Zinc Finger Proteins That Bind Methylated DNA and Repress Transcription," *Molecular and Cellular Biology,* vol. 26, no. 1, p. 169, 2006.

[128] T. Clouaire, J. I. de las Heras, C. Merusi, and I. Stancheva, "Recruitment of MBD1 to target genes requires sequence-specific interaction of the MBD domain with methylated DNA," *Nucleic Acids Research,* vol. 38, no. 14, pp. 4620-4634, 2010.

[129] A. Chatagnon *et al.*, "Preferential binding of the methyl-CpG binding domain protein 2 at methylated transcriptional start site regions," *Epigenetics,* vol. 6, no. 11, pp. 1295-1307, 2011/11/01 2011.

[130] K. H. Wood and Z. Zhou, "Emerging Molecular and Biological Functions of MBD2, a Reader of DNA Methylation," (in English), Review vol. 7, no. 93, 2016-May-26 2016.

[131] C. Stirzaker *et al.*, "Methyl-CpG-binding protein MBD2 plays a key role in maintenance and spread of DNA methylation at CpG islands and shores in cancer," *Oncogene,* Original Article vol. 36, p. 1328, 09/05/online 2016.

[132] J. J. Kasianowicz, E. Brandin, D. Branton, and D. W. Deamer, "Characterization of individual polynucleotide molecules using a membrane channel," *Proceedings of the National Academy of Sciences,* vol. 93, no. 24, pp. 13770-13773, 1996.

[133] B. M. Venkatesan and R. Bashir, "Nanopore sensors for nucleic acid analysis," (in eng), *Nature Nanotechnology,* vol. 6, no. 10, pp. 615-24, Sep 18 2011.

[134] R. D. Maitra, J. Kim, and W. B. Dunbar, "Recent advances in nanopore sequencing," *Electrophoresis,* vol. 33, no. 23, pp. 3418-3428, 11/09 2012.

[135] J. Shim *et al.*, "Detection of methylation on dsDNA using nanopores in a MoS2 membrane," *Nanoscale*, 10.1039/C7NR03092D 2017.

[136] J. E. Reiner, J. J. Kasianowicz, B. J. Nablo, and J. W. F. Robertson, "Theory for polymer analysis using nanopore-based single-molecule mass spectrometry," *Proceedings of the National Academy of Sciences*, vol. 107, no. 27, pp. 12080-12085, 2010.

[137] J. J. Kasianowicz, J. W. F. Robertson, E. R. Chan, J. E. Reiner, and V. M. Stanford, "Nanoscopic porous sensors," *Annual Review of Analytical Chemistry*, vol. 1, no. 1, pp. 737-766, 2008/07/01 2008.

[138] E. C. Yusko *et al.*, "Controlling protein translocation through nanopores with bio-inspired fluid walls," *Nature Nanotechnology*, Article vol. 6, p. 253, 02/20/online 2011.

[139] J. Bello, M. Mowla, N. Troise, J. Soyring, J. Borgesi, and J. Shim, *Increased dwell time and occurrence of dsDNA translocation events through solid state nanopores by LiCl concentration gradients*. 2018.

[140] B. W. Heimer, B. E. Tam, and H. D. Sikes, "Characterization and directed evolution of a methyl-binding domain protein for high-sensitivity DNA methylation analysis," *Protein Engineering, Design and Selection*, vol. 28, no. 12, pp. 543-551, 2015.

[141] H. F. Jørgensen, K. Adie, P. Chaubert, and A. P. Bird, "Engineering a high-affinity methyl-CpG-binding protein," *Nucleic Acids Research*, vol. 34, no. 13, pp. e96-e96, 2006.

[142] J. N. Scarsdale, H. D. Webb, G. D. Ginder, and D. C. Williams, Jr, "Solution structure and dynamic analysis of chicken MBD2 methyl binding domain bound to a target-methylated DNA sequence," *Nucleic Acids Research*, vol. 39, no. 15, pp. 6741-6752, 2011.

[143] H. Bayley, "Nanopore Sequencing: From Imagination to Reality," *Clinical Chemistry*, 10.1373/clinchem.2014.223016 vol. 61, no. 1, p. 25, 2014.

[144] F. Maria, "Threading DNA through nanopores for biosensing applications," *Journal of Physics: Condensed Matter*, vol. 27, no. 27, p. 273101, 2015.

[145] K. Liu, J. Feng, A. Kis, and A. Radenovic, "Atomically Thin Molybdenum Disulfide Nanopores with High Sensitivity for DNA Translocation," *ACS Nano*, vol. 8, no. 3, pp. 2504-2511, 2014/03/25 2014.

[146] A. B. Farimani, K. Min, and N. R. Aluru, "DNA Base Detection Using a Single-Layer MoS2," *ACS Nano,* vol. 8, no. 8, pp. 7914-7922, 2014/08/26 2014.

Appendix A

Supplemental Current Characteristic Traces of Controlled Dielectric Breakdown

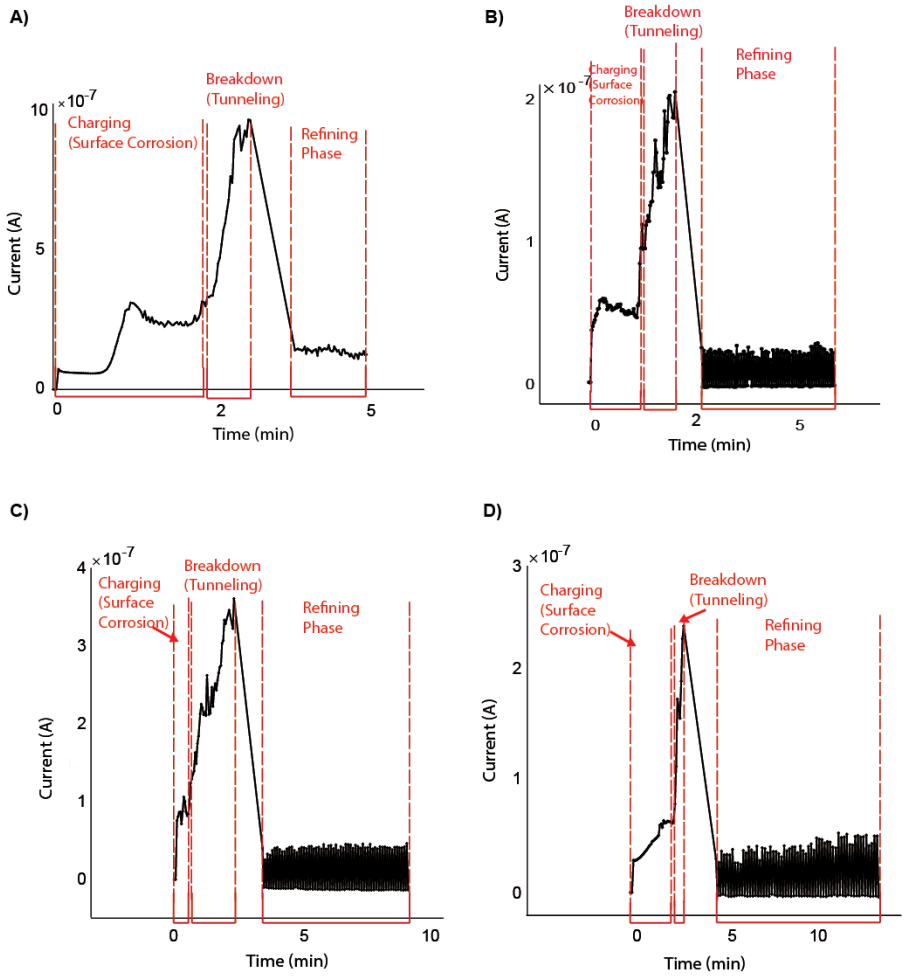

Current Characteristic traces describing progression of nanopore formation during controlled dielectric breakdown. Plots generated by the MATLAB script used for controlled dielectric breakdown describes the mechanism by which the breakdown occurs and highlights three distinct peaks that are indicative of the molecular interactions occurring at that time point. The initial two peaks represent a region driven by surface charge corrosion where the interaction between the ions and membrane cause the accumulation of traps along the center of the free-standing membrane. The third upward spike represents a region of trap assisted tunneling where the breakdown of the membrane occurs. A) illustrates a 5.98 nm pore that was fabricated in 1 M KCl buffer. B) illustrates a 6.37 nm pore fabricated in 1 M LiCl buffer. C) illustrates a 5.46 nm pore fabricated in 1 M KCl buffer. D) illustrates a 5.85 nm pore fabricated in 1 M LiCl buffer.

Appendix B

MATLAB Nanopore Fabrication Code

```
function varargout = Pore_GUI_v5(varargin)
% PORE_GUI_V5 MATLAB code for Pore_GUI_v5.fig
%      PORE_GUI_V5, by itself, creates a new PORE_GUI_V5 or raises the existing
%      singleton*.
%
%      H = PORE_GUI_V5 returns the handle to a new PORE_GUI_V5 or the handle to
%      the existing singleton*.
%
%      PORE_GUI_V5('CALLBACK',hObject,eventData,handles,...) calls the local
%      function named CALLBACK in PORE_GUI_V5.M with the given input
arguments.
%
%      PORE_GUI_V5('Property','Value',...) creates a new PORE_GUI_V5 or raises the
%      existing singleton*.  Starting from the left, property value pairs are
%      applied to the GUI before Pore_GUI_v5_OpeningFcn gets called.  An
%      unrecognized property name or invalid value makes property application
%      stop.  All inputs are passed to Pore_GUI_v5_OpeningFcn via varargin.
%
%      *See GUI Options on GUIDE's Tools menu.  Choose "GUI allows only one
%      instance to run (singleton)".
%
% See also: GUIDE, GUIDATA, GUIHANDLES

% Edit the above text to modify the response to help Pore_GUI_v5

% Last Modified by GUIDE v2.5 22-Jun-2018 13:58:11

% Begin initialization code - DO NOT EDIT
```

```
gui_Singleton = 1;
gui_State = struct('gui_Name',       mfilename, ...
    'gui_Singleton',  gui_Singleton, ...
    'gui_OpeningFcn', @Pore_GUI_v5_OpeningFcn, ...
    'gui_OutputFcn',  @Pore_GUI_v5_OutputFcn, ...
    'gui_LayoutFcn',  [] , ...
    'gui_Callback',   []);
if nargin && ischar(varargin{1})
    gui_State.gui_Callback = str2func(varargin{1});
end

if nargout
    [varargout{1:nargout}] = gui_mainfcn(gui_State, varargin{:});
else
    gui_mainfcn(gui_State, varargin{:});
end
% End initialization code - DO NOT EDIT



% --- Executes just before Pore_GUI_v5 is made visible.
function Pore_GUI_v5_OpeningFcn(hObject, eventdata, handles, varargin)
% This function has no output args, see OutputFcn.
% hObject    handle to figure
% eventdata  reserved - to be defined in a future version of MATLAB
% handles    structure with handles and user data (see GUIDATA)
% varargin   command line arguments to Pore_GUI_v5 (see VARARGIN)


% Choose default command line output for Pore_GUI_v5
handles.output = hObject;
```

```
current = 0;

% handles.current_char = current_char;

% Set axes
handles.current_graph = axes('parent',handles.current_char,....
   'YGrid','on',...
   'YColor',[0 0 0],...
   'XGrid','on',...
   'XColor',[0 0 0],...
   'Color',[1 1 1]);

hold on;
handles.time = now;
handles.current_char =
plot(handles.current_graph,handles.time,current,'Marker','.','LineWidth',1,'Color',[0 0 0]);

xlim(handles.current_graph,[min(handles.time) max(handles.time+0.001)]);

% Create xlabel
xlabel('Time (min)','FontWeight','bold','FontSize',14,'Color',[0 0 0]);

% Create ylabel
ylabel('Current (A)','FontWeight','bold','FontSize',14,'Color',[0 0 0]);

% Create title
title('Current Characteristics','FontSize',15,'Color',[0 0 0]);

% Update handles structure
% disable textfields and button until iniitialized
```

```
set(handles.Cut_Off_Current_edit,'Enable','off');
set(handles.air_bubble_edit,'Enable','off');
set(handles.Voltage_edit,'Enable','off');
set(handles.pulse_dur_edit,'Enable','off');
set(handles.Pulse_volt_min_edit,'Enable','off');
set(handles.pulse_volt_max_edit,'Enable','off');
set(handles.comm_edit,'Enable','off');
set(handles.Exe_comm_button,'Enable','off');
set(handles.Output_edit,'Enable','off');
set(handles.Run_button,'Enable','off');
set(handles.Pause_Button,'Enable','off');
set(handles.e_stop_button,'Enable','off');
set(handles.Export,'Enable','off');
set(handles.refine,'Enable','off');
guidata(hObject, handles);



% UIWAIT makes Pore_GUI_v5 wait for user response (see UIRESUME)
% uiwait(handles.figure1);



% --- Outputs from this function are returned to the command line.
function varargout = Pore_GUI_v5_OutputFcn(hObject, eventdata, handles)
% varargout  cell array for returning output args (see VARARGOUT);
% hObject    handle to figure
% eventdata  reserved - to be defined in a future version of MATLAB
% handles    structure with handles and user data (see GUIDATA)

% Get default command line output from handles structure
varargout{1} = handles.output;
```

```
% --- Executes on button press in intit_button.
function intit_button_Callback(hObject, eventdata, handles)
% hObject    handle to intit_button (see GCBO)
% eventdata  reserved - to be defined in a future version of MATLAB
% handles    structure with handles and user data (see GUIDATA)

% Find a GPIB object.
obj1 = instrfind('Type', 'gpib', 'BoardIndex', 7, 'PrimaryAddress', 20, 'Tag', '');%defines
gpib board (Agilent) as obj1

% Create the GPIB object if it does not exist
% otherwise use the object that was found.

if isempty(obj1)
   obj1 = gpib('AGILENT', 7, 20);
else
   fclose(obj1);
   obj1 = obj1(1);
end

fopen(obj1);               % Connect to instrument object, obj1.

fprintf(obj1,'*RST');       %returns instrument to initial state
fprintf(obj1,':SOURce:VOLTage:LEVel:IMMediate:AMPLitude 0');
fprintf(obj1,'SOURce:VOLTage:RANGe 50');    %sets range of instrument to 50V
(default is 10V)
fprintf(obj1,'SOURce:VOLTage:STATE on');    %Remotely turns on voltage source
operate
```

```
set(handles.Cut_Off_Current_edit,'Enable','on');
set(handles.air_bubble_edit,'Enable','on');
set(handles.Voltage_edit,'Enable','on');
set(handles.pulse_dur_edit,'Enable','on');
set(handles.Pulse_volt_min_edit,'Enable','on');
set(handles.pulse_volt_max_edit,'Enable','on');
set(handles.comm_edit,'Enable','on');
set(handles.Exe_comm_button,'Enable','on');
set(handles.Output_edit,'Enable','on');
set(handles.Run_button,'Enable','on');
set(handles.Pause_Button,'Enable','on');
set(handles.e_stop_button,'Enable','on');
set(handles.Export,'Enable','on');
set(handles.refine,'Enable','on');
set(handles.intit_button,'Enable','off');

handles.obj1 = obj1;
handles.command = get(handles.comm_edit, 'String');
handles.cut_off_current = get(handles.Cut_Off_Current_edit, 'String');
handles.voltage = get(handles.Voltage_edit, 'String');
handles.air_bubble = get(handles.air_bubble_edit, 'String');
handles.pulse_dur = get(handles.pulse_dur_edit, 'String');
handles.pulse_min = get(handles.Pulse_volt_min_edit, 'String');
handles.pulse_max = get(handles.pulse_volt_max_edit, 'String');
handles.refine=get(handles.refine, 'String');
handles.output_log = '';
handles.starttime = '';

handles.output_log = [handles.output_log newline 'Initial Conditions'];
guidata(hObject,handles);
```

```
% --- Executes on button press in Run_button.
function Run_button_Callback(hObject, eventdata, handles)
% hObject    handle to Run_button (see GCBO)
% eventdata  reserved - to be defined in a future version of MATLAB
% handles    structure with handles and user data (see GUIDATA)
%variables
sustain_dur = 3600;   %set duration of sustained voltage application (in seconds)
count = 1;
time = handles.time;
pulse_dur =  str2double(handles.pulse_dur);
cut_off = (str2double(handles.cut_off_current))*10^-09;
air_bubble = (str2double(handles.air_bubble))*10^-09;

q = clock;
sc= num2str(q(4));
sd= num2str(q(5));
se= num2str(q(6));
handles.starttime = [sc ':' sd ':' se];

handles.output_log = [handles.output_log newline ['The start time is '
handles.starttime]];
set(handles.Output_edit, 'String', ['The starttime is '  handles.starttime]);
guidata(hObject,handles);

t5=[];
t10=[];

volt_string=':SOURce:VOLTage:LEVel:IMMediate:AMPLitude ';
timer = 1;

while true      %initiate voltage loop
```

```
    handles.time(count) = datenum(clock);
    fprintf(handles.obj1,'MEASure:CURRent:DC?'); % To measure current the command
is MEASURE:CURRENT:DC?
    current(count) = fscanf(handles.obj1,'%f');  %%#ok<SAGROW>
    set(handles.current_char,'YData',current,'XData',time);
    datetick('x','HH:MM:SS');

    %perform 4 measurements of current and time
    a1=query(handles.obj1,'MEASure:CURRent:DC?');
    time(count) = datenum(clock);
    fprintf(handles.obj1,'MEASure:CURRent:DC?'); % To measure current the command
is MEASURE:CURRENT:DC?
    current(count) = fscanf(handles.obj1,'%f');  %%#ok<SAGROW>
    set(handles.current_char,'YData',current,'XData',time);
    datetick('x','HH:MM:SS');
    count= count+1;
    I1=a1(2:13);

    a2=query(handles.obj1,'MEASure:CURRent:DC?');
    time(count) = datenum(clock);
    fprintf(handles.obj1,'MEASure:CURRent:DC?'); % To measure current the command
is MEASURE:CURRENT:DC?
    current(count) = fscanf(handles.obj1,'%f');  %%#ok<SAGROW>
    set(handles.current_char,'YData',current,'XData',time);
    datetick('x','HH:MM:SS');
    count= count+1;
    I2=a2(2:13);

    a3=query(handles.obj1,'MEASure:CURRent:DC?');
    time(count) = datenum(clock);
    fprintf(handles.obj1,'MEASure:CURRent:DC?'); % To measure current the command
```

```
is MEASURE:CURRENT:DC?
    current(count) = fscanf(handles.obj1,'%f');  %%#ok<SAGROW>
    set(handles.current_char,'YData',current,'XData',time);
    datetick('x','HH:MM:SS');
    count= count+1;
    I3=a3(2:13);

    a4=query(handles.obj1,'MEASure:CURRent:DC?');
    time(count) = datenum(clock);
    fprintf(handles.obj1,'MEASure:CURRent:DC?'); % To measure current the command
is MEASURE:CURRENT:DC?
    current(count) = fscanf(handles.obj1,'%f');  %%#ok<SAGROW>
    set(handles.current_char,'YData',current,'XData',time);
    datetick('x','HH:MM:SS');
    count= count+1;
    I4=a4(2:13);

    I_sum=str2double(I1)+str2double(I2)+str2double(I3)+str2double(I4);      % sum of
Current values

    if (I_sum/4)<50E-09 %If average of measured current points are greater than 15 nA
and less than 50nA iniitiate sustained voltage run (I_sum/4)<15E-09 &&

        message = [volt_string get(handles.Voltage_edit, 'String')];
        fprintf(handles.obj1,message);
        f=query(handles.obj1,':SOURce:VOLTage:LEVel:IMMediate:AMPLitude?');
        h=get(handles.Cut_Off_Current_edit, 'String');
        ff=str2double(f);
        hhh=str2double(h);

        for i=timer:sustain_dur        %counter for sustained voltage run. 1 iteration
```

```
        message = [volt_string get(handles.Voltage_edit, 'String')];
        fprintf(handles.obj1,message);

        if ff==str2double(f)

        else
            z = clock;
            cf= num2str(z(4));
            cg= num2str(z(5));
            ch= num2str(z(6));
            handles.output_log = [handles.output_log newline ['The applied voltage is set
to ' get(handles.Voltage_edit, 'String') ' V at ' cf ':' cg ':' ch]];
            set(handles.Output_edit, 'String', ['The applied voltage is set to '
get(handles.Voltage_edit, 'String') ' V at ' cf ':' cg ':' ch]);
            guidata(hObject,handles);
            f=num2str(ff);
        end

        if hhh==str2double(h)
        else
            c = clock;
            hi= num2str(c(4));
            hn= num2str(c(5));
            ht= num2str(c(6));

            handles.output_log = [handles.output_log newline 'The cutoff current is '
get(handles.Cut_Off_Current_edit, 'String') ' nA at ' hi ':' hn ':' ht];
            set(handles.Output_edit, 'String', ['The cutoff current is '
get(handles.Cut_Off_Current_edit, 'String') ' nA at ' hi ':' hn ':' ht]);
            guidata(hObject,handles);
```

```
            h=num2str(hhh);
        end

        set(handles.Timer_edit, 'String', i);
        pause(0.5)
        b=query(handles.obj1,'MEASure:CURRent:DC?');
        H=b(2:13);
        %           Meas_points2=[meas_points2; str2double(H)];
        T2=[t5; clock];

        if i>5
            if str2double(H)> (str2double(get(handles.Cut_Off_Current_edit,
'String'))*10^-09)
                c = clock;
                hh= num2str(c(4));
                hm= num2str(c(5));
                hs= num2str(c(6));

                handles.output_log = [handles.output_log newline 'The current is ' H ' nA at '
hh ':' hm ':' hs];
                set(handles.Output_edit, 'String', ['The current is ' H ' nA at ' hh ':' hm ':' hs]);
                guidata(hObject,handles);
                pause (0.5)
                l1=query(handles.obj1,'MEASure:CURRent:DC?');
                Check1=l1(2:13);

                pause(0.5)
                l2=query(handles.obj1,'MEASure:CURRent:DC?');
                Check2=l2(2:13);

                pause(0.5)
```

```
                l3=query(handles.obj1,'MEASure:CURRent:DC?');
                Check3=l3(2:13);

                pause(0.5)
                l4=query(handles.obj1,'MEASure:CURRent:DC?');
                Check4=l4(2:13);



check_sum=str2double(Check1)+str2double(Check2)+str2double(Check3)+str2double(C
heck4);

                if (check_sum/4)> (str2double(get(handles.Cut_Off_Current_edit,
'String'))*10^-09)
                    t5=T2;

ff=str2double(query(handles.obj1,':SOURce:VOLTage:LEVel:IMMediate:AMPLitude?')
);
                    fprintf(handles.obj1,':SOURce:VOLTage:LEVel:IMMediate:AMPLitude
0');

                    break
                else
                end
            else
            end
            time(count) = datenum(clock);
            c=query(handles.obj1,'MEASure:CURRent:DC?');

            fprintf(handles.obj1,'MEASure:CURRent:DC?'); % To measure current the
command is MEASURE:CURRENT:DC?
```

```
        current(count) = fscanf(handles.obj1,'%f');  %%#ok<SAGROW>
        set(handles.current_char,'YData',current,'XData',time);
        datetick('x','HH:MM:SS');
        count= count+1;

        t5=T2;


ff=str2double(query(handles.obj1,':SOURce:VOLTage:LEVel:IMMediate:AMPLitude?')
);
        hhh=str2double(get(handles.Cut_Off_Current_edit, 'String'));



        timer = i+2;
    end

  elseif (I_sum/4)> 50E-09
    handles.output_log = [handles.output_log newline 'Membrane has broken...'];
    set(handles.Output_edit, 'String', 'Membrane has broken...');
    guidata(hObject,handles);
    fprintf(handles.obj1,':SOURce:VOLTage:LEVel:IMMediate:AMPLitude 0');

  else
    handles.output_log = [handles.output_log newline 'Nanopore has formed'];
    set(handles.Output_edit, 'String', 'Nanopore has formed');
    guidata(hObject,handles);
    fprintf(handles.obj1,':SOURce:VOLTage:LEVel:IMMediate:AMPLitude 0');
  end

  if ff==str2double(f)
```

```
    else
        z = clock;
        cf= num2str(z(4));
        cg= num2str(z(5));
        ch= num2str(z(6));
        handles.output_log = [handles.output_log newline ['The applied voltage is set to '
get(handles.Voltage_edit, 'String') ' V at ' cf ':' cg ':' ch]];
        set(handles.Output_edit, 'String', ['The applied voltage is set to '
get(handles.Voltage_edit, 'String') ' V at ' cf ':' cg ':' ch]);
        guidata(hObject,handles);
        f=num2str(ff);
    end



    fprintf(handles.obj1,':SOURce:VOLTage:LEVel:IMMediate:AMPLitude 0');

    pause(10)

    fprintf(handles.obj1,':SOURce:VOLTage:LEVel:IMMediate:AMPLitude 1');
    pause(20)

    c1=query(handles.obj1,'MEASure:CURRent:DC?');
    time(count) = datenum(clock);
    fprintf(handles.obj1,'MEASure:CURRent:DC?'); % To measure current the command
is MEASURE:CURRENT:DC?
    current(count) = fscanf(handles.obj1,'%f');  %%#ok<SAGROW>
    set(handles.current_char,'YData',current,'XData',time);
    J1=c1(2:13)

    c2=query(handles.obj1,'MEASure:CURRent:DC?');
```

```
    time(count) = datenum(clock);
    fprintf(handles.obj1,'MEASure:CURRent:DC?'); % To measure current the command
is MEASURE:CURRENT:DC?
    current(count) = fscanf(handles.obj1,'%f');  %%#ok<SAGROW>
    set(handles.current_char,'YData',current,'XData',time);
    J2=c2(2:13)

    c3=query(handles.obj1,'MEASure:CURRent:DC?');
    time(count) = datenum(clock);
    fprintf(handles.obj1,'MEASure:CURRent:DC?'); % To measure current the command
is MEASURE:CURRENT:DC?
    current(count) = fscanf(handles.obj1,'%f');  %%#ok<SAGROW>
    set(handles.current_char,'YData',current,'XData',time);
    J3=c3(2:13)

    c4=query(handles.obj1,'MEASure:CURRent:DC?');
    time(count) = datenum(clock);
    fprintf(handles.obj1,'MEASure:CURRent:DC?'); % To measure current the command
is MEASURE:CURRENT:DC?
    current(count) = fscanf(handles.obj1,'%f');  %%#ok<SAGROW>
    set(handles.current_char,'YData',current,'XData',time);
    J4=c4(2:13)

    J_sum=str2double(J1)+str2double(J2)+str2double(J3)+str2double(J4);

    % Refining

    if (J_sum/4)>15E-09 && (J_sum/4)<50E-09
        handles.output_log = [handles.output_log newline 'Nanopore has formed'];
        set(handles.Output_edit, 'String', 'Nanopore has formed');
        guidata(hObject,handles);
```

```
        fprintf(handles.obj1,':SOURce:VOLTage:LEVel:IMMediate:AMPLitude 0');

        timer=1;



        for i=timer:(str2double(get(handles.pulse_dur_edit, 'String')))
            time(count) = datenum(clock);
            set(handles.Timer_edit, 'String', i);
            volt=query(handles.obj1,':SOURce:VOLTage:LEVel:IMMediate:AMPLitude?');

            T4=[t10; clock];

            if str2double(volt) == str2double(get(handles.pulse_volt_max_edit, 'String'))
%10
                message_min = [volt_string get(handles.Pulse_volt_min_edit, 'String');];

                fprintf(handles.obj1,message_min);

                pause(0.5)
            else
                message_max = [volt_string get(handles.pulse_volt_max_edit, 'String');];

                fprintf(handles.obj1,message_max);
                pause(0.5)
            end
            fprintf(handles.obj1,'MEASure:CURRent:DC?'); % To measure current the
command is MEASURE:CURRENT:DC?
            current(count) = fscanf(handles.obj1,'%f');  %%#ok<SAGROW>
            set(handles.current_char,'YData',current,'XData',time);
            datetick('x','HH:MM:SS');
```

```
            count = count +1;

            t10=T4;

        end
        hold on
        fprintf(handles.obj1,':SOURce:VOLTage:LEVel:IMMediate:AMPLitude 0');
        break

    elseif (J_sum/4)>50E-09

        handles.output_log = [handles.output_log newline 'Membrane has broken...'];
        set(handles.Output_edit, 'String', 'Membrane has broken...');
        guidata(hObject,handles);
        fprintf(handles.obj1,':SOURce:VOLTage:LEVel:IMMediate:AMPLitude 0');


        time(count) = datenum(clock);
        fprintf(handles.obj1,'MEASure:CURRent:DC?'); % To measure current the
command is MEASURE:CURRENT:DC?
        current(count) = fscanf(handles.obj1,'%f');  %%#ok<SAGROW>
        set(handles.current_char,'YData',current,'XData',time);
        datetick('x','HH:MM:SS');
        count = count +1;

        hold on
        break

    elseif (J_sum/4)<15E-09 %(J_sum/4)>08E-09 &&

        handles.output_log = [handles.output_log newline ['There is a small nanopore
```

```
present. Voltage reduced to 8 V. Click \n the mouse to continue or any key to end.' ]];
      set(handles.Output_edit, 'String', 'There is a small nanopore present. Voltage
reduced to 8 V. Click \n the mouse to continue or any key to end.');
      guidata(hObject,handles);
      w = waitforbuttonpress;

      if w == 0
      set(handles.Voltage_edit, 'String', '8')

      else
      handles.output_log = [handles.output_log newline 'SMALL nanopore has formed'];
      set(handles.Output_edit, 'String', 'SMALL nanopore has formed');
      guidata(hObject,handles);
      fprintf(handles.obj1,':SOURce:VOLTage:LEVel:IMMediate:AMPLitude 0');

      timer=1;



      for i=timer:(str2double(get(handles.pulse_dur_edit, 'String')))
         time(count) = datenum(clock);
         set(handles.Timer_edit, 'String', i);
         volt=query(handles.obj1,':SOURce:VOLTage:LEVel:IMMediate:AMPLitude?');

         T4=[t10; clock];

         if str2double(volt) == str2double(get(handles.pulse_volt_max_edit, 'String'))
%10
            message_min = [volt_string get(handles.Pulse_volt_min_edit, 'String');];

            fprintf(handles.obj1,message_min);
```

```
            pause(0.5)
        else
            message_max = [volt_string get(handles.pulse_volt_max_edit, 'String');];

            fprintf(handles.obj1,message_max);
            pause(0.5)
        end
        fprintf(handles.obj1,'MEASure:CURRent:DC?'); % To measure current the
command is MEASURE:CURRENT:DC?
        current(count) = fscanf(handles.obj1,'%f');  %%#ok<SAGROW>
        set(handles.current_char,'YData',current,'XData',time);
        datetick('x','HH:MM:SS');

        count = count +1;

        t10=T4;

    end
    hold on
    fprintf(handles.obj1,':SOURce:VOLTage:LEVel:IMMediate:AMPLitude 0');
    break
    end

else



end
i = clock;
cc= num2str(i(4));
cd= num2str(i(5));
ce= num2str(i(6));
```

```
    handles.output_log = [handles.output_log newline ['The endtime is '  cc ':' cd ':' ce]];
    set(handles.Output_edit, 'String', ['The endtime is '   cc ':' cd ':' ce]);

end

handles.output_log = [handles.output_log newline 'You are done! Click the Export
Button to Save'];
set(handles.Output_edit, 'String', 'You are done! Click the Export Button to Save');

guidata(hObject,handles);

% --- Executes on button press in Pause_Button.
function Pause_Button_Callback(hObject, eventdata, handles)
% hObject    handle to Pause_Button (see GCBO)
% eventdata  reserved - to be defined in a future version of MATLAB
% handles    structure with handles and user data (see GUIDATA)
fprintf(handles.obj1,':SOURce:VOLTage:LEVel:IMMediate:AMPLitude 0');
k = waitforbuttonpress;
if k == 1
else
end
guidata(hObject,handles);




% --- Executes on button press in e_stop_button.
function e_stop_button_Callback(hObject, eventdata, handles)
% hObject    handle to e_stop_button (see GCBO)
% eventdata  reserved - to be defined in a future version of MATLAB
```

```
% handles    structure with handles and user data (see GUIDATA)
fprintf(handles.obj1,':SOURce:VOLTage:LEVel:IMMediate:AMPLitude 0');
quit;
guidata(hObject,handles);

function Cut_Off_Current_edit_Callback(hObject, eventdata, handles)
% hObject    handle to Cut_Off_Current_edit (see GCBO)
% eventdata  reserved - to be defined in a future version of MATLAB
% handles    structure with handles and user data (see GUIDATA)

% Hints: get(hObject,'String') returns contents of Cut_Off_Current_edit as text
%        str2double(get(hObject,'String')) returns contents of Cut_Off_Current_edit as a
double
handles.cut_off_current = get(hObject, 'String');
i = clock;
cc= num2str(i(4));
cd= num2str(i(5));
ce= num2str(i(6));
handles.output_log = [handles.output_log newline ['The cutoff current is set to '
handles.cut_off_current ' nA at ' cc ':' cd ':' ce]];
set(handles.Output_edit, 'String', ['The cutoff current is set to ' handles.cut_off_current '
nA at ' cc ':' cd ':' ce]);
guidata(hObject,handles);

% --- Executes during object creation, after setting all properties.
function Cut_Off_Current_edit_CreateFcn(hObject, eventdata, handles)
% hObject    handle to Cut_Off_Current_edit (see GCBO)
% eventdata  reserved - to be defined in a future version of MATLAB
% handles    empty - handles not created until after all CreateFcns called

% Hint: edit controls usually have a white background on Windows.
```

```
%       See ISPC and COMPUTER.
if ispc && isequal(get(hObject,'BackgroundColor'),
get(0,'defaultUicontrolBackgroundColor'))
    set(hObject,'BackgroundColor','white');
end



function Voltage_edit_Callback(hObject, eventdata, handles)
% hObject    handle to Voltage_edit (see GCBO)
% eventdata  reserved - to be defined in a future version of MATLAB
% handles    structure with handles and user data (see GUIDATA)

% Hints: get(hObject,'String') returns contents of Voltage_edit as text
%        str2double(get(hObject,'String')) returns contents of Voltage_edit as a double
handles.voltage = get(hObject, 'String');
i = clock;
cc= num2str(i(4));
cd= num2str(i(5));
ce= num2str(i(6));
handles.output_log = [handles.output_log newline ['The applied voltage is set to '
handles.voltage ' V at ' cc ':' cd ':' ce]];
set(handles.Output_edit, 'String', ['The applied voltage is set to ' handles.voltage ' V at ' cc
':' cd ':' ce]);

guidata(hObject,handles);

% --- Executes during object creation, after setting all properties.
function Voltage_edit_CreateFcn(hObject, eventdata, handles)
% hObject    handle to Voltage_edit (see GCBO)
% eventdata  reserved - to be defined in a future version of MATLAB
% handles    empty - handles not created until after all CreateFcns called
```

```
% Hint: edit controls usually have a white background on Windows.
%       See ISPC and COMPUTER.
if ispc && isequal(get(hObject,'BackgroundColor'),
get(0,'defaultUicontrolBackgroundColor'))
   set(hObject,'BackgroundColor','white');
end



function air_bubble_edit_Callback(hObject, eventdata, handles)
% hObject    handle to air_bubble_edit (see GCBO)
% eventdata  reserved - to be defined in a future version of MATLAB
% handles    structure with handles and user data (see GUIDATA)

% Hints: get(hObject,'String') returns contents of air_bubble_edit as text
%        str2double(get(hObject,'String')) returns contents of air_bubble_edit as a double
handles.air_bubble_cut_off = get(hObject, 'String');
guidata(hObject,handles);

% --- Executes during object creation, after setting all properties.
function air_bubble_edit_CreateFcn(hObject, eventdata, handles)
% hObject    handle to air_bubble_edit (see GCBO)
% eventdata  reserved - to be defined in a future version of MATLAB
% handles    empty - handles not created until after all CreateFcns called

% Hint: edit controls usually have a white background on Windows.
%       See ISPC and COMPUTER.
if ispc && isequal(get(hObject,'BackgroundColor'),
get(0,'defaultUicontrolBackgroundColor'))
   set(hObject,'BackgroundColor','white');
```

```
end



function Pulse_volt_min_edit_Callback(hObject, eventdata, handles)
% hObject    handle to Pulse_volt_min_edit (see GCBO)
% eventdata  reserved - to be defined in a future version of MATLAB
% handles    structure with handles and user data (see GUIDATA)

% Hints: get(hObject,'String') returns contents of Pulse_volt_min_edit as text
%        str2double(get(hObject,'String')) returns contents of Pulse_volt_min_edit as a
double
handles.pulse_volt_min = get(hObject, 'String');

i = clock;
cc= num2str(i(4));
cd= num2str(i(5));
ce= num2str(i(6));
handles.output_log = [handles.output_log newline ['The min pulse voltage is set to '
handles.pulse_volt_min ' V at ' cc ':' cd ':' ce]];
set(handles.Output_edit, 'String', ['The min pulse voltage is set to '
handles.pulse_volt_min ' V at ' cc ':' cd ':' ce]);

guidata(hObject,handles);

% --- Executes during object creation, after setting all properties.
function Pulse_volt_min_edit_CreateFcn(hObject, eventdata, handles)
% hObject    handle to Pulse_volt_min_edit (see GCBO)
% eventdata  reserved - to be defined in a future version of MATLAB
% handles    empty - handles not created until after all CreateFcns called

% Hint: edit controls usually have a white background on Windows.
```

```
%       See ISPC and COMPUTER.
if ispc && isequal(get(hObject,'BackgroundColor'),
get(0,'defaultUicontrolBackgroundColor'))
    set(hObject,'BackgroundColor','white');
end



function pulse_volt_max_edit_Callback(hObject, eventdata, handles)
% hObject    handle to pulse_volt_max_edit (see GCBO)
% eventdata  reserved - to be defined in a future version of MATLAB
% handles    structure with handles and user data (see GUIDATA)

% Hints: get(hObject,'String') returns contents of pulse_volt_max_edit as text
%        str2double(get(hObject,'String')) returns contents of pulse_volt_max_edit as a
double
handles.pulse_volt_max = get(hObject, 'String');

i = clock;
cc= num2str(i(4));
cd= num2str(i(5));
ce= num2str(i(6));
handles.output_log = [handles.output_log newline ['The max pulse voltage is set to '
handles.pulse_volt_max ' V at ' cc ':' cd ':' ce]];
set(handles.Output_edit, 'String', ['The max pulse voltage is set to '
handles.pulse_volt_max ' V at ' cc ':' cd ':' ce]);

guidata(hObject,handles);

% --- Executes during object creation, after setting all properties.
function pulse_volt_max_edit_CreateFcn(hObject, eventdata, handles)
% hObject    handle to pulse_volt_max_edit (see GCBO)
```

```
% eventdata  reserved - to be defined in a future version of MATLAB
% handles    empty - handles not created until after all CreateFcns called

% Hint: edit controls usually have a white background on Windows.
%       See ISPC and COMPUTER.
if ispc && isequal(get(hObject,'BackgroundColor'),
get(0,'defaultUicontrolBackgroundColor'))
   set(hObject,'BackgroundColor','white');
end



function comm_edit_Callback(hObject, eventdata, handles)
% hObject    handle to comm_edit (see GCBO)
% eventdata  reserved - to be defined in a future version of MATLAB
% handles    structure with handles and user data (see GUIDATA)

% Hints: get(hObject,'String') returns contents of comm_edit as text
%        str2double(get(hObject,'String')) returns contents of comm_edit as a double
handles.command = get(hObject, 'String');
guidata(hObject,handles);

% --- Executes on button press in Exe_comm_button.
function Exe_comm_button_Callback(hObject, eventdata, handles)
% hObject    handle to Exe_comm_button (see GCBO)
% eventdata  reserved - to be defined in a future version of MATLAB
% handles    structure with handles and user data (see GUIDATA)
handles.command = get(handles.comm_edit, 'String');
eval(handles.command);
set(handles.comm_edit, 'String', 'Enter Command');
guidata(hObject,handles);
```

```
% --- Executes during object creation, after setting all properties.
function comm_edit_CreateFcn(hObject, eventdata, handles)
% hObject    handle to comm_edit (see GCBO)
% eventdata  reserved - to be defined in a future version of MATLAB
% handles    empty - handles not created until after all CreateFcns called

% Hint: edit controls usually have a white background on Windows.
%       See ISPC and COMPUTER.
if ispc && isequal(get(hObject,'BackgroundColor'),
get(0,'defaultUicontrolBackgroundColor'))
   set(hObject,'BackgroundColor','white');
end



function pulse_dur_edit_Callback(hObject, eventdata, handles)
% hObject    handle to pulse_dur_edit (see GCBO)
% eventdata  reserved - to be defined in a future version of MATLAB
% handles    structure with handles and user data (see GUIDATA)

% Hints: get(hObject,'String') returns contents of pulse_dur_edit as text
%        str2double(get(hObject,'String')) returns contents of pulse_dur_edit as a double
handles.pulse_dur = get(hObject, 'String');
guidata(hObject,handles);

% --- Executes during object creation, after setting all properties.
function pulse_dur_edit_CreateFcn(hObject, eventdata, handles)
% hObject    handle to pulse_dur_edit (see GCBO)
% eventdata  reserved - to be defined in a future version of MATLAB
% handles    empty - handles not created until after all CreateFcns called

% Hint: edit controls usually have a white background on Windows.
```

```
%       See ISPC and COMPUTER.
if ispc && isequal(get(hObject,'BackgroundColor'),
get(0,'defaultUicontrolBackgroundColor'))
   set(hObject,'BackgroundColor','white');
end

% --- Executes during object creation, after setting all properties.
function current_graph_CreateFcn(hObject, eventdata, handles)
% hObject    handle to current_graph (see GCBO)
% eventdata  reserved - to be defined in a future version of MATLAB
% handles    empty - handles not created until after all CreateFcns called

% Hint: place code in OpeningFcn to populate current_graph

function Timer_edit_Callback(hObject, eventdata, handles)
% hObject    handle to Timer_edit (see GCBO)
% eventdata  reserved - to be defined in a future version of MATLAB
% handles    structure with handles and user data (see GUIDATA)

% Hints: get(hObject,'String') returns contents of Timer_edit as text
%        str2double(get(hObject,'String')) returns contents of Timer_edit as a double
handles.timer = get(hObject, 'String');
guidata(hObject,handles);

% --- Executes during object creation, after setting all properties.
function Timer_edit_CreateFcn(hObject, eventdata, handles)
% hObject    handle to Timer_edit (see GCBO)
% eventdata  reserved - to be defined in a future version of MATLAB
% handles    empty - handles not created until after all CreateFcns called

% Hint: edit controls usually have a white background on Windows.
```

```
%       See ISPC and COMPUTER.
if ispc && isequal(get(hObject,'BackgroundColor'),
get(0,'defaultUicontrolBackgroundColor'))
   set(hObject,'BackgroundColor','white');
end

function Output_edit_Callback(hObject, eventdata, handles)
% hObject    handle to Output_edit (see GCBO)
% eventdata  reserved - to be defined in a future version of MATLAB
% handles    structure with handles and user data (see GUIDATA)

% Hints: get(hObject,'String') returns contents of Output_edit as text
%        str2double(get(hObject,'String')) returns contents of Output_edit as a double
handles.output_edit = get(hObject, 'String');
guidata(hObject,handles);

% --- Executes during object creation, after setting all properties.
function Output_edit_CreateFcn(hObject, eventdata, handles)
% hObject    handle to Output_edit (see GCBO)
% eventdata  reserved - to be defined in a future version of MATLAB
% handles    empty - handles not created until after all CreateFcns called

% Hint: edit controls usually have a white background on Windows.
%       See ISPC and COMPUTER.
if ispc && isequal(get(hObject,'BackgroundColor'),
get(0,'defaultUicontrolBackgroundColor'))
   set(hObject,'BackgroundColor','white');
end



% --- Executes on button press in Export.
```

```
function Export_Callback(hObject, eventdata, handles)
% hObject    handle to Export (see GCBO)
% eventdata  reserved - to be defined in a future version of MATLAB
% handles    structure with handles and user data (see GUIDATA)


% %records start time in output

Fig2 = figure;
copyobj(handles.current_graph, Fig2);
hgsave(Fig2, 'myFigure.fig');

handles.output_log = [handles.output_log newline 'You are done!'];
File = fopen('Output.txt','w');
set(handles.Output_edit, 'String', 'You are done!');
fprintf(File, handles.output_log);
fclose(File);

guidata(hObject,handles);



% --- Executes on button press in refine.
function refine_Callback(hObject, eventdata, handles)
% hObject    handle to refine (see GCBO)
% eventdata  reserved - to be defined in a future version of MATLAB
% handles    structure with handles and user data (see GUIDATA)

handles.refine = get(hObject, 'String');

pulse_dur =  str2double(handles.pulse_dur);
volt_string=':SOURce:VOLTage:LEVel:IMMediate:AMPLitude ';
```

```
      timer=1;



       for i=timer:(str2double(get(handles.pulse_dur_edit, 'String')))
          set(handles.Timer_edit, 'String', i);
          volt=query(handles.obj1,':SOURce:VOLTage:LEVel:IMMediate:AMPLitude?');

          if str2double(volt) == str2double(get(handles.pulse_volt_max_edit, 'String'))
%10
             message_min = [volt_string get(handles.Pulse_volt_min_edit, 'String');];

             fprintf(handles.obj1,message_min);

             pause(0.5)
          else
             message_max = [volt_string get(handles.pulse_volt_max_edit, 'String');];

             fprintf(handles.obj1,message_max);
             pause(0.5)
          end
       end
             fprintf(handles.obj1,':SOURce:VOLTage:LEVel:IMMediate:AMPLitude 0');



guidata(hObject,handles);
```

Published with MATLAB® R2016b

Appendix C

Comparison of I-V Relationship for Pores Post Fabrication and Post Soaking

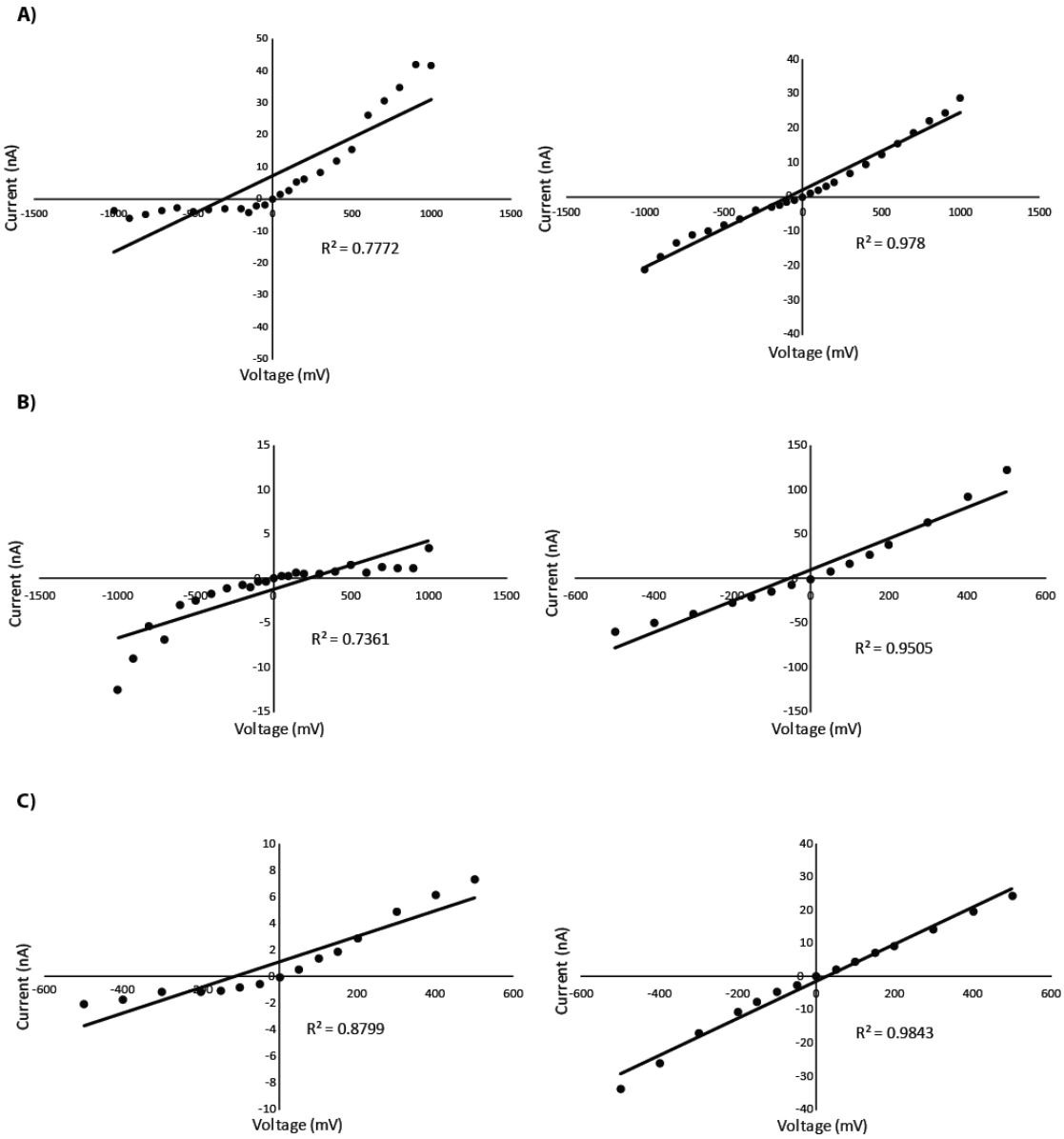

IV curves for various pores acquired immediately after fabrication (left) and after soaking in LiCl stabilization buffer (right)**.** A) nanopore fabricated in 1 M KCl and subsequently soaked overnight in 3.6 M LiCl buffer. The estimated pore size is 5.98 nm in diameter. B) nanopore fabricated in 1 M KCl and subsequently soaked overnight in 3.6 M LiCl buffer. The estimated pore size is 23.9 nm in diameter. C) nanopore fabricated in 1 M LiCl and subsequently soaked overnight in 3.6 M LiCl stabilization buffer. The estimated pore size is 14.45 nm in diameter.

Appendix D

Comparison of I-V Relationship for Pores in Symmetric and Asymmetric Buffer

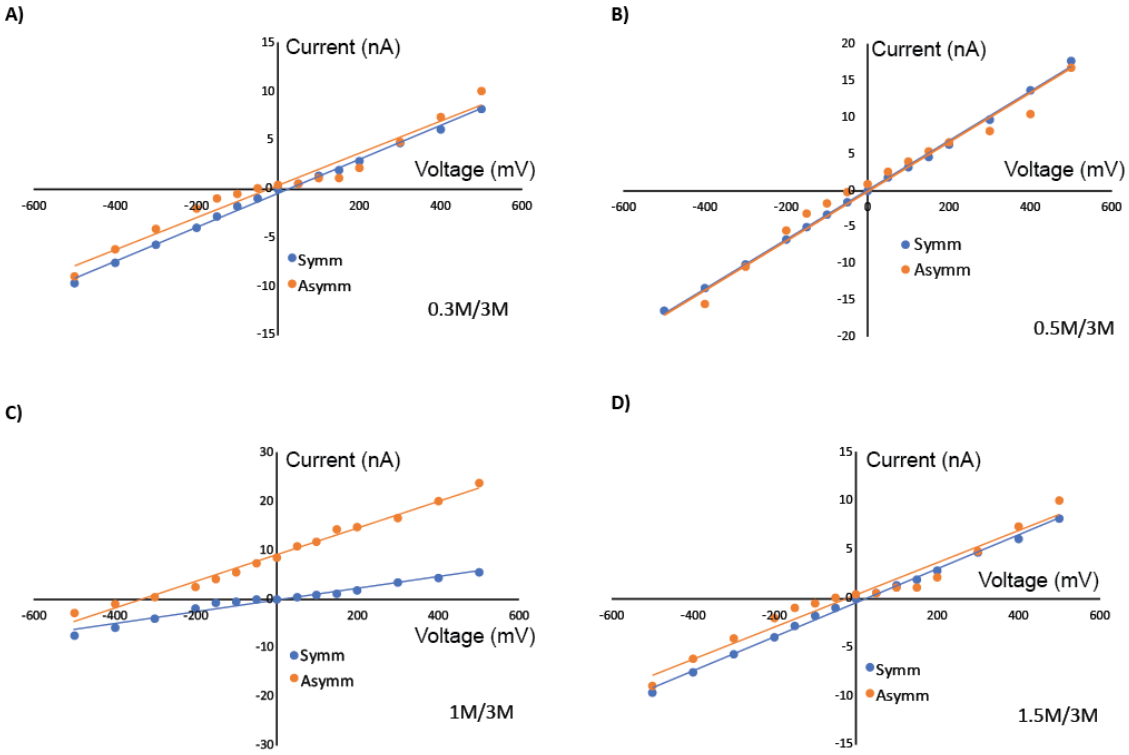

Observable changes in the I-V relationship of the nanopore. I-V relationships were taken in symmetric 1 M LiCl after nanopore fabrication for each pore and then compared to the I-V curve attained after switching media into the asymmetric concentration solution. Linear behavior and a parallel offset to the symmetric conditions were observed in A) 0.3 M/3 M, B) 0.5 M/3 M, and D) 1.5 M/3 M. C) shows a linear behavior, but an offset that has a larger slope.

Appendix E

Methylated DNA Sequence

DNA sequence:

5’-

aaccgtcatgctc^{m}gc^{m}gtcggtgttgcctgcaactgtccgcgttcgacccttgcagcaggtacctcggatgtcccgctctgaga

gc^{m}gc^{m}gctcatacttcac-3’

Control sequence:

5’-

aaccgtcatgctcgcgtcggtgttgcctgcaactgtccgcgttcgacccttgcagcaggtacctcggatgtcccgctctgagagc

gcgctcatacttcac-3’

Appendix F

Mean Dwell Times for DNA-MBP Complexes

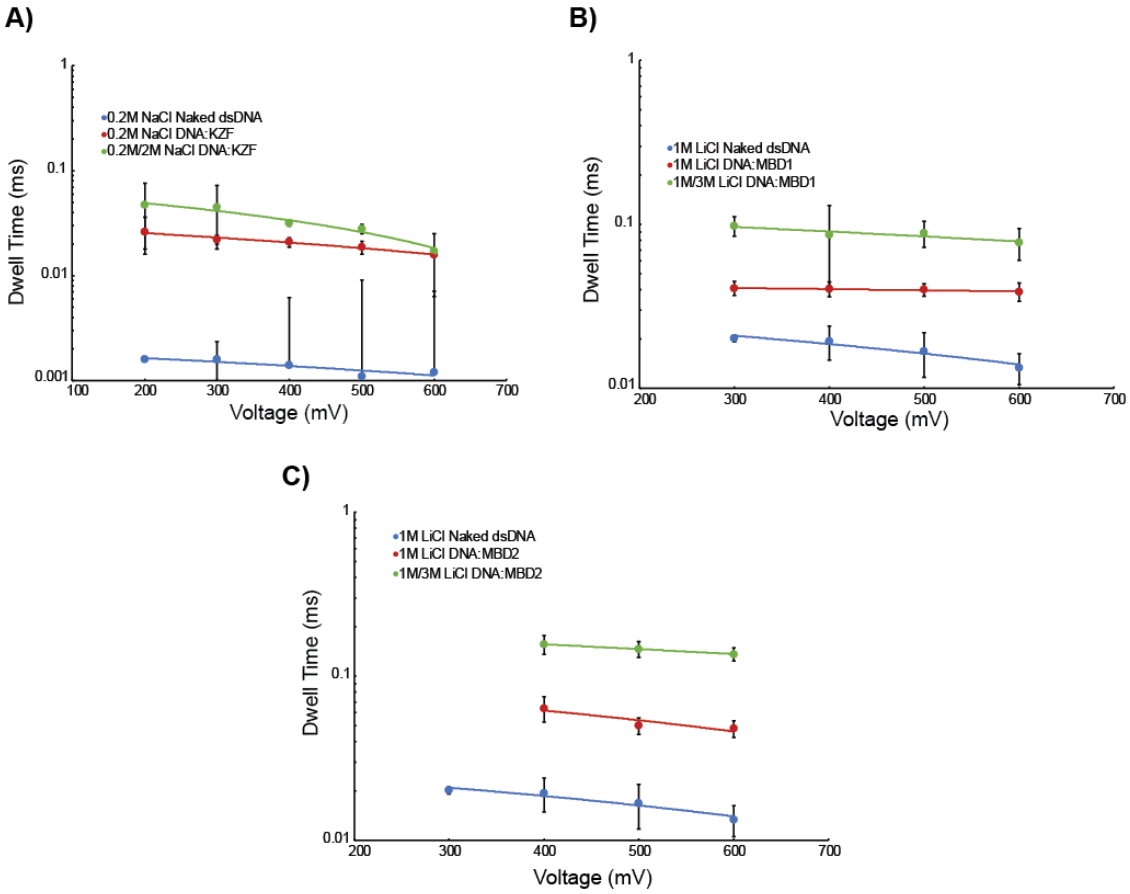

Average dwell times recorded for A) DNA - KZF samples in 0.2 M NaCl and 0.2 M/ 2 M NaCl, B) DNA - MBD1 samples in 1 M LiCl and 1 M/ 3 M LiCl, and C) DNA - MBD2 samples in 1 M LiCl and 1 M/ 3 M LiCl. Experiments were run at applied voltage of 200 mV- 600 mV. A general trend of reduced dwell time with increased applied voltage is observed.

Appendix G

Transport Duration for DNA-MBP Complexes

Table S1

Transport Duration for DNA-MBP Complexes

Sample	Condition	$\tau_{200\ mV}$ (ms)	$\tau_{300\ mV}$ (ms)	$\tau_{400\ mV}$ (ms)	$\tau_{500\ mV}$ (ms)	$\tau_{600\ mV}$ (ms)
Naked DNA	0.2 M NaCl	0.0016 ± 5.00E-06	0.0016 ± 7.49E-04	0.0014 ± 0.005	0.0011 ± 0.008	0.0012 ± 0.006
	1 M LiCl		0.0203 ± 0.001	0.0195 ± 0.005	0.0169 ± 0.005	0.0134 ± 0.003
DNA - KZF	0.2 M NaCl	0.026 ± 0.01	0.0221 ± 0.002	0.0209 ± 0.002	0.0187 ± 0.003	0.0158 ± 0.009
	0.2 M/2 M NaCl	0.047 ± 0.029	0.045 ± 0.027	0.0317 ± 0.002	0.028 ± 0.003	0.017 ± 0.001
DNA - MBD1	1 M LiCl		0.0409 ± 0.004	0.0405 ± 0.004	0.040 ± 0.003	0.039 ± 0.005
	1 M/3 M LiCl		0.0982 ± 0.013	0.0864 ± 0.044	0.0886 ± 0.016	0.0775 ± 0.017
DNA - MBD2	1 M LiCl			0.0640 ± 0.011	0.0502 ± 0.006	0.0481 ± 0.006
	1 M/3 M LiCl			0.1568 ± 0.020	0.1470 ± 0.017	0.1367 ± 0.012

Appendix H

ANOVA Table

Table S2

ANOVA: Single Factor

SUMMARY

Groups	*Count*	*Sum*	*Average*	*Variance*
MBD1 Low	1653	-928943	-561.974	18970.63
MBD1 High	1676	-1476168	-880.768	32987.95
MBD2 Low	1235	-682479	-552.615	21706.39
MBD2 High	2454	-2663770	-1085.48	77492.95
Naked	923	-513441	-556.274	7406.442

ANOVA

Source of Variation	*SS*	*df*	*MS*	*F*	*P-value*	*F crit*
Between Groups	4.34E+08	4	1.09E+08	2775.057	0	2.373052
Within Groups	3.1E+08	7936	39100.17			
Total	7.44E+08	7940				

Appendix I

Histograms for Current Blockage Amplitude for DNA-MBD2 Experiments

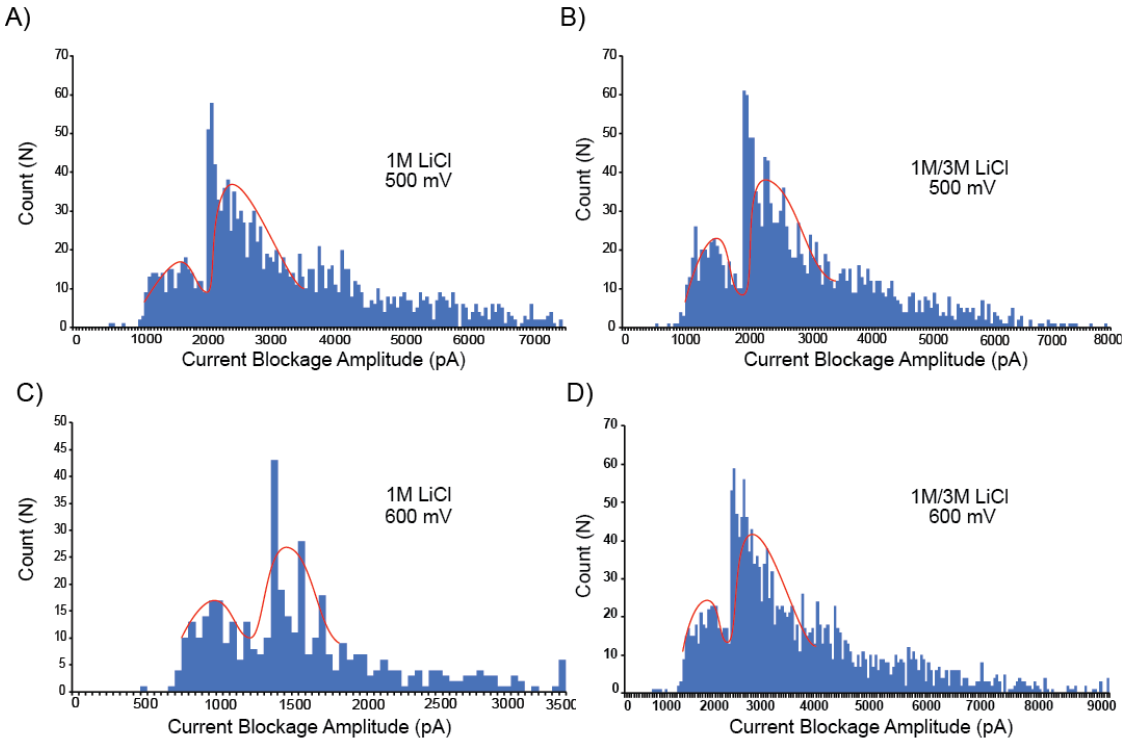

Histograms for current blockage amplitudes of 1:5 ratio DNA - MBD2 samples in A) 1 M LiCl at 500 mV, B)1 M/3 M LiCl at 500 mV, C) 1 M LiCl at 600 mV, and D)1 M/3 M LiCl at 600 mV. Two peaks in each plot show the distinction between bound and unbound DNA in this sample.

Appendix J

Distribution of Different Bound Protein Types

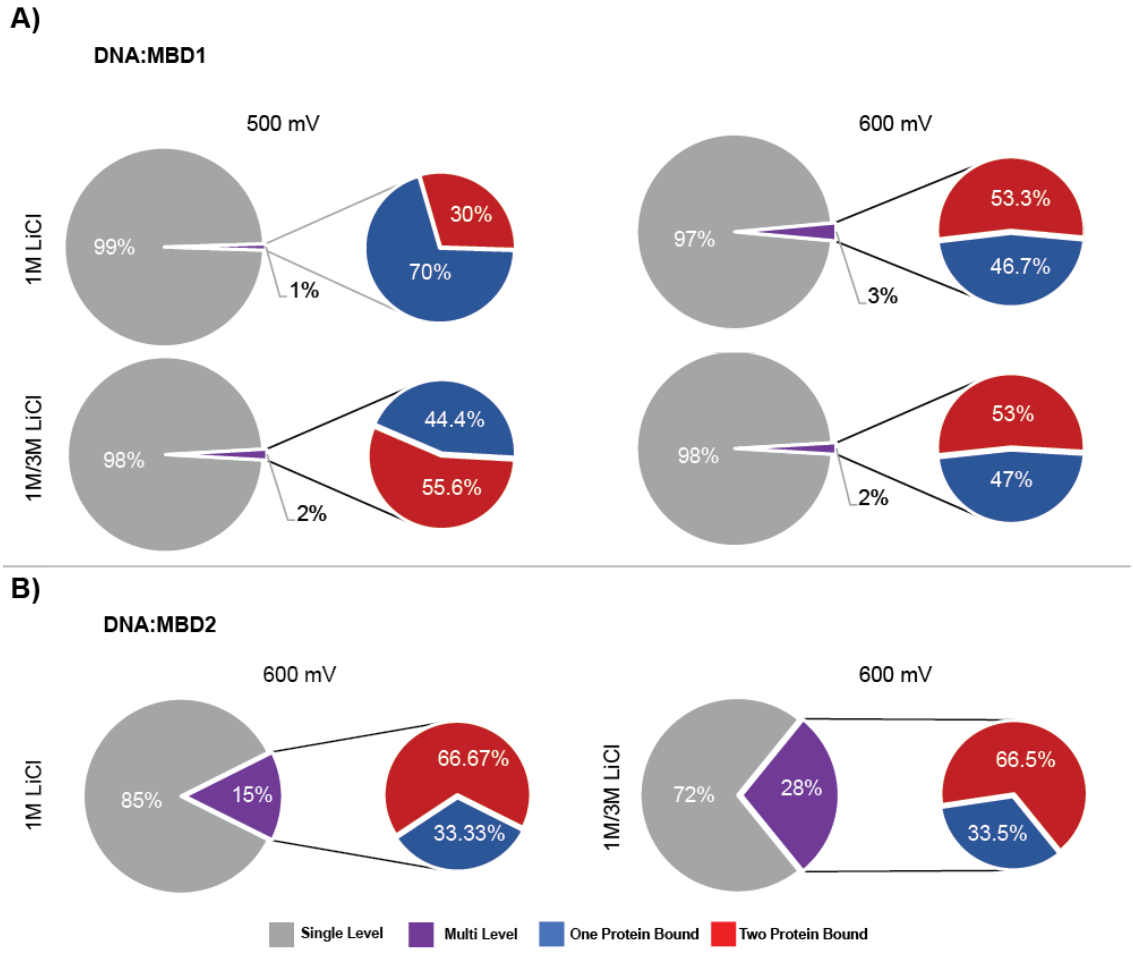

Pie chart depicting the distribution of different types of bound protein events observed in A) 1:1 ratio DNA - MBD1 samples in symmetric 1 M LiCl and asymmetric 1 M/ 3 M LiCl at 500 mV and 600 mV, and B) 1:5 ratio DNA: MBD2 samples in symmetric 1 M LiCl and asymmetric 1 M/ 3 M LiCl at 600 mV.

Appendix K

Supplemental DNA-MBD Multilevel Event Maps

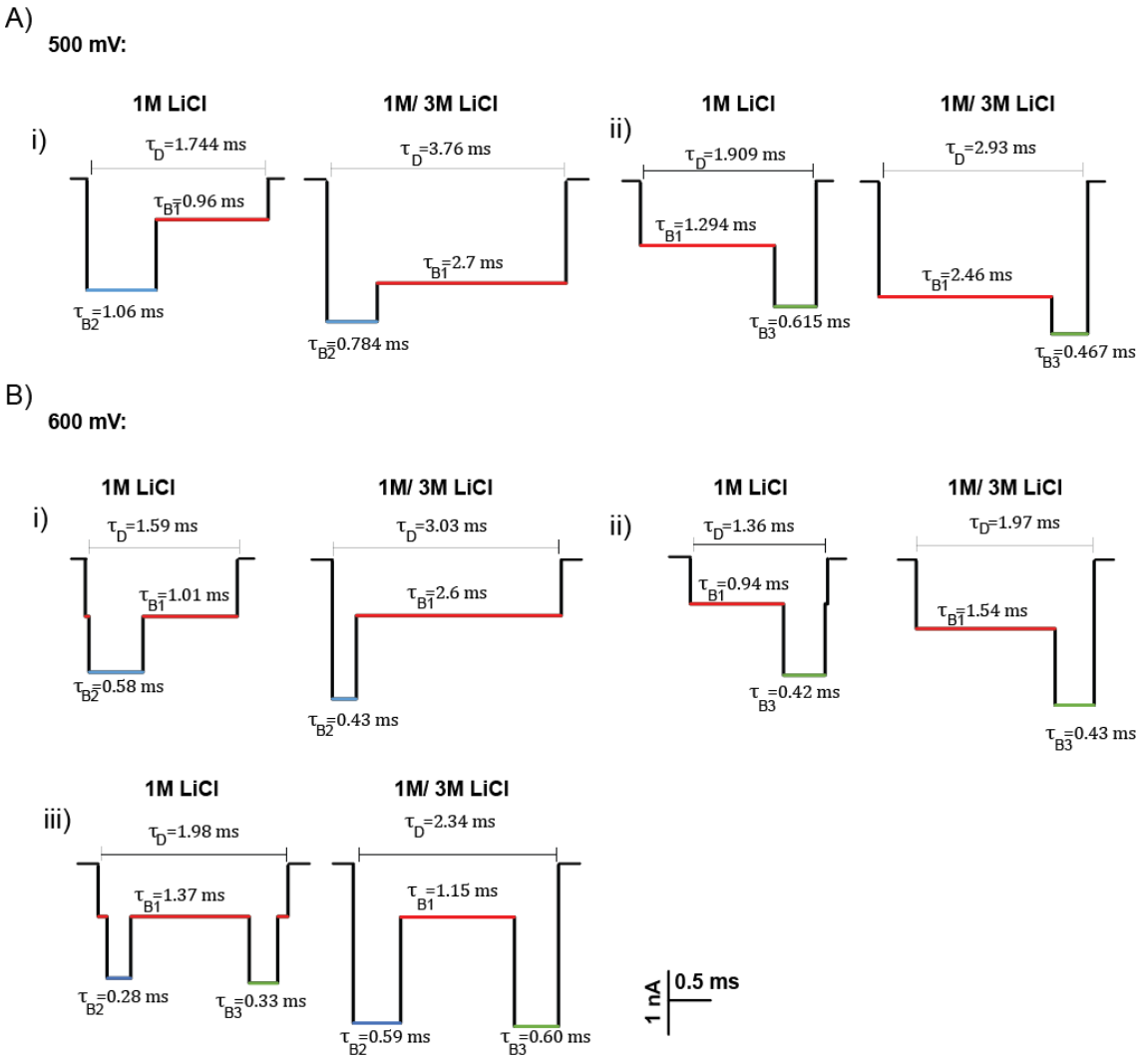

DNA - MBD multilevel event map representing the average temporal duration of each level of current blockage observed in 1:5 ratio DNA: MBD2x samples in 1 M LiCl and 1 M/3 M LiCl. A) Multilevel maps of different current signatures for experiments run at 500 mV applied voltage. Ai) and Aii) correspond to sample events shown in Figure 19E.iv and Figure 19E.iii respectively. B) Multilevel maps of different current signatures for experiments run at 600 mV applied voltage. Bi) and Bii) correspond to Figure 19E.iv and Figure 19E.iii respectively. Biii) corresponds to sample events shown in Figure 19E.v-vi.